2000

The use of atmospheric parameters to account for warm season precipitation variability across the grain-producing region of the US

Paul Stephen Castleberry
Iowa State University

INFORMATION TO USERS

This manuscript has been reproduced from the microfilm master. UMI films the text directly from the original or copy submitted. Thus, some thesis and dissertation copies are in typewriter face, while others may be from any type of computer printer.

The quality of this reproduction is dependent upon the quality of the copy submitted. Broken or indistinct print, colored or poor quality illustrations and photographs, print bleedthrough, substandard margins, and improper alignment can adversely affect reproduction.

In the unlikely event that the author did not send UMI a complete manuscript and there are missing pages, these will be noted. Also, if unauthorized copyright material had to be removed, a note will indicate the deletion.

Oversize materials (e.g., maps, drawings, charts) are reproduced by sectioning the original, beginning at the upper left-hand corner and continuing from left to right in equal sections with small overlaps.

Photographs included in the original manuscript have been reproduced xerographically in this copy. Higher quality 6" x 9" black and white photographic prints are available for any photographs or illustrations appearing in this copy for an additional charge. Contact UMI directly to order.

Bell & Howell Information and Learning
300 North Zeeb Road, Ann Arbor, MI 48106-1346 USA
800-521-0600

The use of atmospheric parameters to account for warm season precipitation variability across the grain-producing region of the U.S.

by

Paul Stephen Castleberry

A dissertation submitted to the graduate faculty

in partial fulfillment of the requirements for the degree of

DOCTOR OF PHILOSOPHY

Major: Agricultural Meteorology

Major Professor: Richard E. Carlson

Iowa State University

Ames, Iowa

2000

Graduate College
Iowa State University

This is to certify that the Doctoral dissertation of

Paul Stephen Castleberry

has met the dissertation requirements of Iowa State University

Signature was redacted for privacy.

Major Professor

Signature was redacted for privacy.

For the Major Program

Signature was redacted for privacy.

For the Graduate College

TABLE OF CONTENTS

ABSTRACT

Warm season precipitation is a necessary ingredient to promote corn growth and development. Above (below) trend corn yields occur in conjunction with above (below) normal precipitation. To isolate potential physical mechanisms responsible for the variations in precipitation across the grain-producing region of the U.S., fields of atmospheric parameters, segregated by a combination of the Positive/Negative phase of the Southern Oscillation Index (SOI) and Warm/Cold phase of the Pacific Decadal Oscillation (PDO) were analyzed. The analysis shows that above (below) trend precipitation and corn yields across portions of the grain-producing region tend to occur with a coupling of the negative (positive) phase of the SOI and warm (cold) phase of the PDO. Fields of atmospheric parameters identified spatial regions of preferential precipitation across the grain producing regions of the U.S. It may be possible to use the atmospheric parameters to infer potential precipitation trends, which can be used to forecast corn yield potential across portions of the grain-producing region of the U.S.

INTRODUCTION

Over the last 100 years, Iowa corn yields have risen from 40 to 120 bushels/acre (Carlson et al. 1996). A portion of this rise in trend can be attributed to the development of better seed varieties, increased use of pesticides, strategic application of nutrients (nitrogen, phosphorous, potassium), and improved farm management practices. While there have been significant improvements in corn yields, there are still periods of marked interannual variability, especially during the past thirty years. The periods of marked interannual yield variability may be related to the changing global climate. It is now recognized that anthropogenic processes may have contributed to a portion of the climatic shift within the past century. Global temperatures are on average 0.5° C warmer now compared to 1900.

Climate model scenarios, such as maintaining current CO_2 or doubling CO_2 concentrations, indicate continued increase in global scale temperatures. Increases in global temperatures may lower yields in southern latitudes, but farm level adjustments in conjunction with CO_2 fertilization should limit midwestern yield reductions to approximately 3% (Kaiser and Drennen 1993). This assumes that weather events are not adversely affected by increasing global temperatures; this, however, may not be the case. Trenberth and Hoar (1996) suggested that increasing global temperatures may be responsible for the frequency and duration of El Nino/Southern Oscillation (ENSO) events in the 1990's. The increasing variability in climate should also signal an increase in yield variabilities.

A measure of the interannual yield variability can be identified by the oscillatory nature it exhibits (Figure 1: Note the oscillatory nature of the "raw" corn yields throughout the last 100 years). There have been extended periods of both amplified (1970-present) and damped (1950-1969) oscillations. The amplified pattern of yield variability since the 1970s is in close agreement with the increase in climate variability as represented by the frequency of occurrences of ENSO/LNSO events.

Mechanisms that account for a portion of climate variability are numerous and complex. Examples of such complex systems are ENSO and LNSO events.

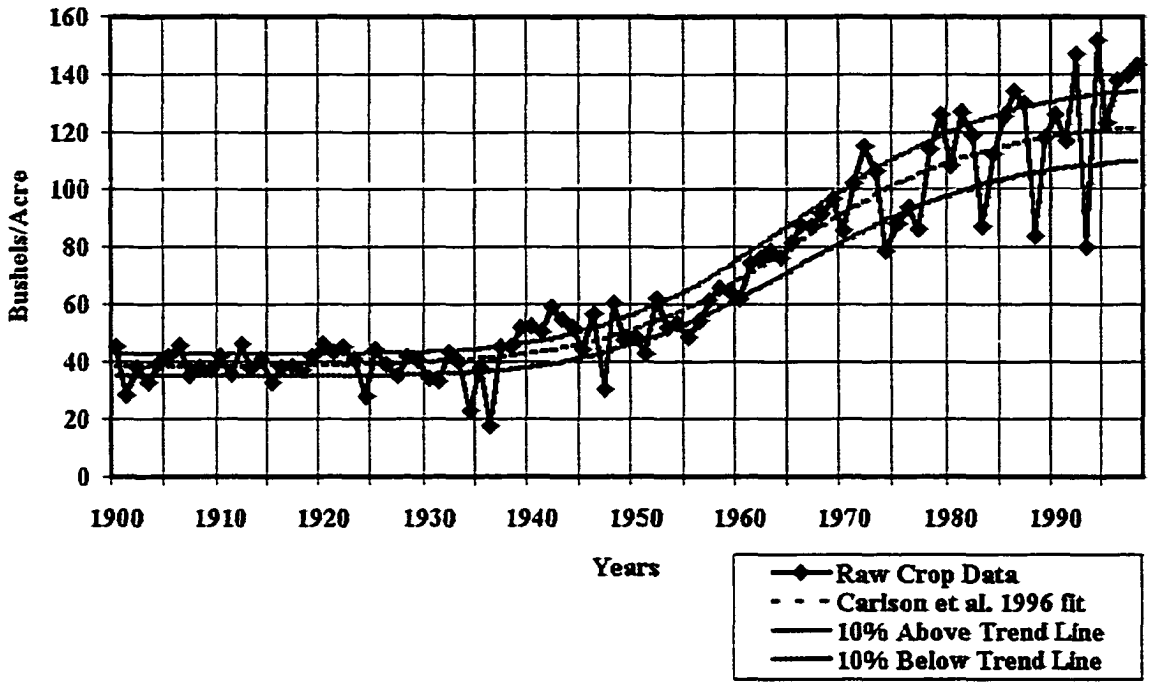

Figure 1. Iowa corn yields for 1900-1998

These systems, which are located in the central and eastern equatorial Pacific regions comprise an intricate connection between the atmosphere and ocean. Although these systems are located in the tropics, ENSO/LNSO systems have accounted for a significant portion of the cold season climate variability in the extratropical regions of the Northern Hemisphere (Wallace and Gutzler 1981; Livezey and Mo 1987). How do systems in the tropics influence remote regions elsewhere? This is an area where the complexities of the system are not completely understood. Modeling studies have suggested a physical link between the tropics and extratropics (Lau and Peng 1992; Hoskins and Karoly 1981). It is conjectured that latent heat release from tropical convection is transported into the extratropics where it "excites," or manifests itself as a perturbation in the Rossby wave flow. These perturbations are then transferred downstream to remote locations such as the U.S. and Canada where they may cause variabilities in atmospheric parameters that, in

turn, influence the variability in temperature and precipitation patterns. The mechanism of transfer described above is referred to as "atmospheric teleconnections." A description of the term atmospheric teleconnection was offered by Leathers et al. (1991). "In short, teleconnections may be used to portray climatological relationships between the planetary-scale atmospheric circulation and surface climate, within the context of the theory, modeling and diagnostics of global climate dynamics."

The effects from atmospheric teleconnections are present throughout the year but often exhibit the strongest correlations during the December-February cold season (Figure 2). Horel and Wallace (1981) explain, "The theoretical results indicate that strong teleconnections to middle latitudes are possible only when the westerlies extend from middle latitudes into the equatorial troposphere over the region of the heat source. For the Northern Hemisphere, this condition is fulfilled only during the winter-half of the year equatorward of the upper tropospheric mid-Pacific and Atlantic troughs. Hence the theoretical results provide a possible explanation for the fact that the teleconnections to high latitudes appear to be present only during the winter half of the year."

Note that the phrase "strong teleconnections" should not exclude links to other seasons, only that these other seasons exhibit a weaker signal (Figure 3). Recent studies have suggested that atmospheric teleconnections are present, albeit weaker, during the Northern Hemisphere warm season. Numerical experiments by Lau and Peng (1992) suggest the presence of these teleconnections through a wave train emanating from the tropics to the extratropics. The forcing for their experiment, a divergence center at 250 mb, was moved into a region of weakened tropical easterlies; thus, any waves propagating poleward are not trapped. Also, note that this region is slightly downstream of the May-August climatological 250 mb trough (one of the necessary conditions needed for tropical-extratropical teleconnections according to Horel and Wallace 1981). The forced wave train consists of a high (near the divergence center), an enhanced Aleutian Low, and a high over North America. They found that the most pronounced wave train occurred in June, with later warm season months not as pronounced, but still identifiable. Lau and Peng (1992) also adjusted the latitudinal location of the forcing and found that the optimal

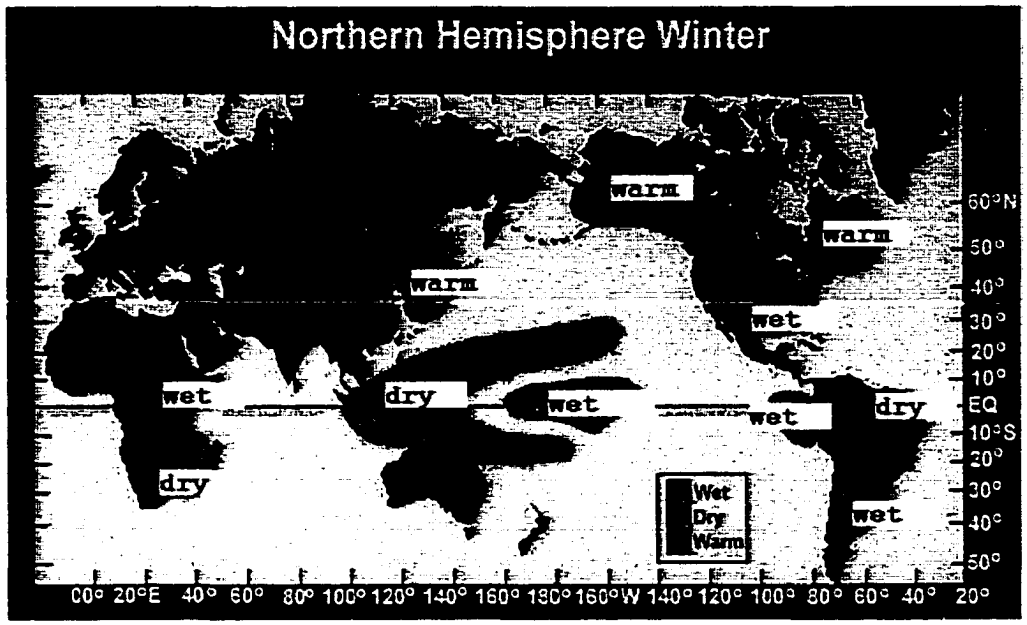

Figure 2. Cold season ENSO teleconnections. (http://www.pmel.noaa.gov/toga-tao/pmel-graphics/gif/winter.gif)

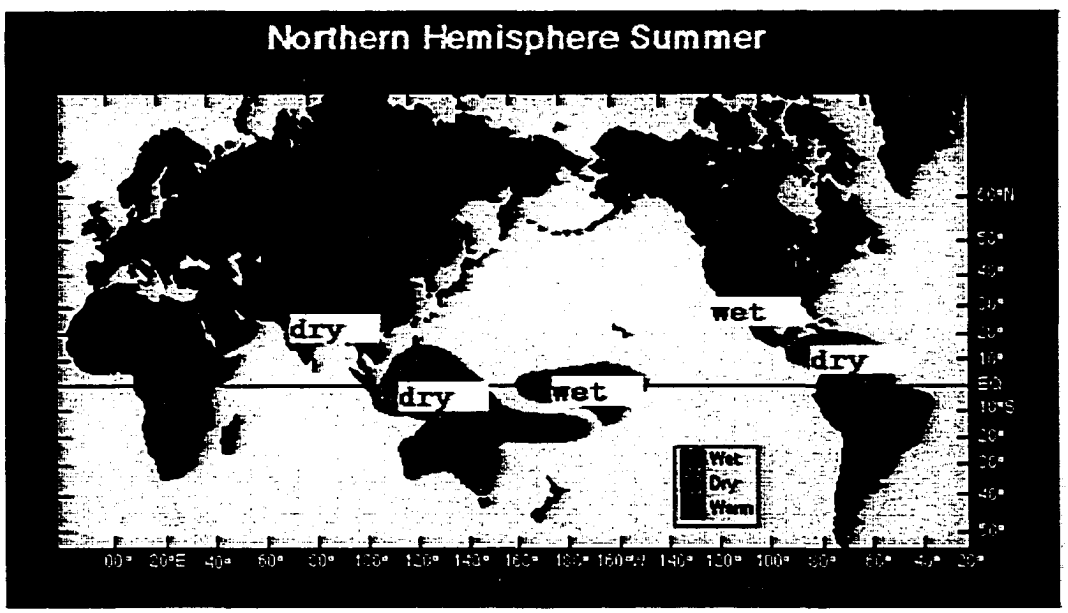

Figure 3. Warm season ENSO teleconnection. (http://www.pmel.noaa.gov/toga-tao/pmel-graphics/gif/summer.gif)

latitude is 13.3^0N. Moving the forcing equatorward of the threshold latitude weakened the tropical-extratropical teleconnection (their Figure 5).

Several observational studies have suggested warm season relationships between the tropics and extratropics. Garnett et al. (1998) identified a significant source of warm season climatic variability in the temperature and precipitation fields over Western Canada, although it was correlated with the previous September-May months. A linear combination of monthly ENSO and 700 mb geopotential height values was used to identify a portion of the variability.

Bunkers et al. (1996) focused on warm season (April-October) forcing from ENSO/LNSO across the Dakotas region. They discovered a coherent warm season precipitation signal based upon the ENSO/LNSO phase. Most ENSO (LNSO) events are associated with above (below) median values of precipitation, with approximately 60% of the ENSO precipitation events in the upper 25% of the distribution. Their study did not attempt to identify physical mechanisms responsible for the precipitation variability, but they speculate that it may be a function of the spatial location of the Bermuda High Pressure system. An anomalous westward displacement of the Bermuda High could support enhanced precipitation in their region of study.

Ting and Wang (1997) identified a warm season relationship between Great Plains precipitation and sea surface temperatures (SSTs) in different regions of the Pacific Ocean. They found that Great Plains warm season (June-August) precipitation is positively correlated with SSTs in the tropical and extratropical Pacific, with extratropical SST correlations stronger than tropical SST correlations. They also analyzed the spatial location of precipitation variability by the contributions from the tropical and extratropical SSTs. Their results suggest that extratropical SSTs are correlated with precipitation variability over the central and eastern U.S., while tropical SSTs influence precipitation variability over the northern portions of the Great Plains. An analysis of atmospheric circulation patterns shows that during wet years an enhanced jet stream was present over the northern Plains. Their work also suggests changes in storm tracks and moisture transport as playing a role in precipitation variability. Compared to other studies, their

results suggest that warm season precipitation variability may be related to both tropical and extratropical SSTs.

Carlson et al. (1996) discovered a warm season statistical relationship between climate (temperature and precipitation) and SOI across portions of the U.S. grain-producing region. Cool and wet summers were associated with an SOI less than or equal to 0.8. This phase of the SOI tended to coincide with corn yields 10% above trend throughout portions of the grain-producing region of the U.S. Conversely, warm and dry summers were associated with SOI values greater than 0.8, along with depressed corn yields (10% below trend).

With the above work suggesting possible warm season teleconnections, a recently identified atmospheric phenomenon in the midlatitude Pacific Ocean (Zhang et al. 1997), referred to as either the Pacific Decadal Oscillation (PDO) or North Pacific Oscillation (NPO), is introduced to help strengthen the idea of "identifiable" warm season teleconnections. Gershunov and Barnett (1997) suggested that an optimal coupling between ENSO/LNSO and the high (warm) and low (cold) phases of the NPO (hereafter, referred to as the PDO) may be responsible for a portion of the climate variability downstream into North America during the cold season. Mantua (2000) has identified October-March climate teleconnections attributed in part to the PDO. Their recent work has suggested that during the warm phase of the PDO (representing above normal SSTs along the west coast of North America and below normal SSTs in the north-central Pacific Ocean) (Figure 4), regions of North America experience a Pacific North American (PNA) temperature pattern (above normal surface temperatures over the Pacific Northwest region). The precipitation pattern is dry across most of the North American continent with wet patterns confined to the southern Plains, southwestern U.S., and Mexico.

These studies of the PDO are focused, like most ENSO/LNSO studies, on the cold season. Is it possible that there may be a warm season connection between climate variability and PDO across portions of the grain-producing region of the U.S., and if so, what is the role of ENSO/LNSO?

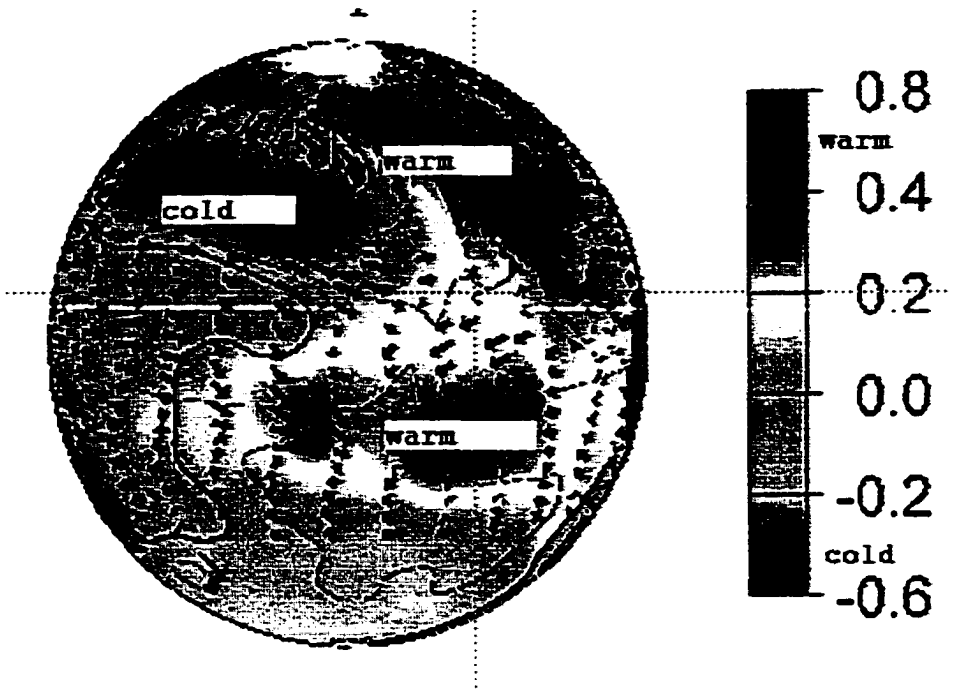

Figure 4. Warm phase of the PDO. (http://tao.atmos.washington.edu/pdo/)

It is already known that not all ENSO/LNSO events are similar in magnitude or location. Part of this change in strength of ENSO/LNSO may be due to the modulating influence of the PDO (Gershunov and Barnett 1997), but modeling studies are needed to further verify their hypothesis.

This research uses couplings of ENSO/LNSO and warm/cold phases of the PDO, which are listed in Table 1. It should be noted that segregating 51 years of data by the four events below decreases sample size. The larger the sample size the more confidence gained in significance tests of differences. All but Event 2 meet minimum requirements of sample size (n=5) for significance testing.

Table 1. Possible combinations of ENSO/LNSO and Warm/Cold PDO events. Sample size of each event is in parenthesis.

Events	Warm Phase of PDO	Cold Phase of PDO
El Nino	1 (8)	3 (7)
La Nina	2 (2)	4 (8)

As previously discussed, midlatitude warm season effects from ENSO/LNSO are weak, but a combination of ENSO/LNSO and the PDO (exerting some type of modulating effect on ENSO/LNSO) may be able to elucidate a more robust teleconnection pattern. Part of the robustness of the signal may be due to the spatial location of the PDO within the midlatitudes, which is within the track of the westerlies. The location of the PDO along the storm track may play a role in warm season climate variability downstream across regions of North America. This research does not attempt to quantitatively identify variations in the storm track or the physics behind a coupling of ENSO/LNSO and PDO. It merely provides a hypothesis for the downstream teleconnections. The coupling itself is used as a way to segregate the data (precipitation, corn yields, and atmospheric parameters) in an attempt to account for the variability of precipitation and corn yields across the grain-producing region of the U.S. during the warm season.

DATA AND METHODOLOGY

Data from April-September 1948-1998 are used for this project. The temporal resolution of this project corresponds to the availability of upper air climate data. The data sets for this project consist of state-division monthly mean precipitation from the National Climatic Data Center (NCDC), five-month centered mean of the SOI from the Climate Prediction Center (CPC), monthly mean atmospheric reanalysis output from the NCEP/NCAR CDAS/Reanalysis Project, monthly standardized values of the PDO index (ftp://ftp.atmos.washington.edu/mantua/pnw_impacts/INDICES/PDO.latest), and corn yields from two sources, Iowa Department of Agriculture (1998) and the USDA (1949-98). Methods of acquisition and/or quality control of state-division monthly mean precipitation, and NCEP/NCAR CDAS/Reanalysis Project can be referenced in Karl et al. (1986), and Kalnay et al. (1996), respectively.

Median values were extracted from state-division monthly mean precipitation data. The choice of using median versus mean values of precipitation was to guard against outlier effects (Wilks 1995); the 1993 warm season precipitation event is an example of such an outlier. A five-month moving mean was performed on the SOI values to stabilize inter-monthly variability (Todey dissertation 1995). Composite analyses of the monthly mean 00 UTC reanalysis data was performed. The choice for 00 UTC was used since it is more representative (presence of instability) of the pre-storm environment during the warm season period. An additional step was performed on the composite analysis; difference fields were computed to elucidate features in the mean atmospheric fields.

El Nino/Warm Phase of PDO (Event 1) and La Nina/Cold Phase of PDO (Event 4) were chosen to segregate the warm season data (Table 1). The decision to segregate the data by these two events was related to previous research (Gershunov and Barnett 1997 and Mantua 1999) suggesting such an optimal coupling; however, their suggested coupling was for cold season events. Before finalizing such a coupling for the warm season, a preliminary analysis of corn yields and of median values of precipitation for the central and northern Plains was performed. Carlson (personal communication 1999) has segregated 99-year corn yield data by combinations of ENSO/LNSO and PDO events (Table 1) and

found evidence of corn yield tendencies to be above (below) trend during Event 1 (Event 4) years (Figure 5). Preliminary analysis of August median precipitation values for state divisions in Nebraska (Figure 6), Iowa (Figure 7), and Illinois (Figure 8) indicates significant differences at the 15% level for Events 1 and 4. Preliminary work with other possible combinations (Events 2 and 3) was not considered for further analysis due to lack of sample size (n=2) for Event 2 years, and smaller precipitation differences (Event 1-Event 3 as compared to Event 1-Event 4 years) across the region of study.

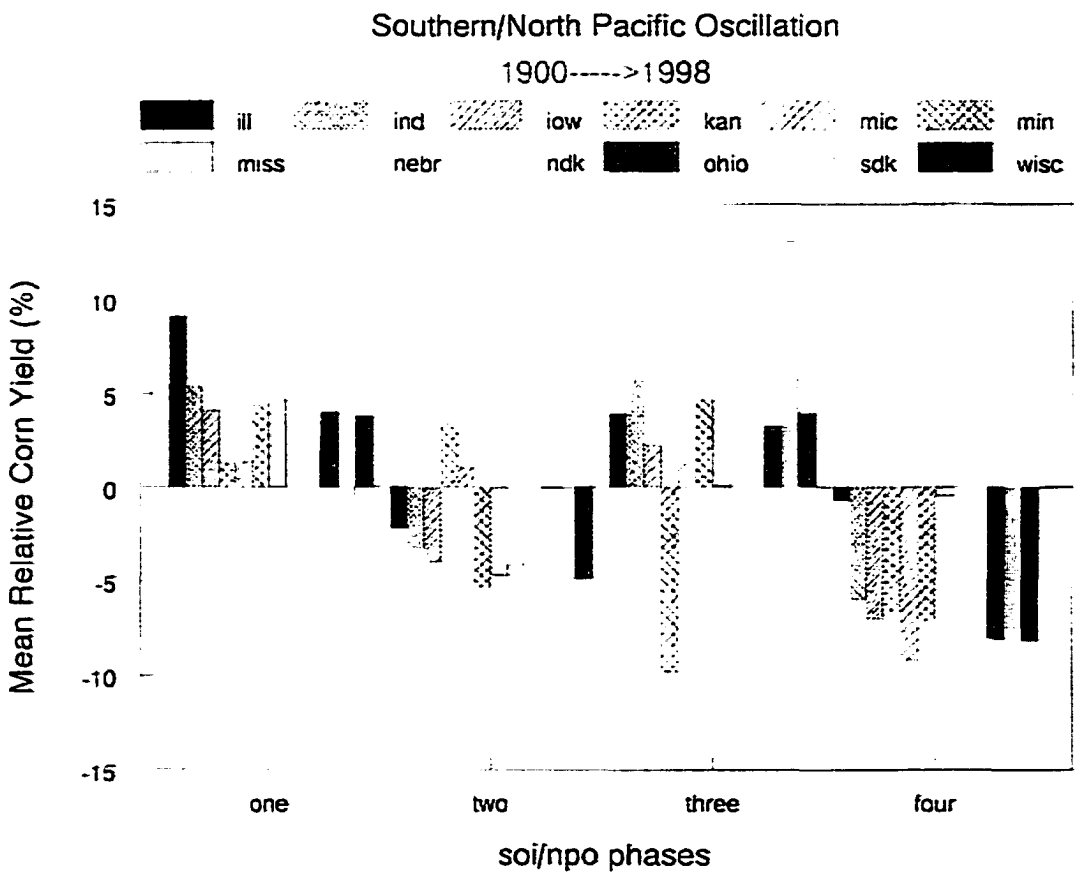

Figure 5. Corn yields segregated by SOI and PDO (1900-1998). On the x-axis "one" represents Event 1 (Table 1), "two" represents Event 2 (Table 1), etc.

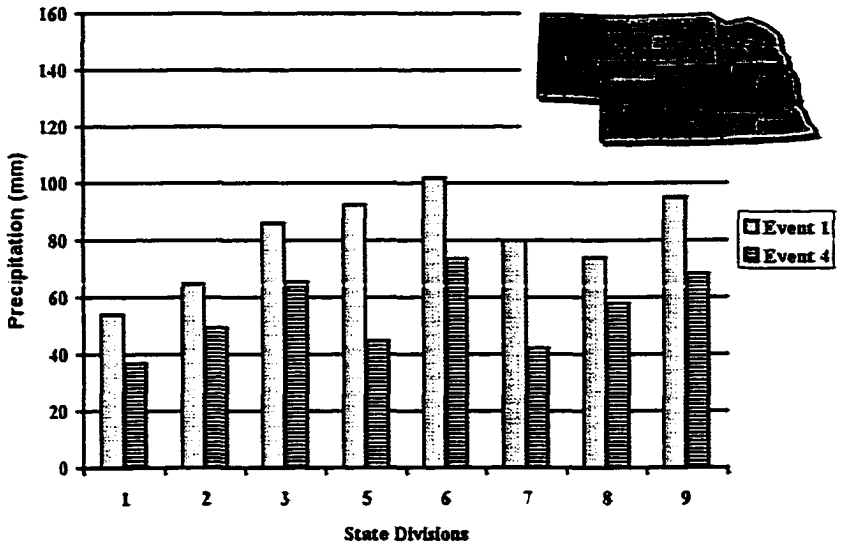

Figure 6. August Nebraska median precipitation by Events 1 and 4. Significance at the 15% level (p-value at 0.15) is denoted by shaded state divisions in upper right portion of graph.

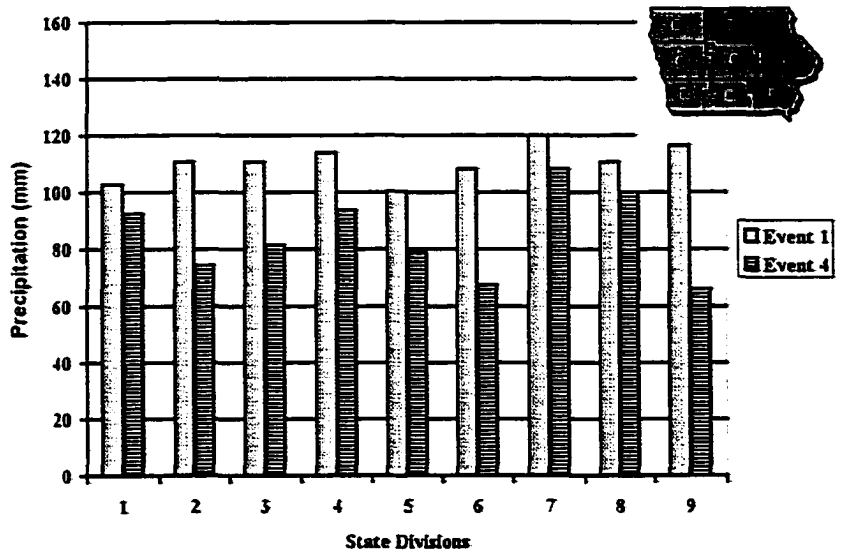

Figure 7. August Iowa median precipitation by Events 1 and 4. Significance at the 15% level (p-value at 0.15) is denoted by shaded state divisions in upper right portion of graph.

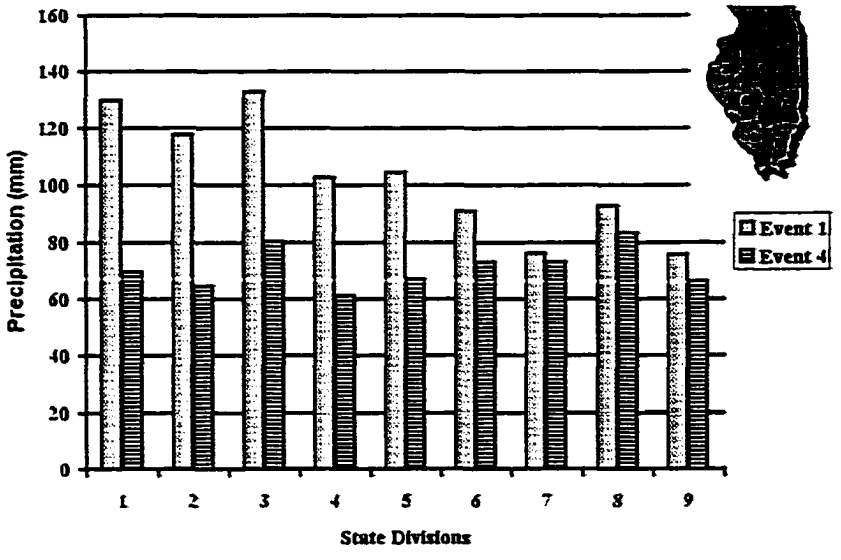

Figure 8. August Illinois median precipitation by Events 1 and 4. Significance at the 15% level (p-value at 0.15) is denoted by shaded state divisions in upper right portion of graph.

Statistics

Atmospheric fields are often used as a visual tool to explain regions of climate variability, which may take the form of physical and/or statistical arguments. Traditional methods of analysis consist of testing for statistically significant differences at individual grid points in a geophysical field (hereafter referred to as "field"). While this method provides statistical information on the individual grid points, it does not accurately evaluate the overall significance of the field. Evaluating the overall statistical significance of a field has its own set of issues that must be addressed, namely, the multiplicity and spatial correlation of geophysical fields (Wilks 1995). The multiplicity issue, which is referred to as "Finiteness" in Livezey and Chen (1983), is described by Wilks (1995) in the context of a 20-sided die example. Assuming that a role of this die has a 5% chance of producing a particular number, the chance of producing the desired number increases beyond 5% when rolling the 20-sided die more than once. This is analogous to the statistical testing of individual grid points in a field. While there may not be a statistically

significant difference at a particular grid point, the probability increases that there will be differences when testing at more than one grid point in a field. Wilks (1995) and Livezey and Chen (1983) have used the binomial test as a means of accounting for the multiplicity in a geophysical field. For this project, the number of independent trials corresponds to the grid points in the field, in this case, 225 and 297. In order to pass the binomial test for significance at the 10% level, the minimum number of successes (represented by t-tests showing statistically significant differences at each grid point) in a field is 29/225 (12.89% of the field) and 37/297 (12.46% of the field), respectively. Therefore, in order to pass the first-tier test accounting for multiplicity in a field, the above threshold values of 12.89% and 12.46% must be met or exceeded in Figure 9. The x and y axis denote the DOF and percent of field exhibiting statistically significant differences, respectively. The curve is constructed by performing calculations using the binomial equation at each of the DOF, with the significance threshold set at 10%. An illustration of using Figure 9 in the first-tier test is demonstrated in the following hypothetical example. Let us assume that a field has

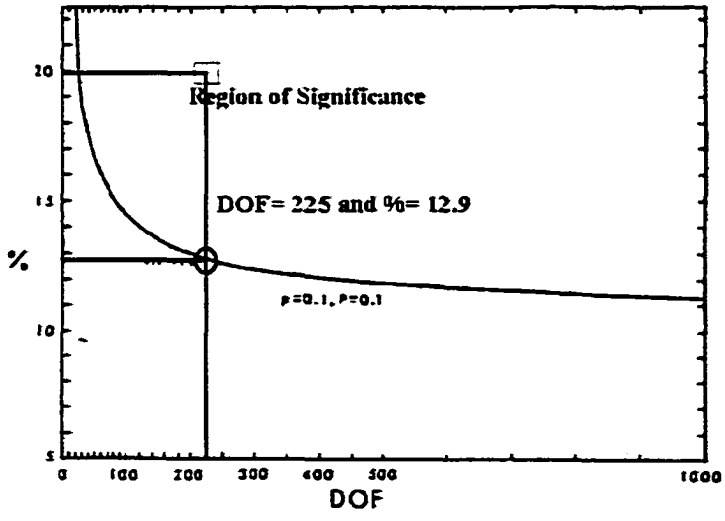

Figure 9. Graphical interpretation of field significance in two-tiers. The x-axis represents the degrees of freedom. The y-axis represents percent of local geophysical field significance. Reproduced from Livezey and Chen (1983) with modifications by Castleberry. Note that the upper limit on the y-axis is at 22%. A reconstructed version of the above graph with extension to 40% can be found in Appendix B.

225 grid points and 20% of the domain exhibits statistically significant differences at the 10% level. The line drawn perpendicular to the DOF set at 225 intersects the curve at approximately 12.9% (oval). The oval represents the minimum value of percent field significance. In this example the percent field significance is 20 (45 of the 225 grid points are significantly different). This is beyond the minimum threshold of 12.9% and can be seen graphically as above the curve (rectangle) in the "Region of Significance." This example shows an experiment that passes the first-tier test of significance, the test of field multiplicity.

The above adjustment for multiplicity assumed independence between grid points, however, it is recognized that many atmospheric parameters are correlated in both time and space. 500 mb geopotential heights and 200 mb wind fields are two such examples of temporal and spatially correlated fields (Livezey and Chen 1983). Correlations in time and space often violate the assumption of independence between gridpoints in a geophysical field, thus invalidating most parametric tests of significance. This invalidation of the test statistic is reflected in an underestimation of the variance, leading to an inflated test statistic, which may then lead to an erroneous conclusion of significance (Wilks 1995). The serial correlation issue was addressed in this project for both the state-division precipitation and reanalysis data by using monthly, not seasonal composites that met the predefined criteria. Accounting for the spatial correlation in atmospheric fields requires a more sophisticated approach. The methods described in the following paragraphs are the second-tier of testing to account for spatial correlation in a field, in order to assess the statistical significance of geophysical fields.

The spatial correlation in fields often acts to decrease the degrees of freedom (DOF), thus, requiring a method to estimate this reduction in DOF in the field. The DOF correspond to the number of grid points in a field. Since there is a strong spatial correlation in warm season atmospheric fields, especially geopotential height fields, the distance between independent observations increases, thus reducing the degrees of freedom. There is a variety of methods to estimate the "reduced degrees of freedom (RDOF)" in a geophysical field problem (Fraedrich et al. 1995 and Madden et al. 1993).

The method used for this project was based upon work done by Madden et al.(1993) and confirmed by Wikle (personal communication 1998). They suggested calculating an "integral space scale," which is used to estimate the spatial distance between gridpoints to ensure that the assumption of independence is met. The integral space scale (A_o) is defined as:

$$A_0 = \int_{\theta=0}^{2\pi} \int_{\phi=0}^{\pi} r(s)\, R^2 \sin\phi \, d\phi \, d\theta \qquad (1)$$

R = radius of the earth

s = distance between gridpoints

$J_o = 0^{th}$ order Bessel Function

$r(s) = \exp(-\lambda * s^{\alpha}) J_0(\beta s)$

λ, α, β = estimated coefficients determined by a first guess vector

r(s) is a correlation function between gridpoints across a finite spatial domain. To estimate r(s) a Fortran program was written to calculate correlations among all gridpoints in the spatial domain. The correlation values were binned into 200 km intervals from 100 to 2900 km, plotted, and then r(s) were fitted to the binned data. According to Madden et al. (1993), the correlation function (r(s)) is both homogeneous (independent of location) and isotropic (independent of direction). The isotropic assumption allows A_0 to be simplified to A_I:

$$A_I = 2\pi R \cdot \int_0^{\pi R} r(s) \sin\left(\frac{s}{R}\right) ds \qquad (2)$$

since r is not a function of θ. The spatial RDOF are calculated as the ratio of:

$$RDOF = A_1/A_2 \tag{3}$$

where A_2 is:

$$A_2 = 2\pi R \cdot \int_0^{\pi R} \sin\left(\frac{s}{R}\right) ds \tag{4}$$

The limits of integration must be adjusted to represent the spatial domain of study. The spatial domain for this project was 25^0N to 50^0N latitude, and 65^0W to 130^0W longitude, thus, a domain spanning a latitude of 25^0, and a longitude of 65^0. The adjustment for the domain in this project produces the following forms of A_1 and A_2, respectively:

$$A_1 = \frac{13\pi R}{36} \cdot \int_0^{\frac{5\pi R}{36}} r(s) \sin\left(\frac{s}{R}\right) ds \tag{5}$$

$$A_2 = \frac{13\pi R}{36} \cdot \int_0^{\frac{5\pi R}{36}} \sin\left(\frac{s}{R}\right) ds \tag{6}$$

With the determination of the RDOF (Equation 3), it is now possible to complete the second-tier of significance testing using Figure 9. Adding an additional component to the previous hypothetical example, let us assume that the calculated RDOF is 30. Locate

the rectangle from Figure 9 and move toward the y-axis until you reach 30 (RDOF). Note that this point (30) lies to the right of the curve, which is the "Region of Significance," thus, a proclamation of global significance can be declared.

The term "global significance" is used in the context of declaring the entire domain significant, assuming passing of the two-tiered test described in the above paragraphs. One other caveat to note, as pointed out in Livezey and Chen (1983), and can be seen graphically in Figure 9, is failure to pass the first-tier test (multiplicity) will terminate further testing (spatial correlation). *It is not possible to be in the region above the curve* (Region of Significance) in the second-tier test (spatial correlation) if the experiment is not located in the region above the curve in the first-tier test (multiplicity).

Statistics used to test for differences between Events 1 and 4 (Table 1) for the monthly mean state-division precipitation data consisted of the Mann-Whitney test. The Mann-Whitney test is the nonparametric version of the Student's t-test. The Mann-Whitney test, however, does not require a Gaussian assumption to the distribution. This non-parametric test was used on the precipitation data since amounts are not Gaussian but are positively skewed, and therefore, the use of parametric tests such as the Student's t-test would be invalid (Wilks 1995).

Statistics were also used to test for the distribution of extreme events; in this case, corn yields. The Hypergeometric Distribution was performed to see how corn yields separated into the top, middle, and bottom one-third of the distribution (Kalbfleisch 1985).

Factors Affecting Crop Development

The motivation for this warm season project is related, in part, to corn yield variability. Corn is grown in various amounts across the grain-producing region of the U.S. (Figure 10). Note that portions of Nebraska, South Dakota, Minnesota, Iowa, Wisconsin, Illinois, and Indiana make up the bulk of the crop acreage planted. This region will make up a subset of interest to this research project.

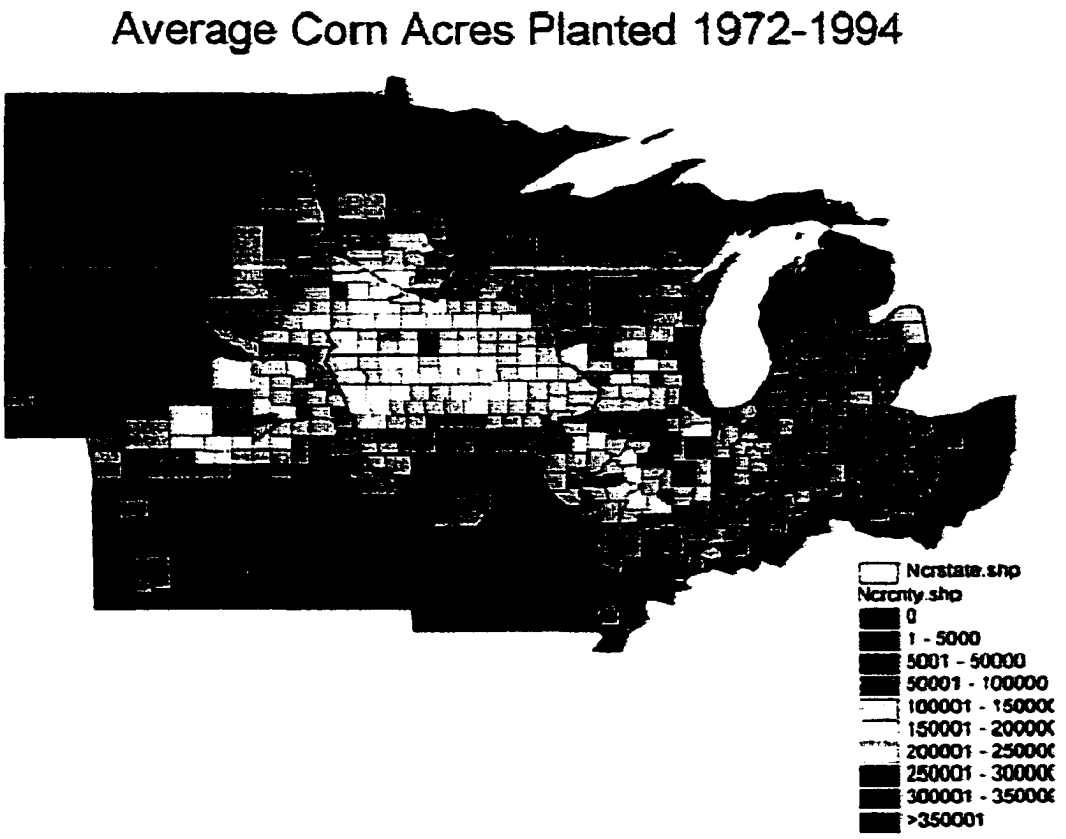

Figure 10. Average corn acres planted averaged over the 1972-1994 period (NC-94)

The crop season can be divided into three phases; preseason (April-mid May), season (mid May-September), and postseason (October). Preseason planting data is important since the five-foot subsurface soil moisture profile plays a role in potential yield variability. The five-foot soil profile across Iowa can typically hold 8 to 10 inches of plant available moisture, and the profile can hold up to a foot of moisture, assuming a silt loam soil texture (Cooperative Extension Service, Iowa State University 1980). In other states across the grain-producing region, such as Nebraska and the Dakotas, subsurface soil moisture profile may be lower due to a steppe climate and soil texture across the western grain-producing region, thus, excessive precipitation may not negatively impact yields

there. However, excessive values of subsurface soil moisture in eastern portions of the region may actually inhibit crop development later in the season. As crops begin to develop, the rooting system begins to grow. The growth may be downward, lateral, and in most cases a combination of downward and lateral movement. Some functions of the rooting system are to transport water and nutrients throughout the crop (Shibles 1998). If there is excessive soil moisture in the five-foot profile, the roots may not develop downward; this is due, in part, to the presence of soil moisture at shallow depths. As the growing season begins to progress towards summer the subsurface moisture begins to be depleted by both the crops and lack of recharge from precipitation. If rooting depth is shallow due to excessive preseason (April and May) precipitation, this type of soil moisture profile will not allow the roots to tap into the soil moisture at lower depths in the profile. Conversely, insufficient moisture in the subsurface soil profile may inhibit downward movement of roots by providing an impediment due to hard soil. Therefore, a critical balance of soil moisture is needed in the five-foot soil profile during the preseason to ensure proper biological development of the crop.

As the crop moves into the seasonal phase of development, subsurface soil moisture becomes a crucial factor in the continued physiological development of the crop. Typically, the soil moisture in the five-foot profile begins to be depleted by the crop and atmosphere. Part of the depletion caused by the crop itself is due to physiological processes, while the sink of subsurface soil moisture by the atmosphere is a function of the moisture gradient between the crop and atmosphere. During the seasonal phase, ambient temperatures begin to increase; as does the crop leaf area and the water potential differences between soil and atmosphere. Increasing temperatures and saturation vapor pressure values begin to create an increasing moisture gradient between the crop and atmosphere. The coupling between the atmosphere and crop can quickly deplete soil moisture reserves if conditions are conducive to this setup. The crop will continue to exchange water vapor with the atmosphere until moisture becomes a limiting factor; at which point, the process will slow down by restricting of the stomata, reducing of exposed leaf surface or reducing of leaf area (leaf death). The closing of the stomata will slow the

loss of water from the crop, but will create an environment that is harmful to crop development. The exchange of vapor and gas by the leaf is crucial to growth. If loss of water vapor is restricted, the gain of CO_2 is simultaneously limited. Additionally, transpiration is a contributing process since a portion of the water available is used to regulate leaf temperature and to transport nutrients from the soil through the roots and to the rest of the crop (Shibles 1998). The movement of water through the crop contributes to continued growth and eventual maturation of the plant; thus, the importance of moisture availability to the crop.

During the seasonal phase of the growing season, subsurface moisture is often depleted by the processes discussed in the previous paragraph. That is one reason why warm season precipitation is so crucial to the overall development of crops across the grain-producing region of the U.S. Timely precipitation events are important to the recharging of the subsurface soil moisture profile.

Carlson et al. (1996) identified possible teleconnective climate patterns for the warm season variability in precipitation across the grain-producing region of the U.S. Their work indicated that warm season precipitation across portions of the grain-producing region shows marked variability based upon the phase of the SOI. They identified threshold values of SOI. SOI values less than or equal to 0.8 were associated with above median precipitation, while SOI values greater than 0.8 were associated with below median precipitation. These differences were statistically significant at the 5-15% level across portions of the grain-producing region. Their suggestions for future research consisted of identifying physical reasons for the precipitation variability based upon the phase of the SOI, thus, the genesis for portions of this research project.

Precipitation Factors across the Grain-Producing Region of the U.S.

Adequate, but not excessive amounts of precipitation are essential to agronomic crops in the grain-producing region of the U.S. Excessive or scant precipitation can negatively impact yields, which can lead to a shortage of food, negatively impacting

farmers and consumers. Atmospheric scientists have recognized for years the importance of precipitation to the grain-producing region of the U.S. and many have concentrated their research in this area. Results from past and current research have shown that the bulk of warm season (April-September) precipitation across the grain-producing region is in the form of Mesoscale Convective Weather Systems (MCWS) (Tollerud and Collander 1993; Fritsch et al. 1986). Results suggest that 30% to 70% of warm season precipitation is attributed to MCWS, and during the months of June, July, and August, it may even by higher (Fritsch et al. 1986). Subsets of the MCWS are the Mesoscale Convective Complex (MCC) and Persistent Elongated Convective Systems (PECS), and are important since they are capable of producing large amounts of precipitation (Tollerud and Collander 1993).

Maddox (1980) classified MCCs by their shape, size, and temporal characteristics. He found that these systems exhibit a well-defined vertical structure in the mature stage, consisting of areas of cold downdrafts near the surface (mesohigh), which acts as a wedge to aid in the inflow of warm moist air into the system at mid-layers (700-400 mb). The mid-layers of the system exhibit a mesoscale cyclonic circulation due to latent heat release from precipitation, which produces a region of ascent. Upper-levels of the system are represented by anticyclonic flow. The vertical structure helps to produce and maintain these systems over large temporal (six hours) and spatial (> 50,000 km) dimensions. The above description on the vertical structure of the MCC is representative of the mature stage of the system, which typically occurs at approximately 0700 UTC. However, the data from this project are taken from 0000 UTC. The 0000 UTC period is more representative of the initiation and growth stage of MCCs.

MCCs typically start out as a group of disjointed convective systems in an environment of conditional instability and low-level warm air advection (Cotton et al. 1989). During the early evening hours (02 UTC), the individual convective cells begin to organize into a single system, and then track along the mean 700-500 mb flow pattern overnight (Maddox 1983). Mean tracks of MCCs are from the lee of the Rockies across east central Nebraska, southwestern and southeastern Iowa (McAnelly and Cotton 1989).

This track is along a portion of the grain-producing region of the U.S., thus, influential in warm season crop development.

Anderson and Arritt (1998) identified PECS as systems that meet the same criteria as MCCs with the exception of the shape criterion. During portions of the 1992 and 1993 warm seasons, PECS occurred more frequently than MCCs (their figures 3 a. and b.); thus, the importance of this type of convective system to the grain-producing region of the U.S. PECS, like MCCs, are nocturnal events with similar seasonal north-south shifts across the grain-producing region. Historical cataloguing of PECS events are small compared to MCCs; therefore, discussion of factors affecting precipitation variability will be in relation to the MCC from this point on. It is recognized that PECS are an important component of warm season precipitation variability and form in environments (synoptic scale ascent, and sufficient moisture) similar to MCCs.

One of the focuses of this research is to identify synoptic scale conditions that can account for the precipitation variability via segregation by Events 1 and 4 across the grain-producing region. Since MCCs account for a large portion of this variability, it is logical to identify synoptic scale conditions favorable/unfavorable for MCC development in this region.

A study by Cotton et al. (1989) focused on synoptic-scale conditions present in each of the stages of MCC development. Their study had increased temporal resolution compared to Maddox's 1983 study, but results were similar, such as the warm (cold) core nature of the system in the middle (upper) portion of the atmosphere, and the synoptic scale ascent found in the low to mid-levels of the system. While recognizing the importance of middle and upper air dynamics (especially during the 1993 warm season, refer to Anderson and Arritt 1998), such as the presence of shortwaves, results suggests that, "the primary forcing apparently is due to (1) low-level warm advection" and (2) the presence of sufficient moisture. The emphasis on low-level forcing versus upper-level forcing during the warm season appears warranted since upper-level dynamics are not as strong compared to the cold season of the year. However, Augustine and Howard (1991) describe a "vertical phasing" between the low and mid-levels of the atmosphere as an

environment conducive to MCC production through synoptic scale ascent. They do note however, that differences such as the positioning of a thermal ridge, where the low-level thermal forcing is focused, and moisture transport by the LLJ, were most pronounced in the lower levels of the atmosphere between active and inactive MCC periods in both 1986 and 1987. Since previous work has found contributions from all levels of the atmosphere in regard to MCC production, this project will analyze all such levels.

Cotton et al. (1989) will often be used as a point of reference since their work focused on warm-season MCC development and segregation by eight different stages, ranging from twelve hours before MCC occurrence, through initial and growth stages (0000 UTC), maturity, and finally three stages of termination. Two specific stages of MCC development are of interest in this project, initial and growth stages, which correspond with the temporal resolution of this project.

Using a combination of the above studies on MCCs, it was discovered that conditions conducive to initiation and growth of are as follows:

- Development near a low-level thermal gradient
- Favorable low to mid-level thermal advection and moisture present in the genesis region
- A trough and ridge at 850 mb located, respectively, over the western and eastern portion of the genesis region
- LLJ present at 850 mb
- Short-wave at 700 mb moves across the northern portion of the genesis region
- MCCs typically move along the periphery of a 500 mb ridge
- Favorable moisture content in the low to mid-levels of the atmosphere
- A weak jet streak at 200 mb is located to the north of the genesis region
- The thermodynamic environment is unstable over portions of the genesis region

A comparison between the above synoptic-scale environments of Events 1 and 4 will be analyzed for differences. It is hypothesized that the large-scale environment

conducive to the genesis of MCWS more often occur in an Event 1 than Event 4, thus, producing more precipitation across the grain-producing region of the U.S.

Portions of the above criteria are strongly tied to the low-level jet stream (LLJ) during the warm season period. The LLJ is defined as a wind maximum in the lower regions (approximately 800 m above ground) of the troposphere (Bonner 1968). Various studies have shown the importance of the LLJ to precipitation production across the nation's breadbasket. Mo et al. (1997) discovered that warm season precipitation in the central U.S. is inversely related to precipitation in the Gulf coast states and portions of the southern Plains. Like Fritsch et al. (1986) they found that dry events across the central U.S. are related to increasing geopotential heights, but they take it a step further by suggesting that the drought itself is related to the strength and position of the LLJ. Their study shows that during a drought event, such as 1988, the ITCZ (represented by negative values of OLR) moves northward to approximately 10^0-15^0 N (note that this latitudinal position is similar to the one suggested by Lau and Peng 1992). The upper-level divergence from this region moves towards the Gulf of Mexico and begins to sink in this region, thus, weakening and repositioning the LLJ away from the central U.S. During wet periods, they suggest that the LLJ is strengthened across the central U.S. by a trough found along the lee side of the Rocky Mountains. Arritt et al. (1997) took this idea a step further and categorized the magnitude of 1993 LLJs. They found that the most intense precipitation events occurred with very strong LLJs on the order of 20 m/s or greater. Their results also suggested leeside troughing at lower levels of the atmosphere (their figure 16c.) as playing a role in the strengthening of the LLJ.

The LLJ is critical to the horizontal movement of heat, moisture and vertical movement of mass by convergence. The importance of heat, moisture and vertical movement of mass is important to the development of MCWS, which, in turn, are responsible for most of the warm season precipitation across the grain-producing region of the U.S. Any change in magnitude or direction of the LLJ may affect precipitation variability, leading to variability in crop production over the region.

Atmospheric Parameters

Environmental conditions necessary for the production of precipitation and crop development depend upon the delicate balance of atmospheric conditions throughout the depth and breadth of the atmosphere. The linkage between precipitation production through the MCC and its effects on crop development has been documented in previous studies. In this section, we will discuss the role that atmospheric parameters play at each of the levels (low, mid, and upper) of the atmosphere in producing favorable/unfavorable environments for precipitation production. The atmospheric parameters, as are the precipitation and other data, are segregated by Events 1 and 4. Difference fields (Event 1 - Event 4) were constructed in cases where monthly averaging smoothed out most distinct features of the field (i.e. geopotential height fields) or atmospheric parameters exhibiting positive or negative magnitudes (i.e. divergence, convergence). It is noted that since the reanalysis data consist of monthly mean fields and composite means are performed on the data, the magnitudes will be smaller compared to other studies, as suggested by Cotton et al. 1989. Therefore, the results should be weighted more on the qualitative end, although, there is quantitative information to be gleaned from the data. The quantitative information will describe the significance of the fields by taking into account the spatial correlation in the field.

Low-Level Atmosphere Parameters

Low-level atmospheric parameters play an essential role in the production and maintenance of warm season precipitation across the grain-producing region of the U.S. The following subsections provide a description of some influencing parameters.

850 mb Wind Field

The essential feature to look for at this level is the LLJ. The LLJ can provide warm moist convergent air, supportive ingredients for the production of warm season precipitation. The LLJ typically reaches its maximum speed sometime between 0600 UTC and 0900 UTC. The monthly reanalysis data are taken from 0000 UTC, some six to nine

hours before the maximum LLJ, but since this study is focusing on an environment conducive to the initiation and growth of MCCs, this temporal resolution will suffice.

850 mb Specific Humidity

Relative humidity was the only measure of moisture directly available from the monthly reanalysis data and since relative humidity is temperature dependent, it will not serve as a stable indication of the change in moisture alone. Therefore, specific humidity was derived from an integrated form of the Clausius-Clapeyron equation (Stull 1995) and the equation of state applied to water vapor (Fleagle and Businger 1980). Once saturated vapor pressure was calculated from the Clausius-Clapeyron equation, it was used to derive the vapor pressure from the known value of relative humidity. The final step consisted of using the derived vapor pressure value in the equation of state to solve for specific humidity. Specific humidity is a quantity that is not temperature dependent, therefore, a more stable parameter to represent moisture available to a system. Cotton et al. 1989 used the 850 mb mixing ratio in their study to quantify moisture availability to the MCC. It is noted that other studies have used columnar precipitable water (Mo et al. 1997) or vertically integrated water (Bell and Janowiak 1995) as a means to quantify moisture available to the system, but this study analyzes moisture at a single level, therefore choosing to use specific humidity. It is also recognized that 850 mb may not be the optimal level for the analysis of low-level moisture over portions of the Western Plains and Rocky Mountain region since this is often the location of the surface and within the planetary boundary layer.

850 mb Temperature Advection

Low-level temperature advection is an ingredient that can provide buoyancy to the air, thus providing a lifting mechanism to produce precipitation. The omega equation expresses vertical motion as a function of two terms, differential vorticity advection and thickness advection (the thickness of a layer is analogous to its temperature (Holton 1979)). Assuming equivalent magnitudes of contribution from both terms in the omega

equation, then a Q-vector analysis would be advisable since the two terms often cancel each other out (Hoskins et al. 1978). Since this work is focused on warm season events, the contributions from both terms are not equivalent. Differential vorticity advection often exhibits a weaker magnitude during this season. As discussed in previous work by Cotton et al. (1989), Augustine and Howard (1991), and Maddox (1983), most of the forcing for the development of MCCs is due to low-level thermal advection. 850 mb thermal advection was computed using a centered differencing scheme.

850 mb Convergence

Convergence (as defined by the continuity equation) at this level provides an additional lifting mechanism to warm moist air. The LLJ plays a significant role in convergence in the area of initiation and growth of MCCs.

Middle to Upper Atmosphere Parameters

While the atmospheric dynamics are typically weaker during the warm season, they can still play an active role in the production and maintenance of precipitation. The following paragraphs provide a description of some middle-upper atmospheric influencing parameters.

500 mb Geopotential Heights

A general rule of forecasting is that surface systems tend to move parallel to the 500 mb isohypse pattern (Wallace and Hobbs 1977). Surface temperature and precipitation patterns can also be inferred from patterns of 500 mb troughs and ridges. Recall that Augustine and Howard (1991) noted that MCCs tend to propagate along the periphery of ridges at this level.

200 mb Divergence

According to Dines Compensation, lower atmospheric convergence balanced by upper atmospheric divergence leads to large-scale ascension of air. Upper atmospheric

divergence is not common, since generally, the Midwest experiences subsidence during the warm season (Bell and Janowiak 1995). This is due, in part, to the positioning of the upper level jet stream over the northern U.S. The Midwestern portion of the country is typically located in a convergent part of the jet stream, which leads to large-scale descent. It will be shown later that upper atmospheric convergence tends to weaken during some years. Also, there is evidence of optimal phasing between lower level convergence and upper level divergence during portions of the warm season.

200 mb Winds (Jet Stream)

The warm season positioning of the jet stream can play an important role in determining spatial temperature and precipitation patterns across the grain-producing region of the U.S. The warm season positioning of the jet stream is usually confined to Canada, but on occasion as in 1993, the jet stream may be located as far south as 43^0 N latitude. This southward positioning of the jet stream reduced temperatures and increased precipitation amounts as compared to the climatological mean during portions of the 1993 warm season. Cotton et al. (1989) noted that most MCCs tended to be located in the right rear quadrant of a jet streak, which is a favorable position for producing (maintaining) upward motion.

RESULTS AND DISCUSSION

Hypothesis:

Previous work by Carlson et al. (1996) has identified a statistical relationship between corn yields and climate (precipitation and temperature) when segregated by the phase of the SOI. The purpose of this project is to explain their results in terms of physical and statistical connections related to atmospheric parameters. In order to do this, data associated with this project has been segregated by Event 1 (Low Phase of the SOI coupled with the Warm Phase of the PDO) and Event 4 (High Phase of the SOI coupled with the Cold Phase of the PDO). The segregation by these particular couplings appears to separate the positive yield years (0 to 10% above trend) from the negative yield years (1 to 10% below trend). Therefore, it is hypothesized that parameters in the atmosphere that are conducive to precipitation production occur in Event 1 years, while Event 4 years depict unfavorable parameters for precipitation production across the grain-producing region of the U.S. It is also hypothesized that some of these fields of atmospheric parameters will show spatially significant statistical differences.

Yield Patterns across the Grain-Producing Region of the U.S.

Iowa corn yields from the last century have exhibited interannual variability (Figure 1). Corn yield variability is a function of many variables as discussed in the introduction section. However, corn yield variability during the last half of the century has been mainly a function of climate variability. In the grain-producing region of the U.S., the last 15 years have exhibited extreme variability in the form of the 1988 drought and 1993 floods. Crop physiology is closely tied to both temperature and precipitation; therefore, variability in these parameters can have a significant effect on yields. Climate variability in itself is a function of many aspects of the physical world, such as the interplay between the ocean and atmosphere (ENSO/LNSO, PDO). A more complete

understanding of observational effects based upon this coupling should elucidate climatic trends such as precipitation, which, in turn, can be used to forecast crop yield tendencies. Carlson et al. (1996) discovered a relationship between corn yields and the phase of the SOI. Note that during the last thirty years crop yields that were 10% above trend tended to occur in years associated with El Nino, while the corresponding signal of below 10% yield trend was just as robust with La Nina years (Figure 11).

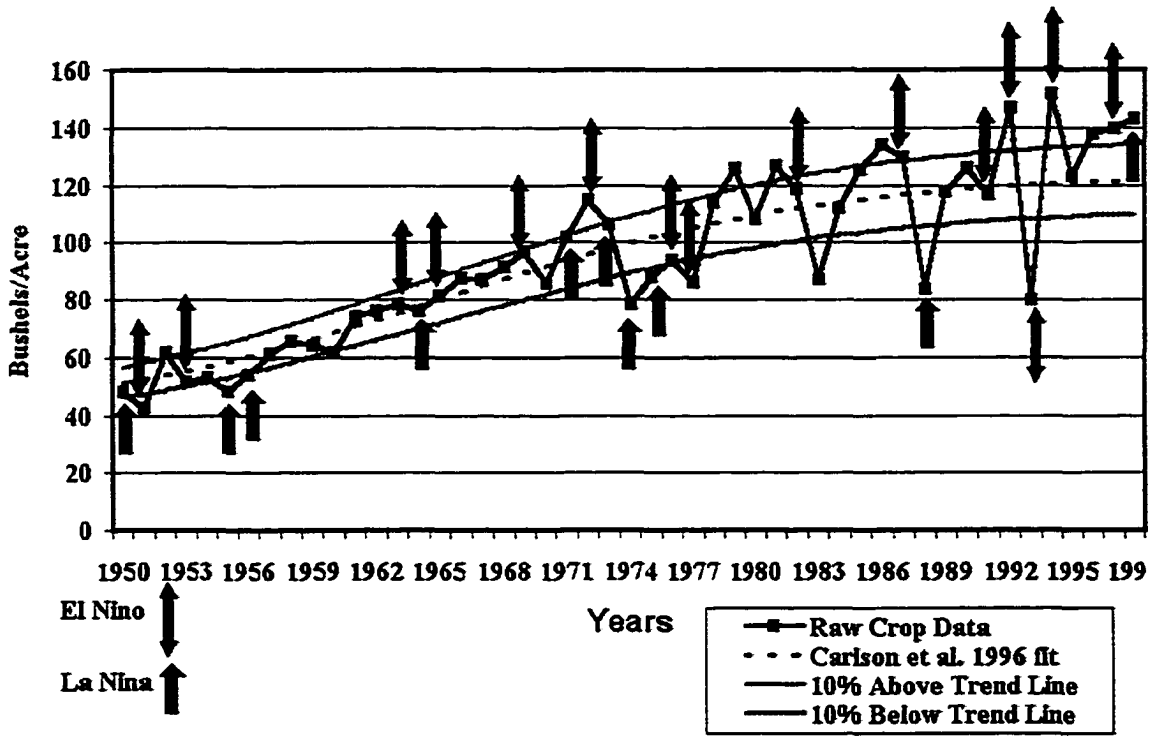

Figure 11. Iowa Corn Yields for 1900-1998

Their conclusions were that cool-wet growing seasons tended to be associated with years exhibiting SOI values < 0.8 (El Nino), but warm-dry growing seasons were associated with years of SOI values > 0.8 (La Nina). As has been shown by previous research (observational and modeling) tropical-extratropical signals are weaker during the growing season period, but coupling the tropical Pacific with the extratropical Pacific region produces interesting results in corn yields across the grain-producing region of the

U.S. (Figure 5). Notice that in general Events 1 and 3 show yields above trend, while Events 2 and 4 depict yields below trend. Kansas corn yields do not follow the general overall trend in the region during Events 2 and 3. Assuming that climate is the main limiting factor with corn yields it may be possible to forecast yield trends based on the above coupling of ENSO/LNSO and PDO. Carlson et al. (1996) has shown statistically significant evidence that above trend corn yields correlate positively with above median precipitation during the warm season.

To identify tendencies with the distribution of yields by segregation into Events 1 and 4, the hypergeometric distribution is used. The hypergeometric distribution is used to calculate probabilities that the observed data will fall into a particular category (Walpole and Myers 1989). Mauget and Upchurch (1998) used the hypergeometric distribution to identify extreme yield events across portions of the grain-producing region and found a coherent signal associated with ENSO/LNSO. A similar analysis on the corn yields found in Table 2 presents some interesting results. It appears that Event 4 years negatively impact corn yields across portions of the grain-producing region. This is in very good agreement with crop model simulations which indicated that LNSO events tend to negatively impact maize yields more than ENSO events help them (Phillips et al. 1998). Iowa, Kansas, Michigan, Minnesota, Nebraska, and Wisconsin are states in which corn yields are in the lower third of the distribution during Event 4 years. This may be interpreted as below trend corn yields during Event 4 years. Conversely, only two states, Indiana and North Dakota, show statistically significant corn yields in the upper third of the distribution during Event 1 years. However, many of the grain-producing states, such as Illinois, Minnesota, Ohio, and Wisconsin, show a statistically moderate signal (p-value = 0.77) during Event 1 years. Note that it would take only one additional case in the upper third of the Event 1 distribution to move the signal from moderate to strong in Illinois, Minnesota, Ohio, and Wisconsin. While these results are in general agreement with Carlson et al. (1996) showing a warm season yield signal when segregating by SOI and PDO, the signal is weaker than their negative SOI segregation. Part of this may be due to differing sample sizes (their data were from 1900-1994, this study is from 1950-1998), and

Table 2. Distribution of Corn Yields Segregated by Events 1 and 4.[1]

State	Corn Yields	Lower 1/3	Middle 1/3	Upper 1/3	P-Value
Illinois Event 1	8	2	2	4	0.77 ¶
Indiana Event 1	8	2	1	5	0.94 §
Iowa Event 1	8	3	2	3	0.48
Kansas Event 1	8	1	6	1	0.03
Michigan Event 1	8	1	5	2	0.18
Minnesota Event 1	8	2	2	4	0.77 ¶
Missouri Event 1	8	2	3	3	0.48
Nebraska Event 1	8	2	4	2	0.18
North Dakota Event 1	8	2	1	5	0.94 §
Ohio Event 1	8	2	2	4	0.77 ¶
South Dakota Event 1	8	2	3	3	0.48
Wisconsin Event 1	8	2	2	4	0.77 ¶
Illinois Event 4	8	3	3	2	0.48
Indiana Event 4	8	4	3	1	0.77 ¶
Iowa Event 4	8	5	1	2	0.94 §
Kansas Event 4	8	5	0	3	0.94 §
Michigan Event 4	8	6	2	0	0.99 §
Minnesota Event 4	8	5	1	2	0.94 §
Missouri Event 4	8	4	1	3	0.77 ¶
Nebraska Event 4	8	5	2	1	0.94 §
North Dakota Event 4	8	3	4	1	0.48
Ohio Event 4	8	4	4	0	0.77 ¶
South Dakota Event 4	8	4	3	1	0.77 ¶
Wisconsin Event 4	8	6	0	2	0.99 §

[1] ¶, § indicates a statistically moderate and strong signal, respectively.

the segregation of the data by SOI alone versus a coupling of SOI and PDO. Still, the similarity of results between the two studies is encouraging.

Since Event 1 years depict above trend corn yields compared to Event 4 years (Figure 12), and according to Table 2 there is a statistically significant separation of the events into lower and upper distributions, it is hypothesized that Event 1 years have significantly more precipitation across the grain-belt versus Event 4 years. We assume that precipitation is the limiting factor based upon the previous discussion relating to crop physiology. To test this hypothesis an analysis of the monthly state-division precipitation values follows. It is noted that ambient temperatures play a role in crop development but are not the focus in this study, although, inferences will be made about temperature when presenting the analysis of the atmospheric parameters.

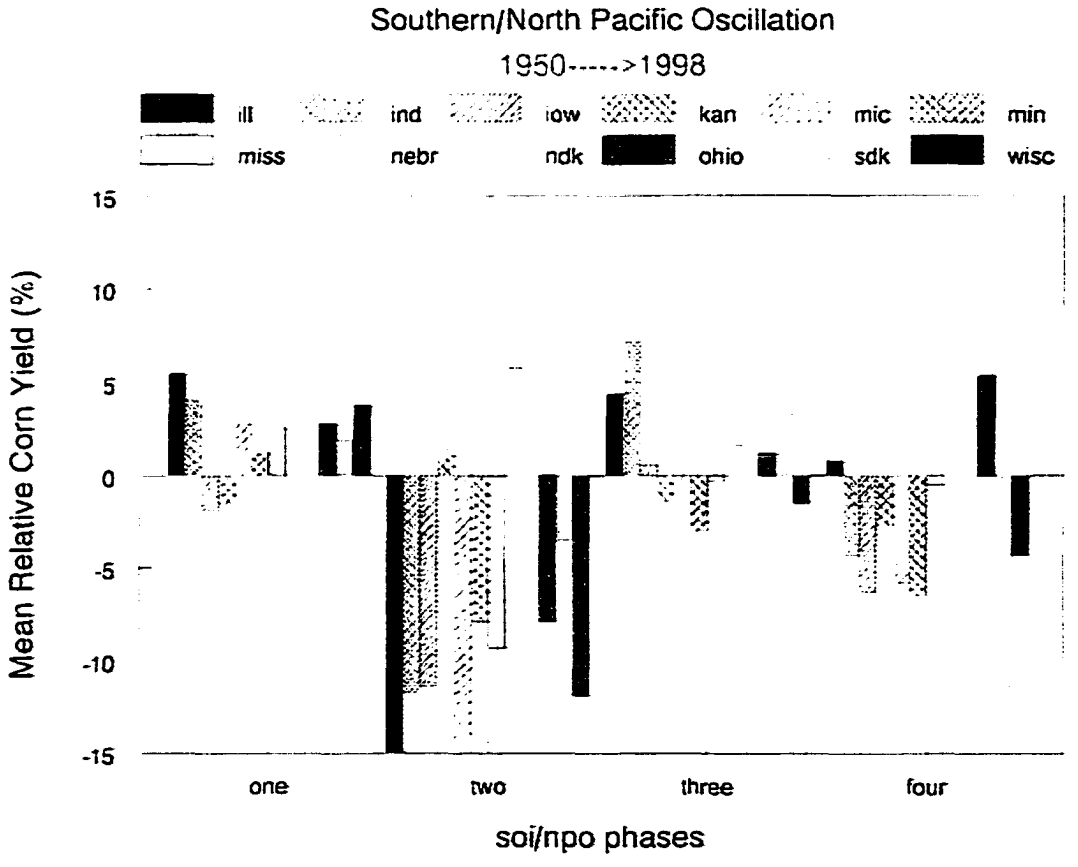

Figure 12. Corn Yields segregated by SOI and PDO (1950-1998). On the x-axis "one" represents Event 1 (Table 1), "two" represents Event 2 (Table 1), etc.

Precipitation Patterns across the Grain-Producing Region of the U.S.

Precipitation patterns across the grain-producing region of the U.S. exhibit spatial cohesiveness during most months of the warm season. The exception to this occurs in May and June. This is not unexpected since these are transitional months in regards to both dynamics and thermodynamics of the atmosphere. The jet stream has moved somewhat poleward during these two months, and the overall wind and temperature gradients begin to weaken into their warm season pattern.

During a portion of the preseason (April) crop phase, significant precipitation differences (Event 1 - Event 4) occur mainly across portions of the central Plains of Kansas, Missouri, and Iowa (Figure 13). Although Figures 13-16 depict the continental U.S., the analysis was limited to the grain-producing region of the U.S. (Figure 10).

The seasonal portion (July, August, and September) of the crop phase exhibits a well-developed spatial pattern. During July, portions of the northern Plains (Dakotas,

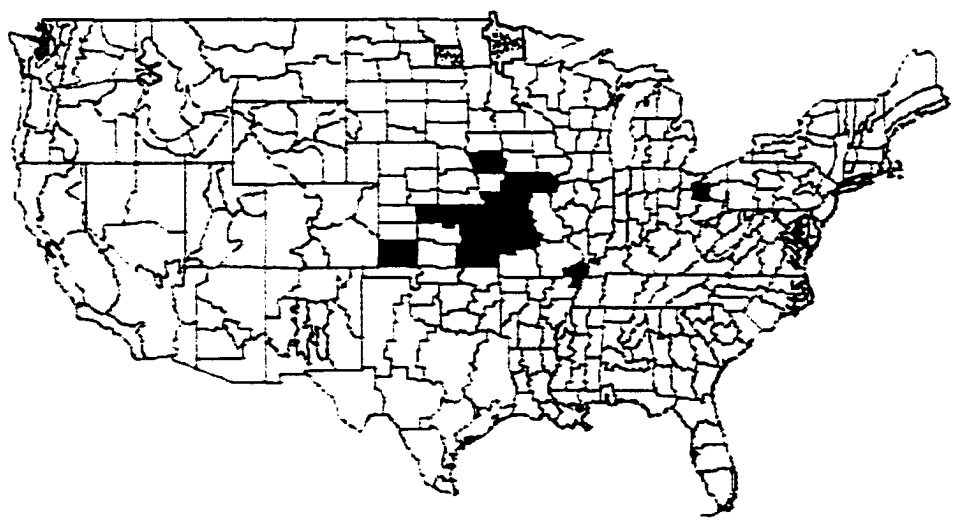

Figure 13. April precipitation differences between Event 1 and Event 4 significant at the 15% level (p-value at 0.15). Positive (negative) differences are shaded solid (spots). Magnitudes of the precipitation differences can be referenced in Appendix D.

Minnesota, Wisconsin, and northeastern Iowa) show the most significant precipitation differences between Event 1 and 4 years (Figure 14).

In August, the spatial pattern of precipitation differences moves southward to Nebraska, Kansas, Iowa, and Illinois (Figure 15). The spatial pattern of precipitation differences in September moves back into portions of Wisconsin, Minnesota, and South Dakota (Figure 16). The following section will elaborate on the precipitation differences across portions of the grain-producing region of the U.S. for April. A description of July-September precipitation characteristics, segregated by Event 1 and 4 years, along with state and division, are provided in Appendix C.

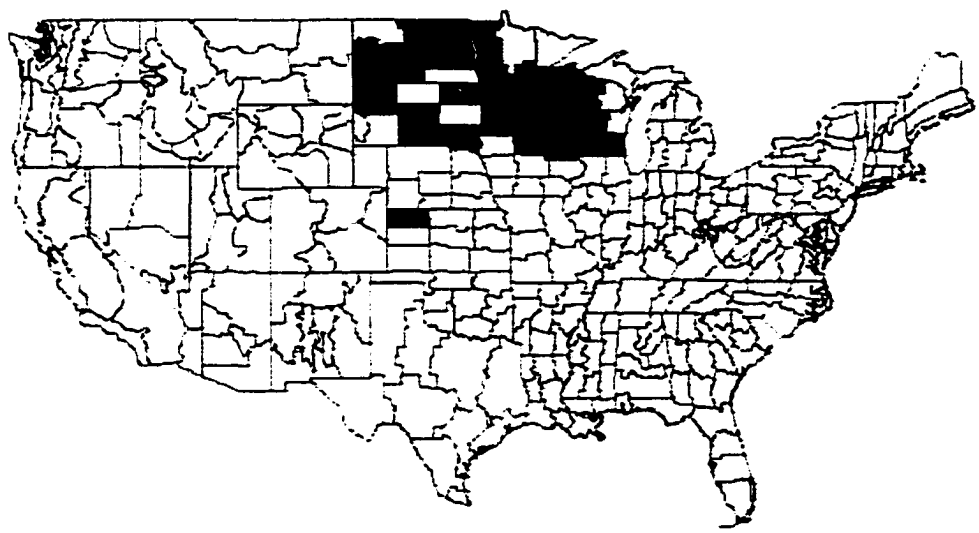

Figure 14. July precipitation differences between Event 1 and Event 4 significant at the 15% level (p-value at 0.15). Positive (negative) differences are shaded solid (spots). Magnitudes of the precipitation differences can be referenced in Appendix D.

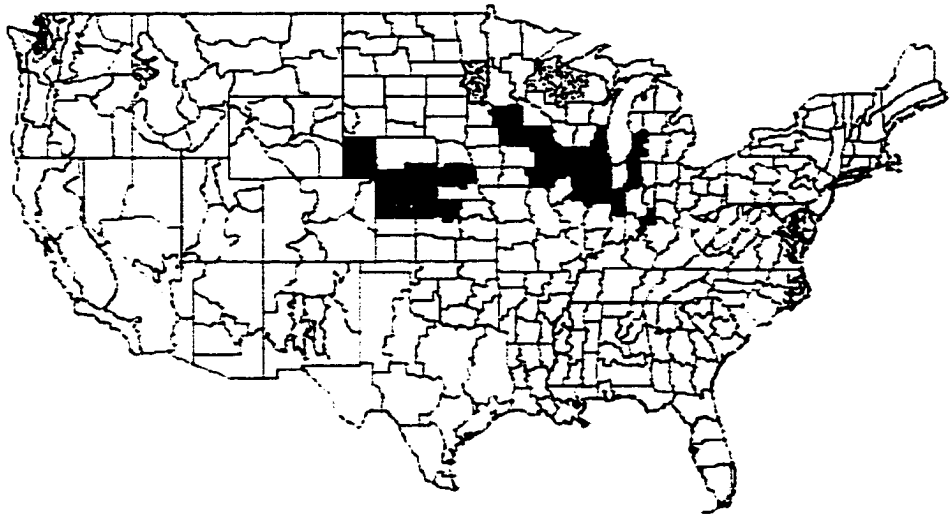

Figure 15. August precipitation differences between Event 1 and Event 4 significant at the 15% level (p-value at 0.15). Positive (negative) differences are shaded solid (spots). Magnitudes of the precipitation differences can be referenced in Appendix D.

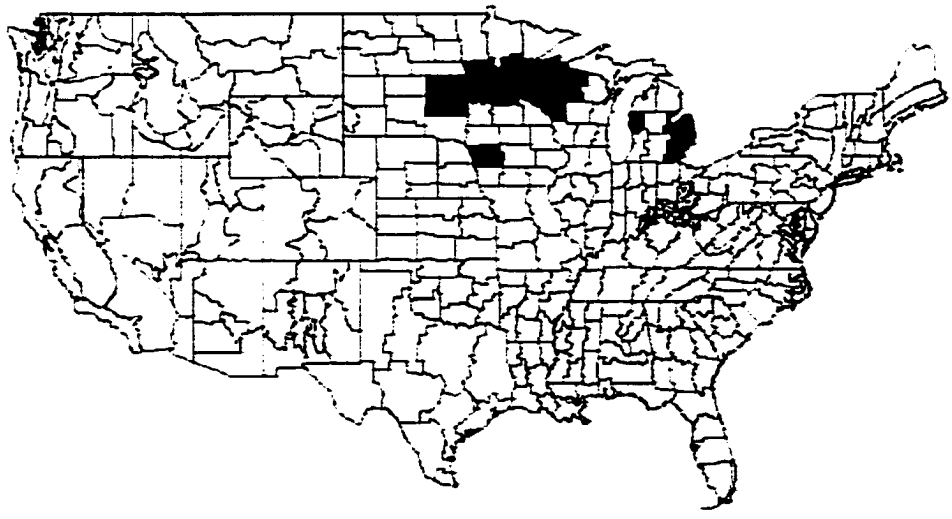

Figure 16. September precipitation differences between Event 1 and Event 4 significant at the 15% level (p-value at 0.15). Positive (negative) differences are shaded solid (spots). Magnitudes of the precipitation differences can be referenced in Appendix D.

April Precipitation

Kansas- Five of the nine state divisions show significant median precipitation differences between Events 1 and 4 at the 15% level (Figure 17). Event 1 median precipitation values are larger in magnitude than Event 4, with the exception of state division 4. Differences range from 4 mm to 52 mm, with the largest differences (> 30 mm) located in state divisions 3, 6, 8, and 9.

Missouri- Two of the six state divisions show significant median precipitation differences between Events 1 and 4 at the 15% level (Figure 18). Event 1 median precipitation values are larger in magnitude than Event 4. Differences range from 2 mm to 69 mm, with the largest differences (> 30 mm) located in state divisions 1, 3, and 6.

Iowa- Three of the nine state divisions show significant median precipitation differences between Events 1 and 4 at the 15% level (Figure 19). Event 1 median precipitation values are larger in magnitude than Event 4, with the exception of state division 3. Differences range from 0 mm to 30 mm, with the largest differences located in state divisions 1, 4, and 8.

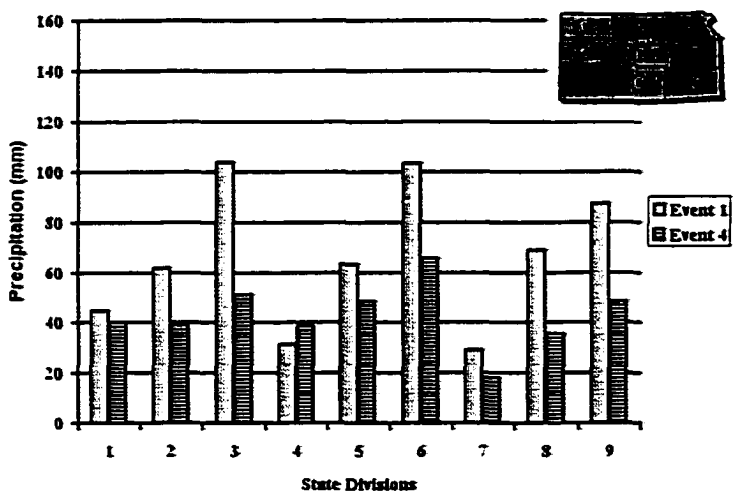

Figure 17. April Kansas median precipitation by Events 1 and 4. Significance at the 15% level (p-value at 0.15) is denoted by shaded state divisions in upper right portion of graph.

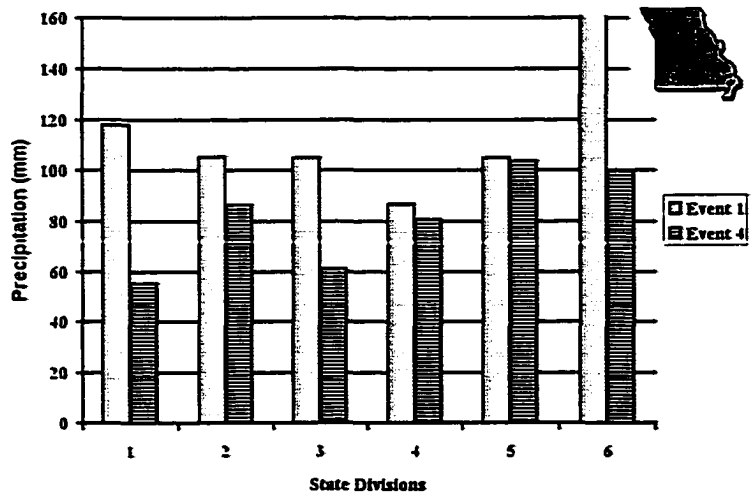

Figure 18. April Missouri median precipitation by Events 1 and 4. Significance at the 15% level (p-value at 0.15) is denoted by shaded state divisions in upper right portion of graph.

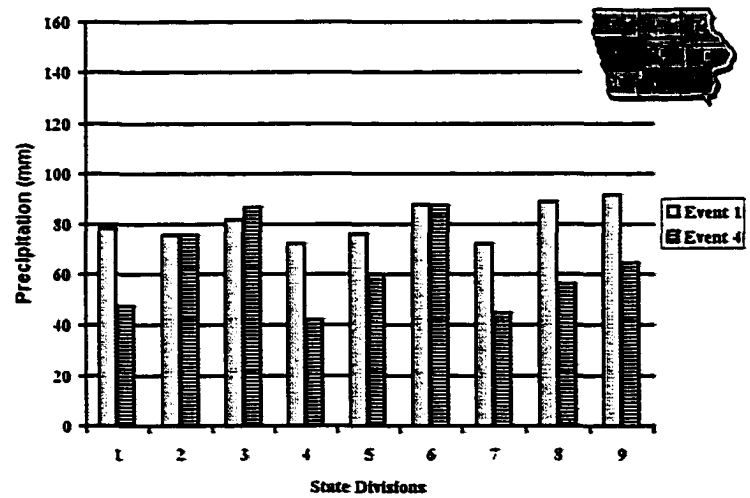

Figure 19. April Iowa median precipitation by Events 1 and 4. Significance at the 15% level (p-value at 0.15) is denoted by shaded state divisions in upper right portion of graph.

Summary of Warm Season Precipitation Events

To summarize, significant differences between Event 1 and 4 precipitation events occur throughout the warm season with the most spatially coherent signals occurring in April and July-September. Precipitation amounts are higher during an Event 1 compared to Event 4 for most of the warm season, the exception being September where Ohio and portions of South Dakota receive more rainfall during Event 4. Magnitude differences range from 0 mm to 80 mm over portions of the grain-producing region of the U.S.

During April the strongest precipitation signal is over portions of the central Plains states such as Kansas, Missouri, and Iowa (Figure 13). In July, the signal moves into the northern Plains states of the Dakotas, Minnesota, and Wisconsin (Figure 14). August finds the strongest signal moving back into the central and eastern Plains states of Nebraska, Kansas, Iowa, Illinois, and Indiana (Figure 15). In September, the signal fractures into two regions, the northern Plains states of South Dakota, Minnesota, and Wisconsin, and the Ohio Valley region of Ohio and Michigan (Figure 16). It is interesting to note that only Ohio exhibits a statistically significant precipitation difference with Event 4 precipitation being greater than Event 1 precipitation during September.

It is apparent that there are coherent precipitation signals throughout portions of the grain-producing region of the U.S. during Event 1 and 4 years. It is also known that MCCs play a significant role in precipitation production and that the genesis and initiation of these systems are dependent upon factors present in the atmosphere. Therefore, a segregation of these atmospheric parameters by Events 1 and 4 is performed to account, in part, for the variation in precipitation and yields across the grain-producing regions of the U.S.

Atmospheric Patterns across the Grain-Producing Region of the U.S.

Precipitation production is a function of many atmospheric variables. For this project, two factors will be under consideration: (1) sufficient atmospheric moisture and (2) atmospheric lifting. Specific humidity was the variable used for the measure of

moisture in the atmosphere, and low-level convergence, upper-level divergence, and thermal advection were used to represent lifting. Low-level convergence and thermal advection are partly a function of the position and strength of the LLJ. Upper-level divergence is a function of the positioning of the jet stream; the jet stream may also imply synoptic-scale storm tracks.

These atmospheric parameters, along with others, are segregated (by Events 1 and 4) and analyzed in an attempt to account for a portion of the interannual precipitation variability and, in turn, yield variability. The discussion will center on both the spatial pattern of precipitation during the warm season and the positioning and strength of the atmospheric parameters. Recall that July and August showed preferred patterns of precipitation across portions of the northern and central Plains, respectively. The results presented below will describe the relationship between the spatial patterns of atmospheric parameters and precipitation across portions of the grain belt.

April Atmospheric Parameters

In most of the grain belt states, April is the month preceding planting of crops. Excessive preseason precipitation at this time can delay or, in severe cases, eliminate planting. Conversely, a deficit in preseason precipitation can create a problem in that the subsurface soil moisture profile will not have a buffer against a normal or drier than normal July and August. Both above scenarios underscore the importance of balanced preseason precipitation. One only needs to look at recent history (April 1999) for an example of an excessive preseason moisture regime. In 1999 excessive preseason precipitation waterlogged many farms which led to a delay in planting in some sections of the grain belt. While corn yields were above trend in Iowa during 1999, other years, such as 1993, which exhibited excessive precipitation from preseason through postseason did not fare so well (37% below yield trend in Iowa).

Systems that produce preseason precipitation across the grain belt in April are typically synoptic in scale. Synoptic scale systems in April can produce both stratiform

and convective type precipitation. Stratiform type precipitation often occurs with synoptic scale frontal systems; whereas, convective type precipitation is often a product of mesoscale processes such as the MCC. MCCs often initiate along thermal gradients (synoptic scale frontal systems) to produce precipitation across the grain-producing region of the U.S. (Maddox 1983). An analysis of the spatial distribution of precipitation differences across regions of the breadbasket and the atmospheric parameters responsible for their development are discussed below.

Figure 13 shows that most of the precipitation differences between Events 1 and 4 are found in the central Plains states of Kansas, Missouri, and Iowa (hereafter referred to as the KMI region). There are other state divisions outside this region with precipitation differences, but spatially they are incoherent compared to the central Plains.

The April KMI region is favorable for increased precipitation in an Event 1 year. Iowa experienced a median increase of 27.3 mm in an Event 1 year versus Event 4. Kansas' median increase is 23.1 mm, while Missouri shows a median increase of 31.6 mm. This increase may be due, in part, to favorable atmospheric parameters, which are described in the following paragraphs.

As discussed earlier, low-level thermal advection, which can be used to infer upward motion, is an important parameter in the initiation of MCCs. Warm air advection is present across the grain-producing region of the U.S. throughout the warm season, but with differing magnitudes. During an April Event 1 year the maximum warm air advection pattern is centered to the south of the KMI region (Figure 20). In an Event 4 year the center of the warm air advection is located along and south of the KMI region (Figure 21). A maximum in the difference fields of thermal advection is centered over the KMI region with a stronger magnitude during Event 4 years (Figure 22); a result that is inconsistent with the precipitation field over the KMI region (stronger warm air advection implies stronger buoyancy).

The April 200 mb wind field pattern over the KMI region shows the presence of a weaker jet stream during an Event 1 year (Figure 23). This is due, in part, to the southward displacement of the jet stream over the Gulf of Mexico during an Event 1 year (Figure 24).

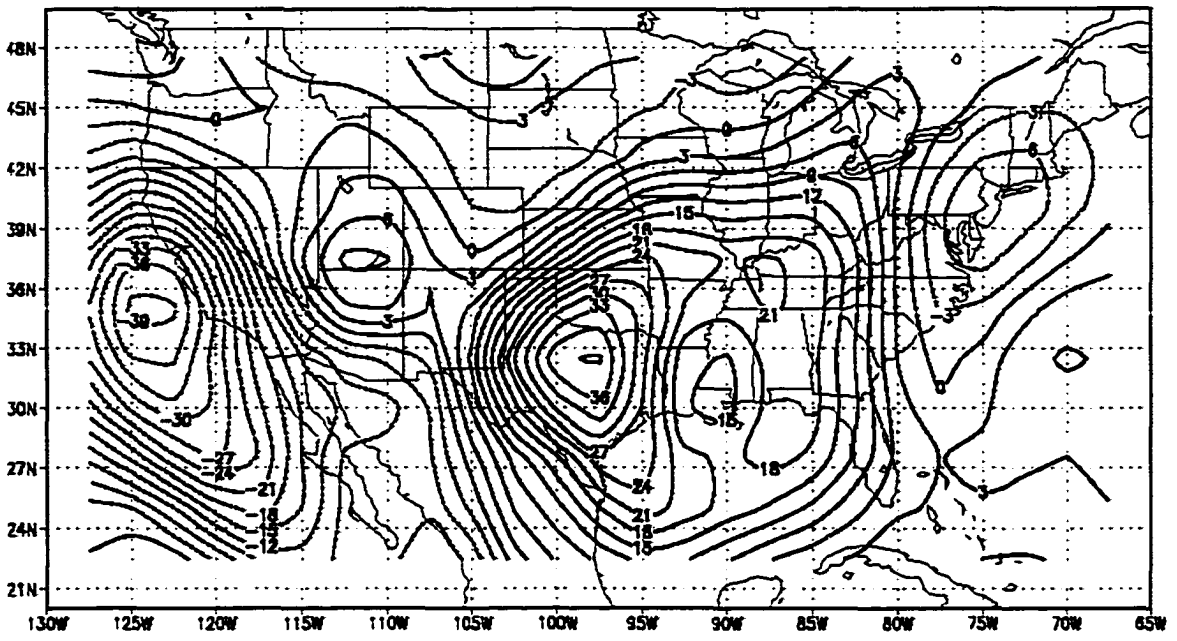

Figure 20. April 850 mb Temperature Advection for Event 1 Years. Contours are $3x10^{-6}$ K s^{-1}

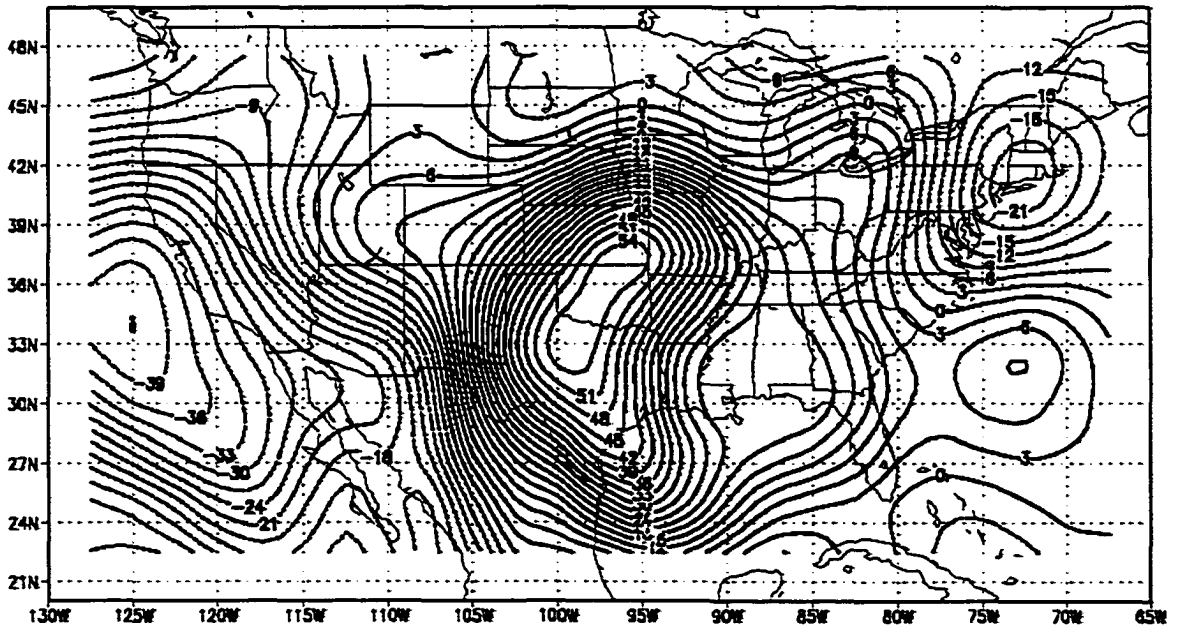

Figure 21. April 850 mb Temperature Advection for Event 4 Years. Contours are $3x10^{-6}$ K s^{-1}

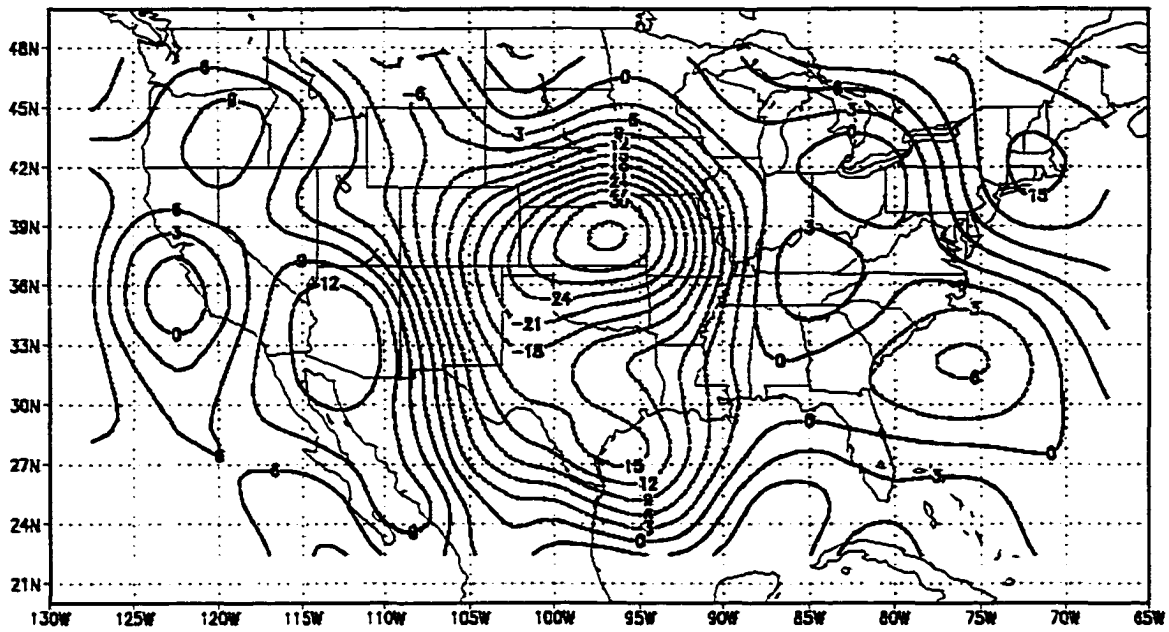

Figure 22. April 850 mb Temperature Advection for Event 1 - Event 4 Years. Contours are $3x10^{-6}$ K s^{-1}

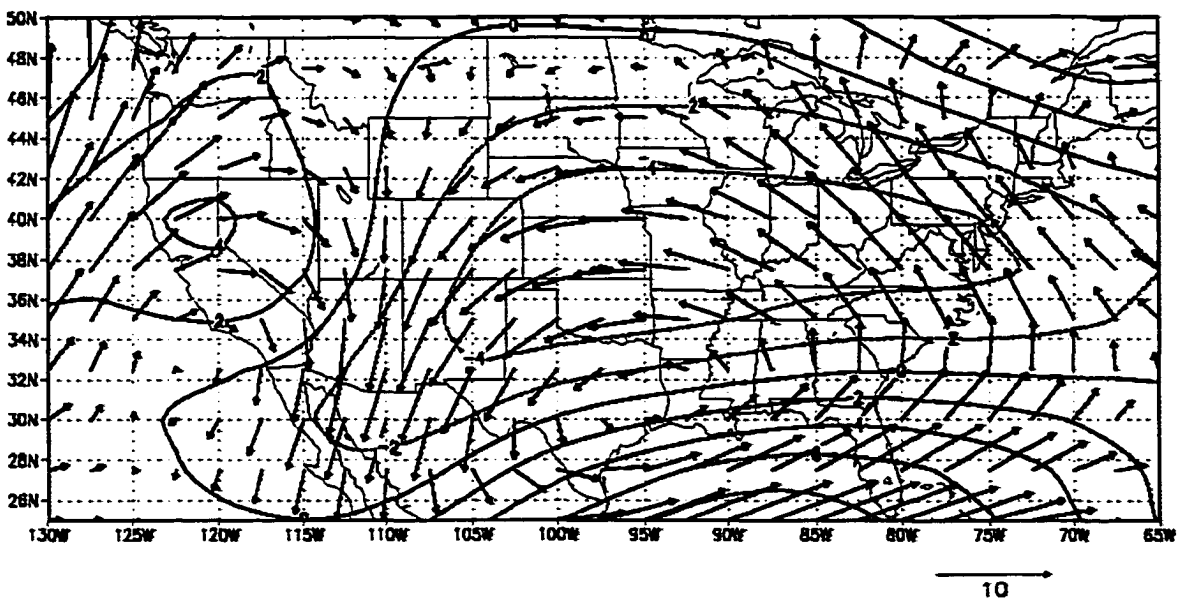

Figure 23. April 200 mb Winds for Event 1 - Event 4 Years. Contours are 2 m s^{-1}

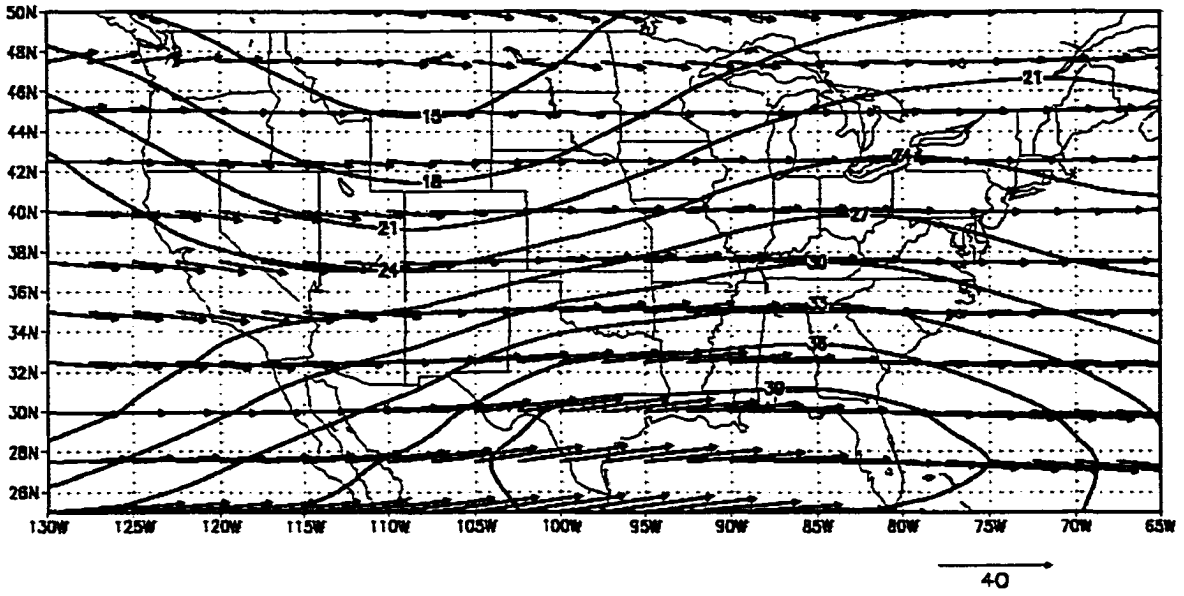

Figure 24. April 200 mb Winds for Event 1 Years. Contours are 2 m s^{-1}

Previous studies have shown the presence of an amplified jet stream across the southern U.S. during ENSO events (Rasmusson and Wallace 1983). Since this study uses a partitioning of events by ENSO (LNSO)/PDO, there is some consistency present with the previous studies mentioned above; but again, physically inconsistent (weaker wind field in Event 4 years) with the precipitation field over the KMI region (Figure 13).

There is a large spatial pattern of 200 mb convergence present in both Event 1 (Figure 25) and Event 4 (Figure 26) years. The difference field shows weaker values of convergence (5-40x10^{-7} s^{-1}) over the KMI region during an Event 1 compared to an Event 4 year (Figure 27). While large-scale descent is present at upper levels, it is of weaker magnitude during an Event 1 year, thus, a slightly less inhibiting environment for large-scale upward motion.

The second portion of Dines Compensation is the lower-level convergence pattern. The KMI region is under an area of lower-level convergence during both Event 1 (Figure 28) and Event 4 years (Figure 29). It is interesting to note that during an Event 1 year the center of lower-level convergence is located at approximately 36^0 N and 100^0 W (Figure 42), this location is equatorward of its position during an Event 4 year (Figure 29).

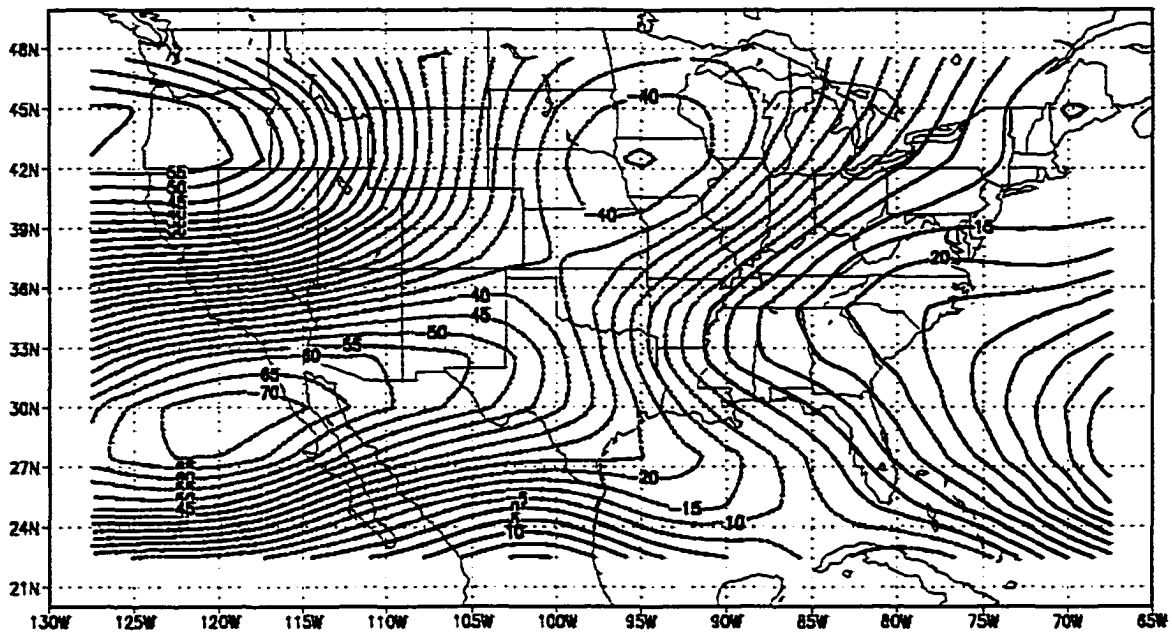

Figure 25. Event 1 April 200 mb Divergence. Contours are $5x10^{-7}$ s^{-1}

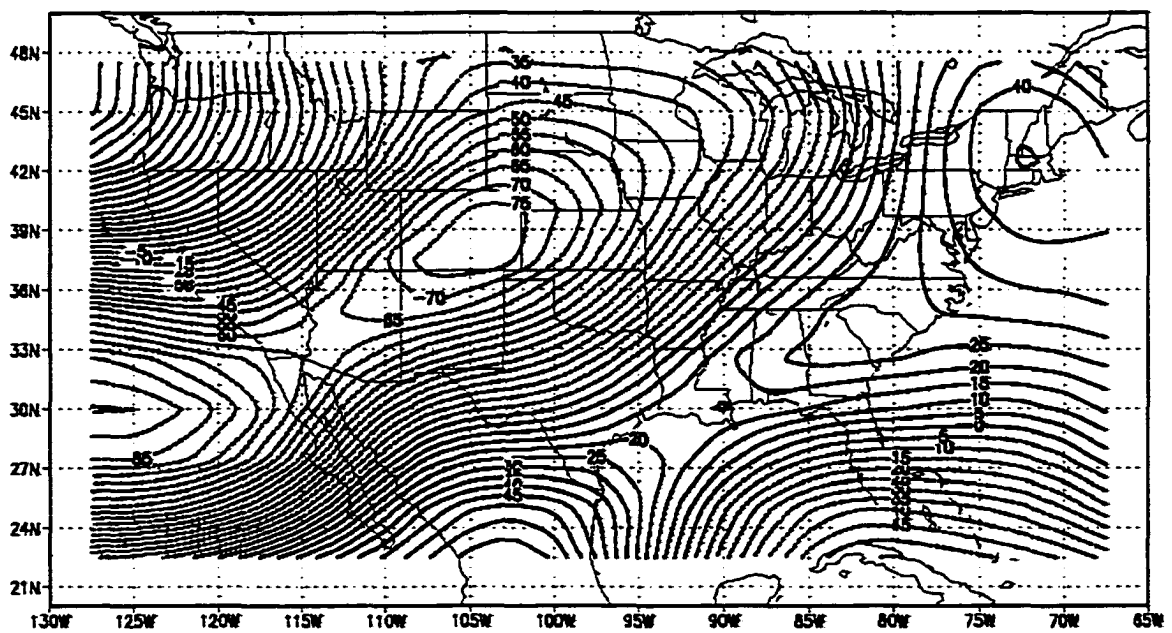

Figure 26. Event 4 April 200 mb Divergence. Contours are $5x10^{-7}$ s^{-1}

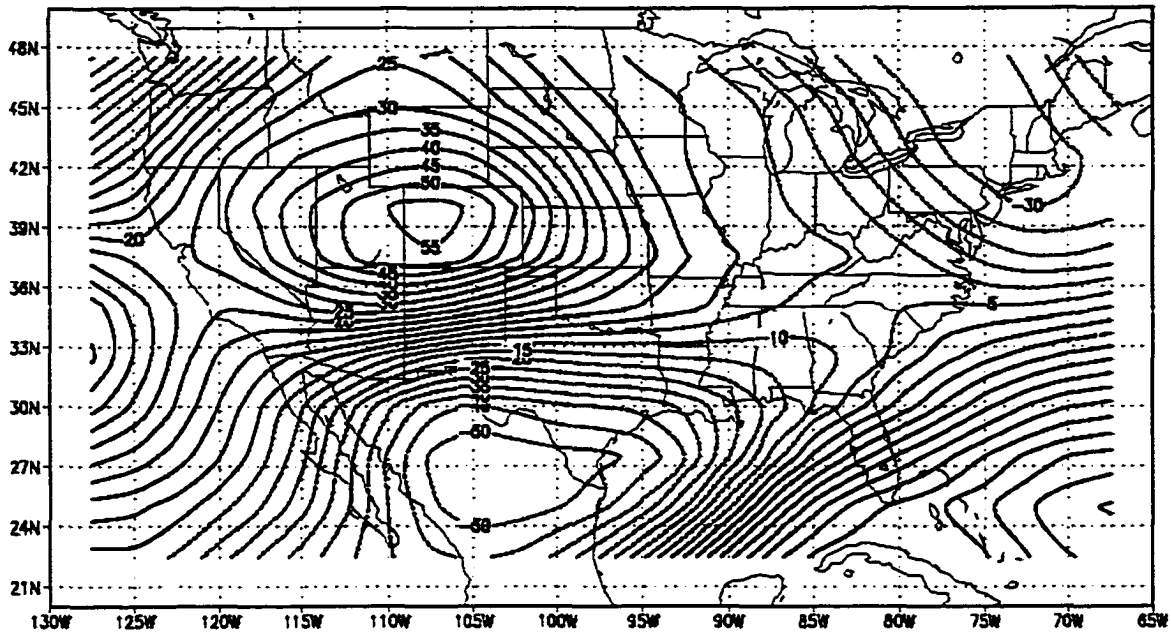

Figure 27. April 200 mb Divergence for Event 1 - Event 4 Years. Contours are $5x10^{-7}$ s^{-1}

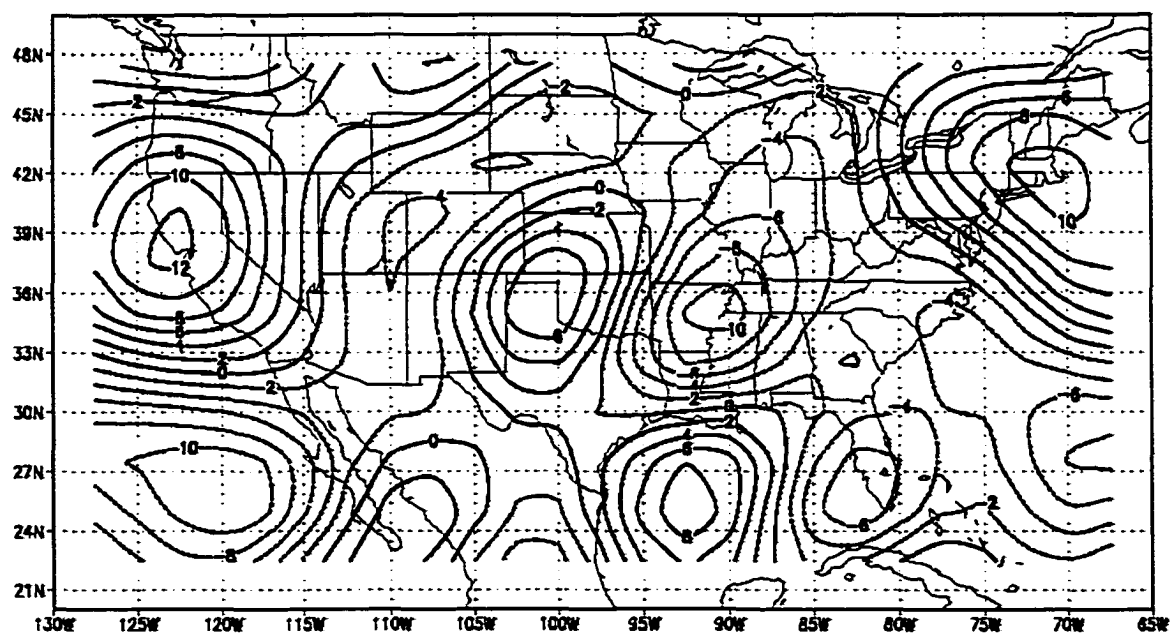

Figure 28. April 850 mb Convergence for Event 1 Years. Contours are $2x10^{-7}$ s^{-1}

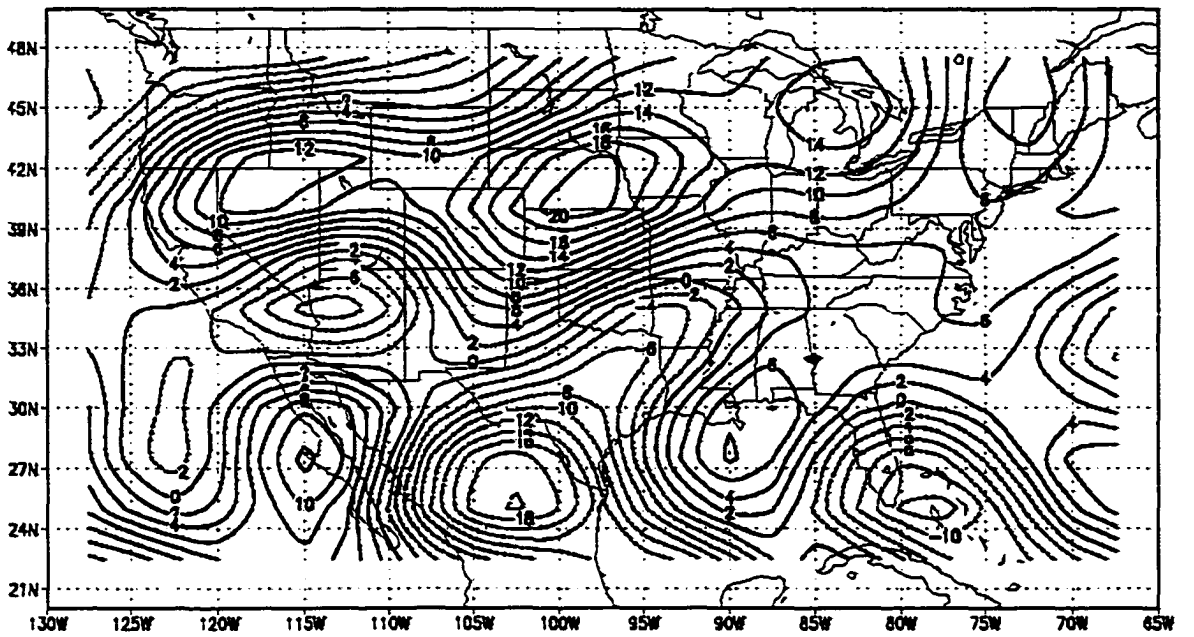

Figure 29. April 850 mb Convergence for Event 4 Years. Contours are $2x10^{-7}$ s^{-1}

However, the convergence pattern is weaker during Event 1 years as indicated by the difference field in Figure 30. Part of the decrease in strength of the convergence pattern during an Event 1 year may be related to the strength of the LLJ. Figure 31 shows that the magnitude of the LLJ is weaker over the KMI region in an Event 1 year compared to Event 4.

If precipitation production were simply a product of large scale lifting, then one could infer that precipitation magnitudes should be larger in an Event 4 compared to Event 1; this, however, is not the case. Precipitation production is also dependent on the amount of moisture available.

The next parameter, specific humidity, shows excess low-level moisture present throughout a large portion of the continental U.S. during an Event 1 year (Figure 32), the only exception is in Texas. The KMI region shows values ranging from 0.3 to 0.5 g kg^{-1} in excess during an Event 1 year, with magnitudes decreasing both north and south of the KMI region. It is helpful to examine the magnitudes of specific humidity in terms of dewpoint temperature, which is also an indicator of moisture. To convert from specific

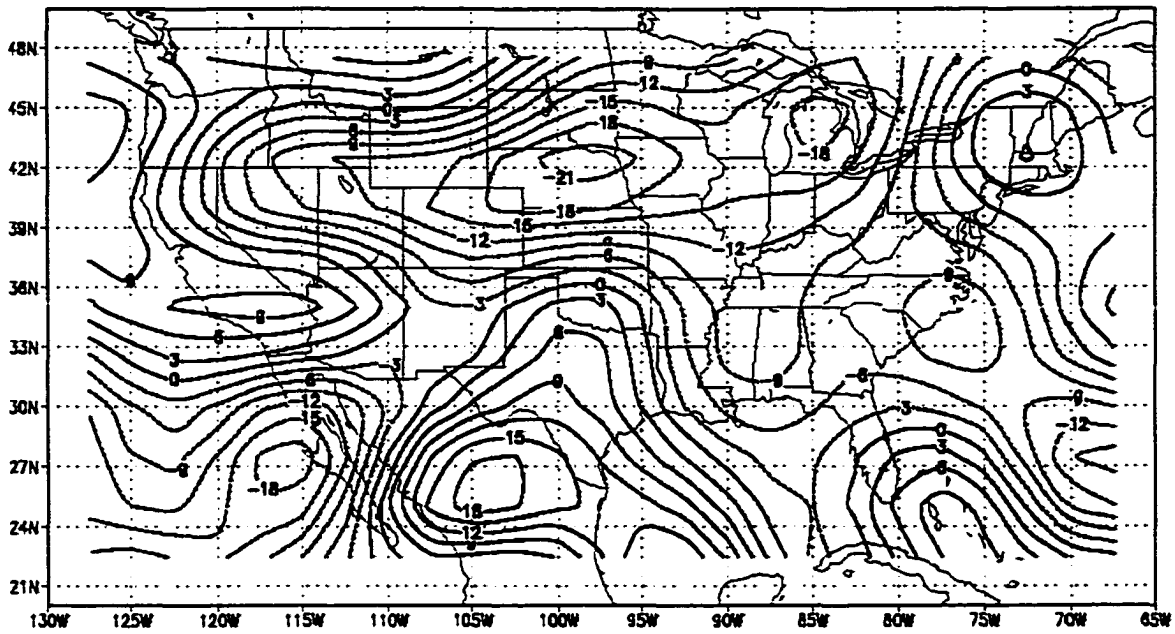

Figure 30. April 850 mb Convergence for Event 1 - Event 4 Years. Contours are $3x10^{-7}$ s^{-1}

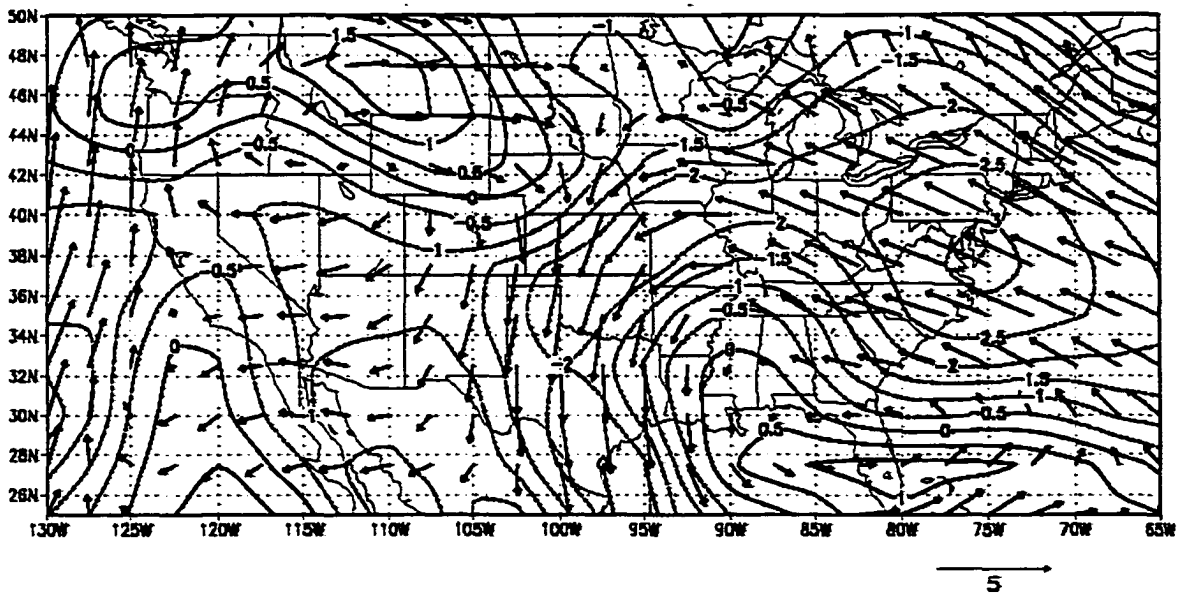

Figure 31. April 850 mb Total Wind Field for Event 1 - Event 4 Years. Contours are 0.5 m s^{-1}

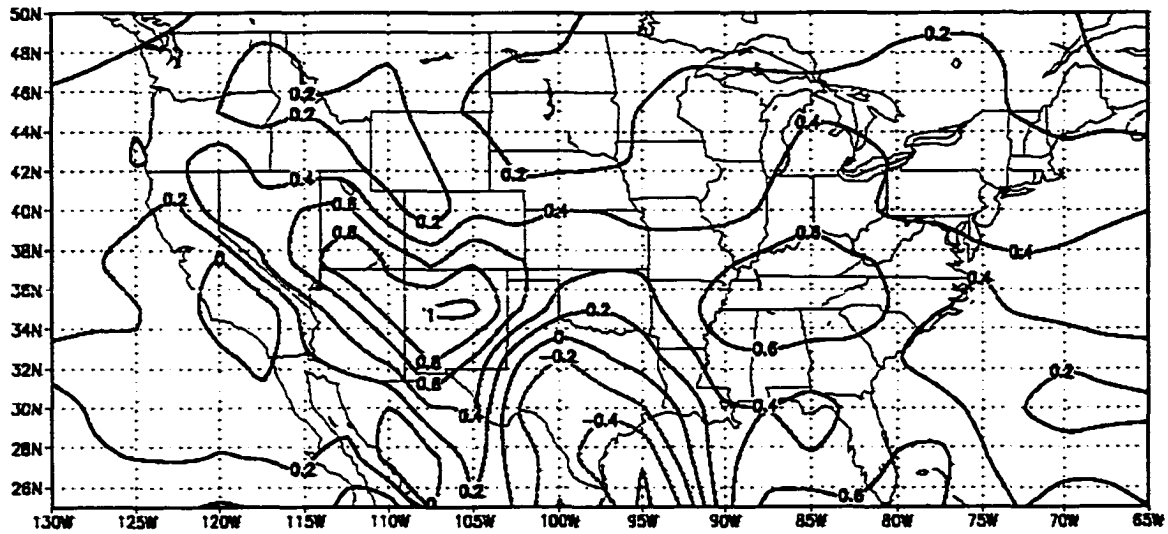

Figure 32. April 850 mb Specific Humidity for Event 1 - Event 4 Years. Contours are 0.2 g kg^{-1}

humidity to dewpoint temperature the following procedures were performed. Specific humidity was converted to vapor pressure using the equation of state applied to water vapor (Fleagle and Businger 1980):

$$q = \frac{\varepsilon e}{p} \tag{7}$$

where:

q = specific humidity in kg/kg
ε = ratio of molecular masses of water vapor and dry air
e = vapor pressure in mb
p = pressure in mb

Using the calculated value of vapor pressure from the above equation the dewpoint temperature can be determined by the use of Table 94 in the Smithsonian Meteorological Tables (List 1966). The 0.5 g/kg increase corresponds to approximately a 1.5^0 C increase in dewpoint temperature over the KMI region during an April Event 1 year.

During April, the difference field of 500 mb geopotential heights depicts higher (lower) heights over the western (central) Plains (not shown). This orientation provides a southeastward oriented duct for convective systems into the KMI region.

Summary of April Atmospheric Parameters

Atmospheric parameters that are conducive to precipitation production in the KMI region during April appear to be mainly a function of low-level thermal advection, low-level convergence, and sufficient moisture. Note that the thermal advection pattern is displaced equatorward of the KMI region during an Event 1 year, but difference fields depict a minimum (still warm air advection) over the KMI region; although, this would imply stronger lifting during Event 4 years, possibly resulting in higher precipitation amounts. Low-level convergence and moisture appear to be in phase over the KMI region. Convergence occurs during both Event 1 and 4 years, but the convergence pattern during Event 1 is collocated with higher values of moisture in the KMI region, thus a physical explanation for the precipitation differences. Other parameters such as upper level convergence, LLJ, and 500 mb geopotential heights do not appear to enhance the production of precipitation during Event 1 years in the KMI region.

July Atmospheric Parameters

While crops use water throughout the entire crop season, July is the month where moisture availabilty is most crucial for corn crops (Thompson, 1986). Figure 33 illustrates the sensitivity of crops to above/below normal precipitation. A 20 mm increase in July precipitation can enhance yields by approximately 200 kg ha^{-1} (assuming that water is the only limiting factor); therefore, emphasizing the importance of July precipitation to corn yields.

During July, statistically significant precipitation differences occur over the northern Plains states of the Dakotas, Wisconsin, northeastern Iowa, and Minnesota

(hereafter referred to as the DWIM region). The precipitation signal for July is the most spatially coherent signal, compared to other months during the warm season (Figure 14).

The July DWIM region is favorable for increased precipitation in an Event 1 versus Event 4 year. North and South Dakota experienced a median increase of 33.02 and 31.50 mm, respectively, in an Event 1 versus Event 4 year. Likewise, Wisconsin's median increase is 34.29 mm, Iowa's median increase is 20.07, and Minnesota's median increase is 36.07 mm.

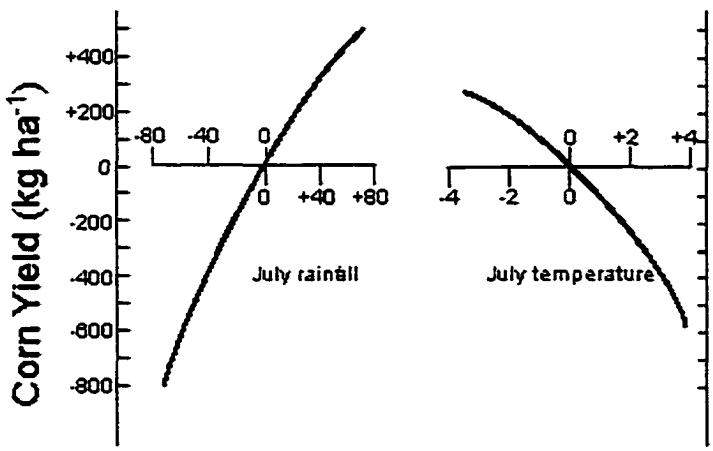

Figure 33. The response of corn yields to precipitation (mm)

Note the decrease in median precipitation differences from north to south across the DWIM region. The north to south decrease of median precipitation differences across the DWIM region may be indicative of MCC tracks. McAnelly and Cotton (1989) found that the heaviest precipitation amounts are typically 50 to 100 km south of the MCC path. It is also interesting to note the much more coherent spatial pattern of precipitation differences in July (Figure 13) as compared to April (Figure 14). This may be attributed, in part, to a more positive spatial phasing of precipitation fields and atmospheric parameters across the DWIM region, as will be shown below.

The 200 mb jet stream pattern across the DWIM region in July shows a strengthened and southward displacement into regions of the U.S. during Event 1 years as

shown by the 200 mb wind difference field (Figure 34). This spatial displacement of the 200 mb wind field is in good agreement with the Bell and Janowiak (1995) study, which showed a southward-displaced jet during the 1993 warm season. Also, note that the DWIM region is located near the right rear divergent portion of the jet in an Event 1 year (Figure 35), although this is the weaker of the two divergent quadrants of the jet.

The 200 mb surface depicts regions of convergence across portions of the DWIM region in both Event 1 (Figure 36) and 4 (Figure 37) years. Notice however, that during an Event 1 year the central Plains region is in an area of upper level divergence. This area of divergence also encroaches into southern portions of the DWIM region. Recall that MCCs initiate in portions of the western and central Plains region, which provides a more favorable upper level environment for these convective systems. Difference fields of this parameter depict enhanced upper level divergence across the initiation region of the western and central Plains and along the eastern portions of the DWIM region in an Event 1 versus Event 4 years (Figure 38). Stronger subsidence across portions of the north and northwestern portions of the DWIM region occurs during an Event 1 year, which is resultant of the orientation of the 200 mb jet (left rear quadrant).

With upper level patterns of divergence conducive to precipitation development present, an analysis of low-level convergence patterns follows. Low-level convergence at 850 mb shows a favorable pattern over the DWIM region. Figure 39 shows that low-level convergence is concentrated in the southeastern portion of the DWIM region, near the genesis region of mean MCC tracks (Cotton et al. 1989; Augustine and Howard 1991). During Event 4 years (not shown) low-level convergence is located in the heart of the DWIM region near the U.S.-Canadian border; however, as will be seen later, moisture is a limiting factor further north into the DWIM region. A difference field of low-level convergence (Figure 40) shows a maximum over eastern Kansas, which is in phase with the upper-level divergence field (Figure 38) over the central Plains; providing a large-scale mechanism to support lifting in the initiation region (Dines Compensation). The difference field of convergence at 850 mb is shown to be a result of the spatial difference field of winds, as shown in Figure 41.

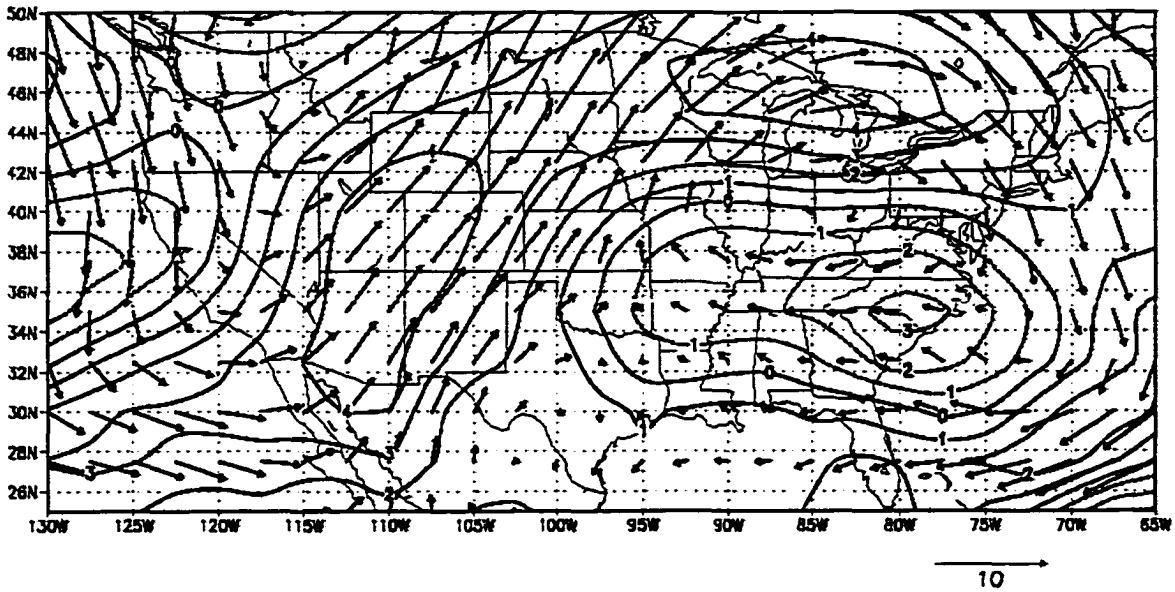

Figure 34. Event 1 - Event 4 July 200 mb Winds. Contours are 1 m s^{-1}

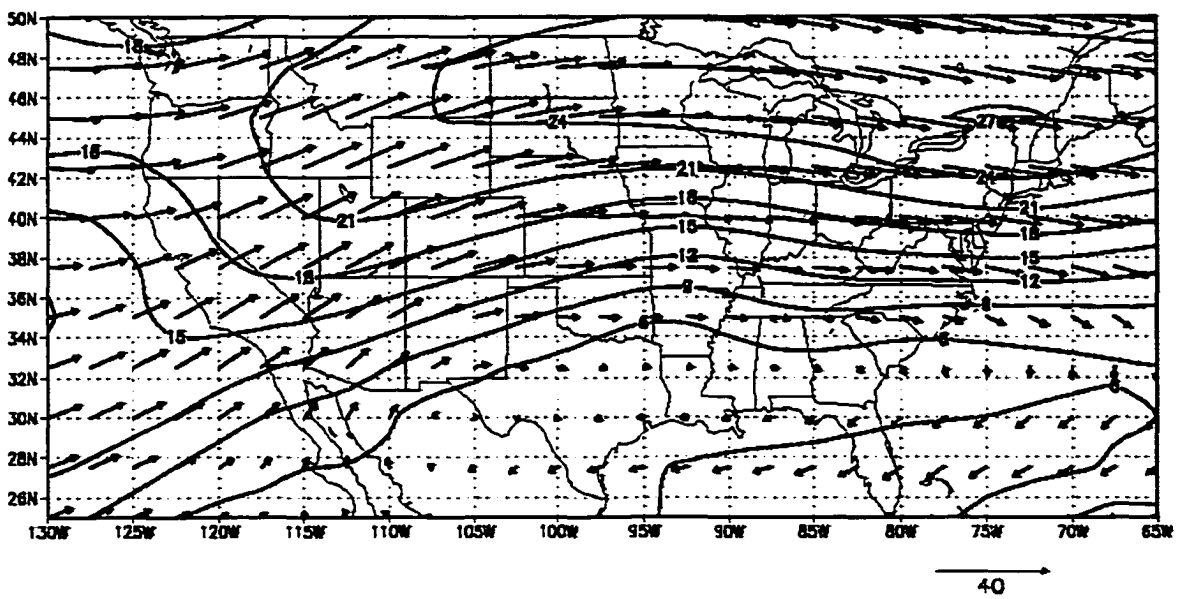

Figure 35. Event 1 July 200 mb Winds. Contours are 3 m s^{-1}

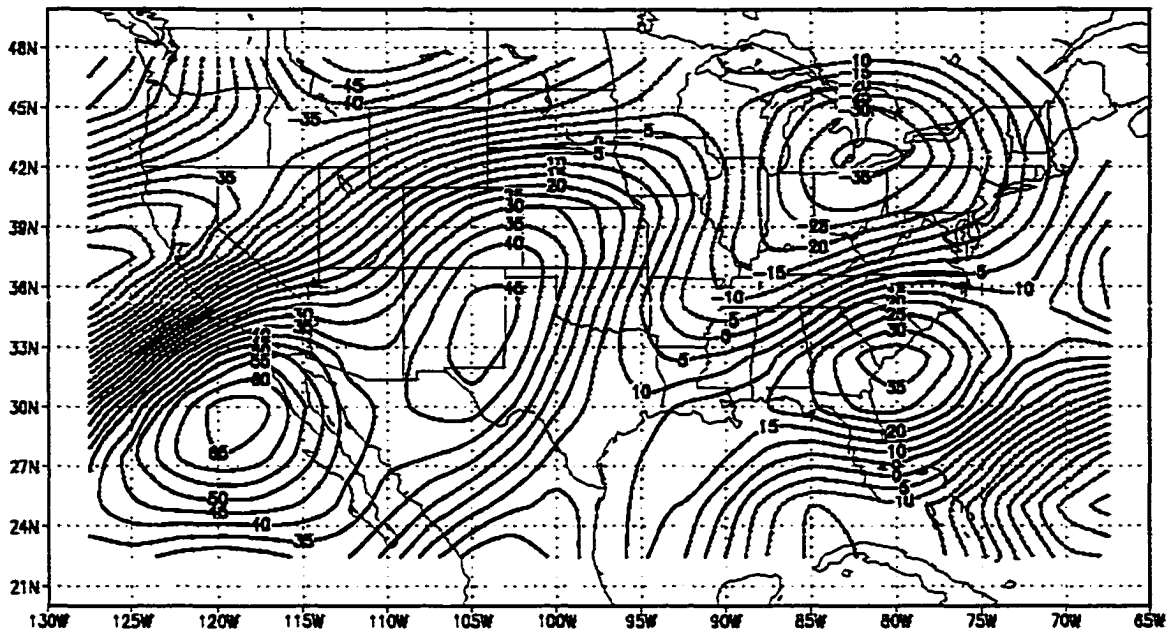

Figure 36. Event 1 July 200 mb Divergence. Contours are $5x10^{-7}$ s^{-1}

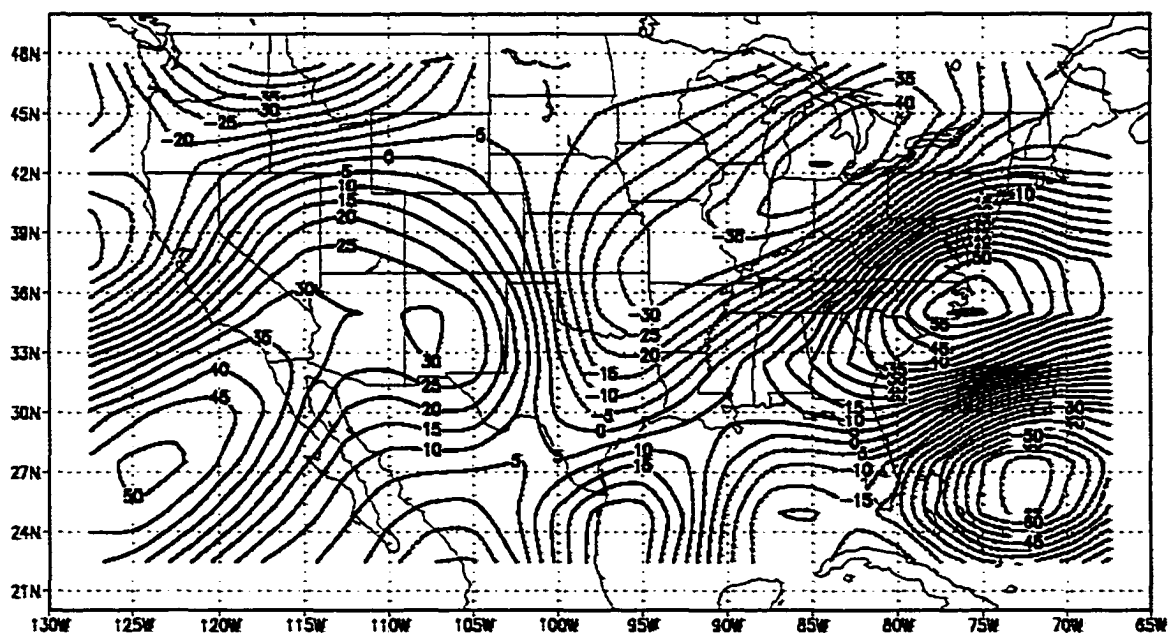

Figure 37. Event 4 July 200 mb Divergence. Contours are $5x10^{-7}$ s^{-1}

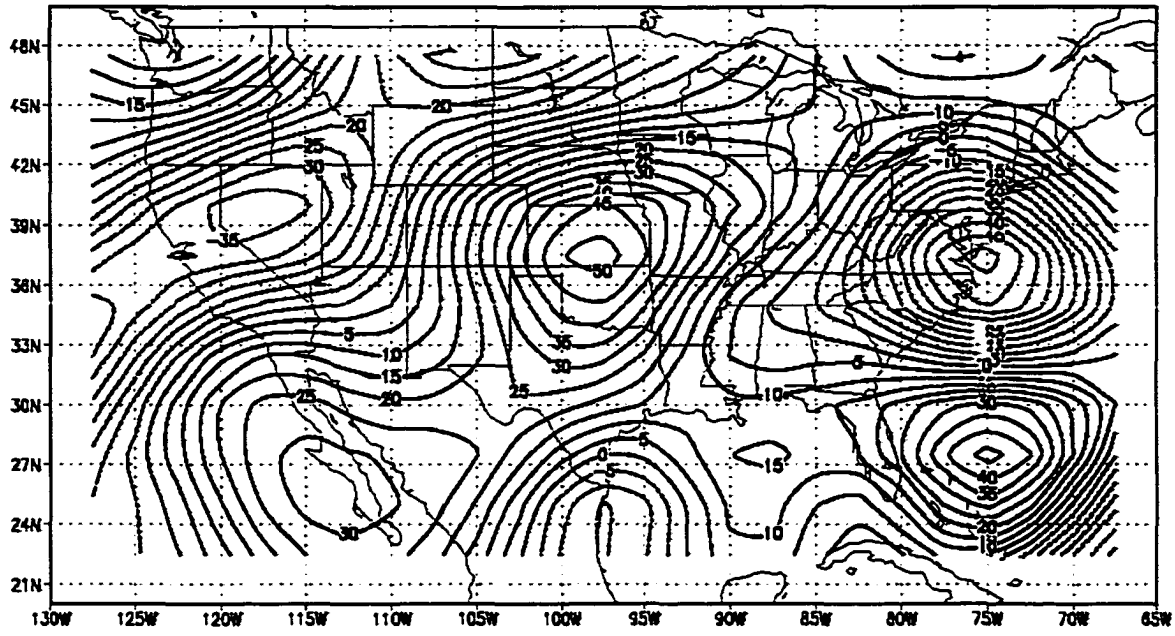

Figure 38. Event 1 - Event 4 July 200 mb Divergence. Contours are $5x10^{-7}$ s^{-1}

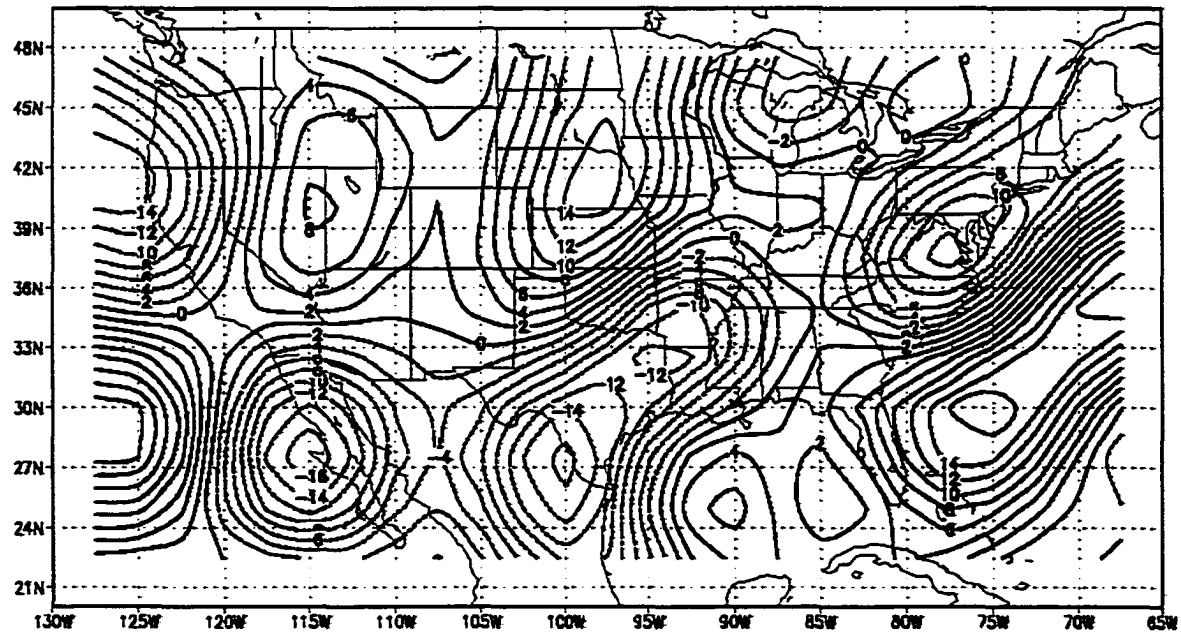

Figure 39. Event 1 July 850 mb Convergence. Contours are $2x10^{-7}$ s^{-1}

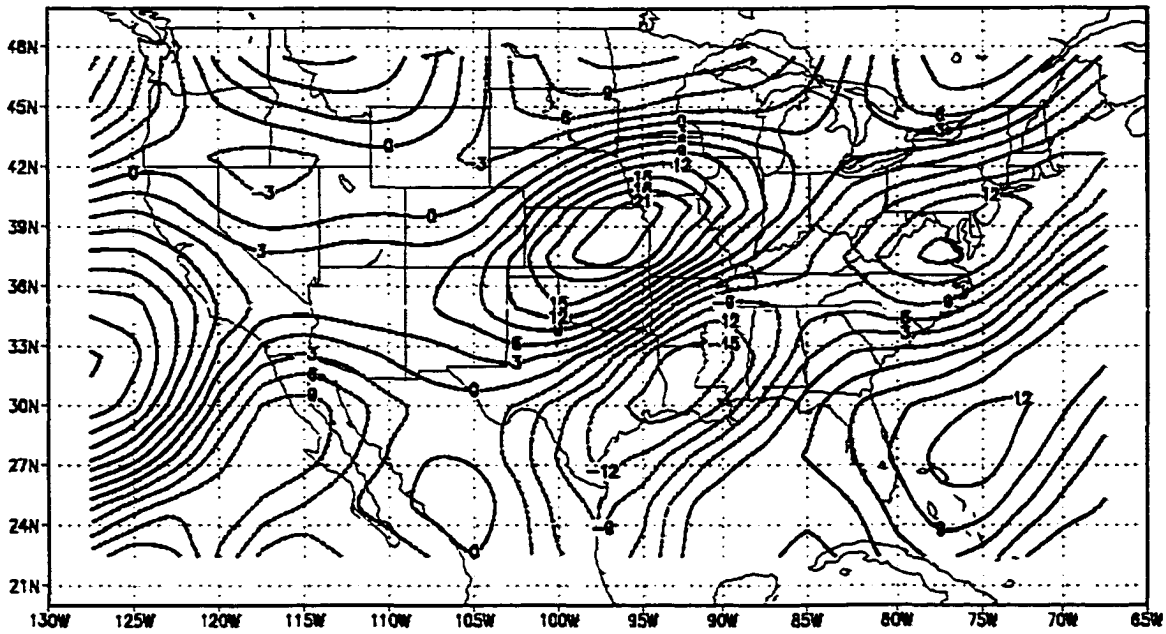

Figure 40. Event 1 - Event 4 July 850 mb Convergence. Contours are $3x10^{-7}$ s^{-1}

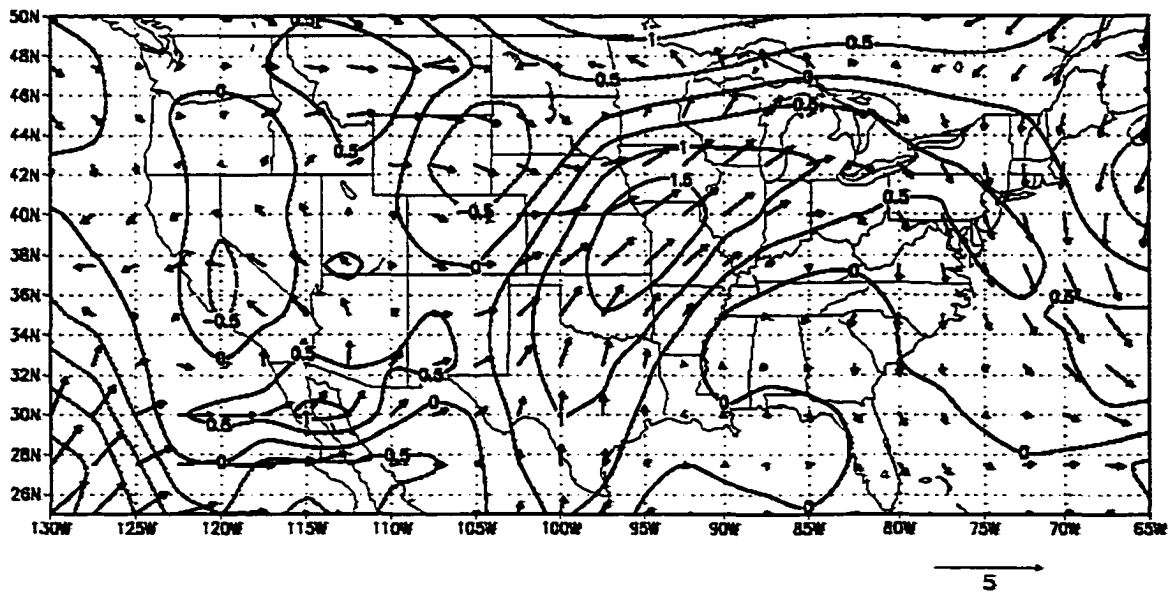

Figure 41. Event 1 - Event 4 July 850 mb Winds. Contours are 0.5 m s^{-1}

During Event 1 years (Figure 42) the 850 mb wind field exhibits a stronger poleward shift into the central Plains versus Event 4 years (Figure 43) (increase of approximately 2 m s^{-1}). This is evidenced by the 6 m s^{-1} isotach that has moved into southwestern Iowa in an Event 1 year as compared to an Event 4 year, when it is located further south along the Kansas-Oklahoma border. The intensification of the low-level wind field may be attributed, in part, to the enhanced pressure gradient that is depicted in the Event 1 - Event 4 difference field of 850 mb heights (Figure 44). The enhanced pressure gradient is a result of the strengthening (8 m) and westward positioning of the Bermuda High pressure system over the eastern Gulf of Mexico interacting with an anomalous trough in the central and northern Plains; thus, increasing the low-level winds. Also, note the southwest-northeast orientation of the isotachs (Figure 41), which strongly resemble the 850 mb height difference field (Figure 44). The trough/ridge orientation in Figure 44 enhances not only the wind field and downstream convergence, but may also enhance moisture transport into the region favorable for MCC development.

Low-level moisture in July is more abundant in Event 1 versus Event 4 years (Figure 45). The excess low-level moisture is located in a large swath from the lee of the Rockies to the central Plains, a region favorable for MCC initiation. Also note the magnitude of the moisture present in portions of the region; it is on the order of 1 g kg^{-1}. Putting this in terms of dewpoint temperature, it is an increase of approximately 1.5^{0} C at 850 mb from Event 4 to Event 1 years. Moisture availability appears to play the key role for precipitation differences across the DWIM region in July. While lower-level convergence is present in both Event 1 and 4 years over portions of the DWIM region, the convergence field in Event 4 years is displaced northward, away from the axis of increased moisture; therefore, less precipitation occurs during these years.

July thermal advection fields support vertical motion in and around the DWIM region. Event 1 years show warm air advection present in the central and northern Plains (Figure 46). Event 4 years also depict warm air advection in the same region (Figure 47), but note that the magnitude of warm air advection is not as pronounced as in Event 1 years (Figure 46).

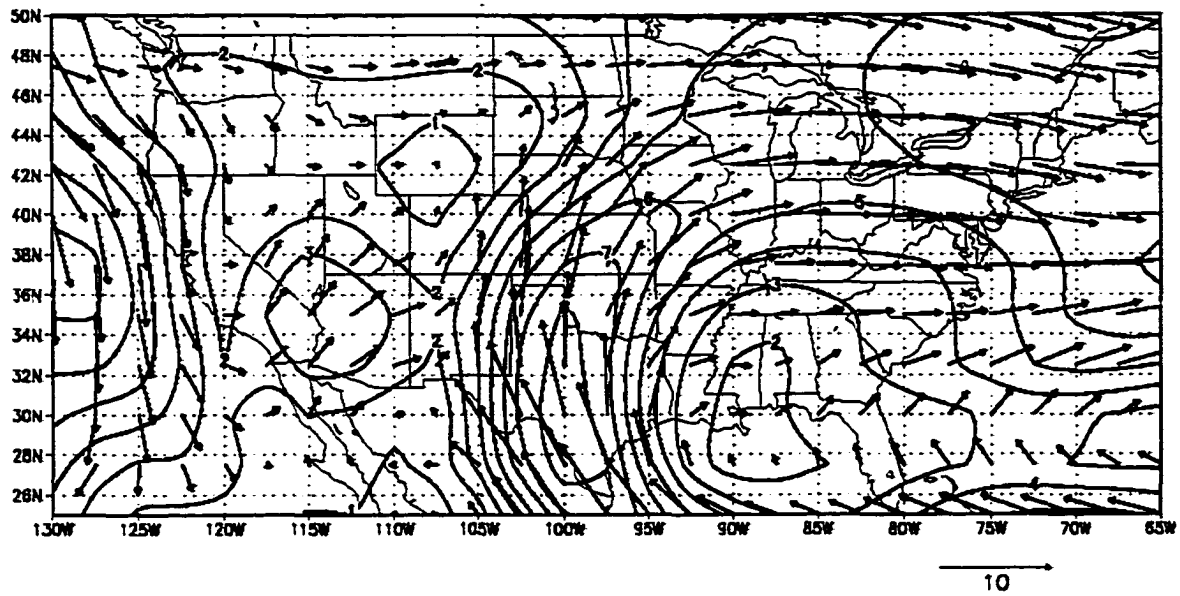

Figure 42. Event 1 July 850 mb Winds. Contours are 1 m s^{-1}

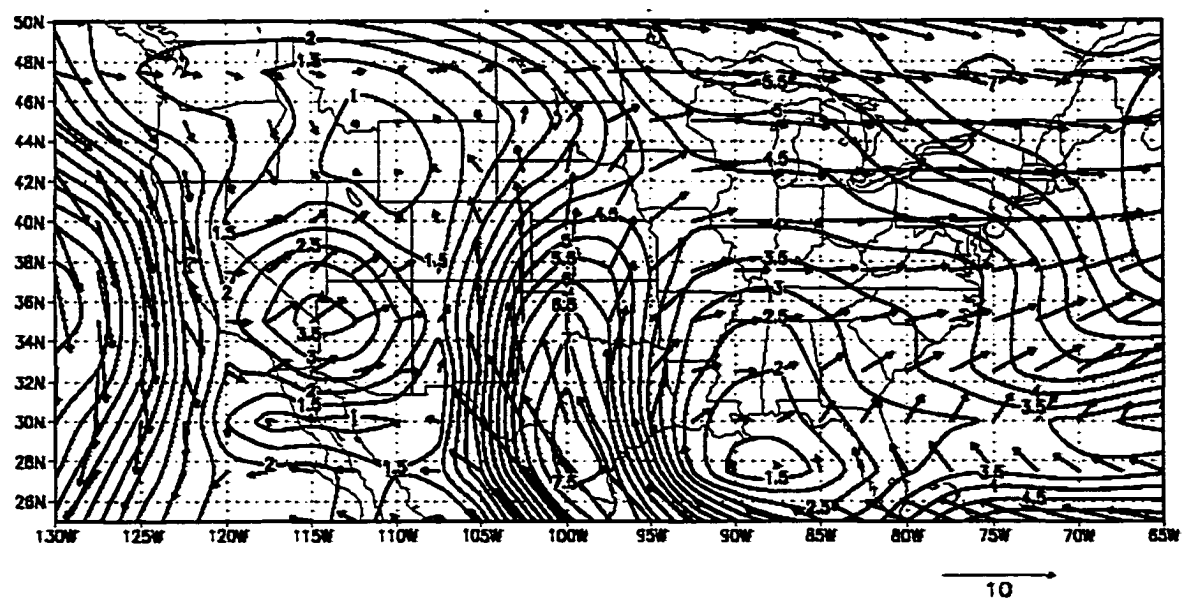

Figure 43. Event 4 July 850 mb Winds. Contours are 0.5 m s^{-1}

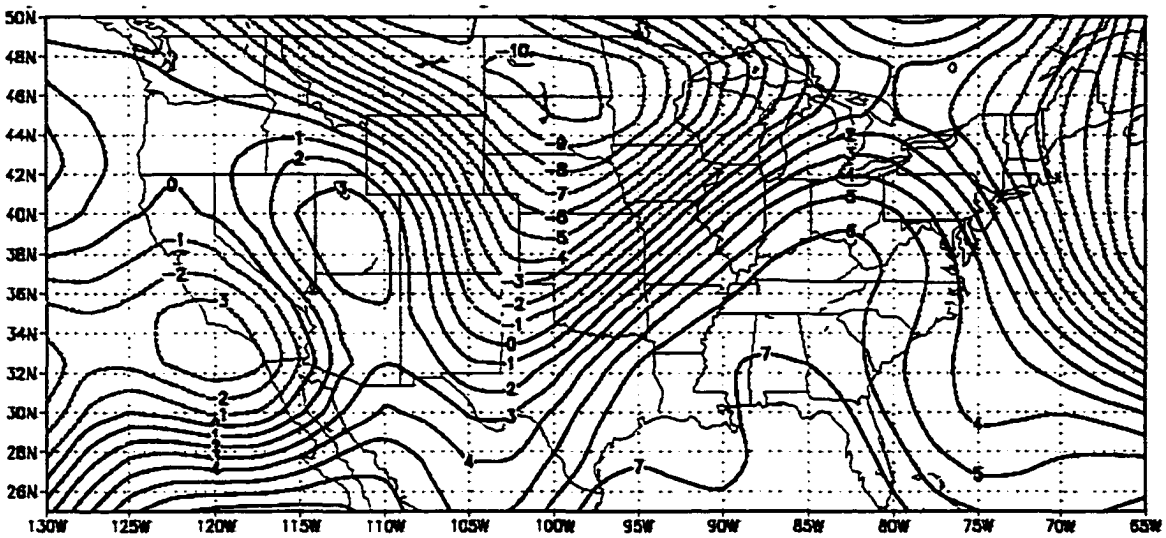

Figure 44. Event 1 - Event 4 July 850 mb Heights. Contours are 1 m

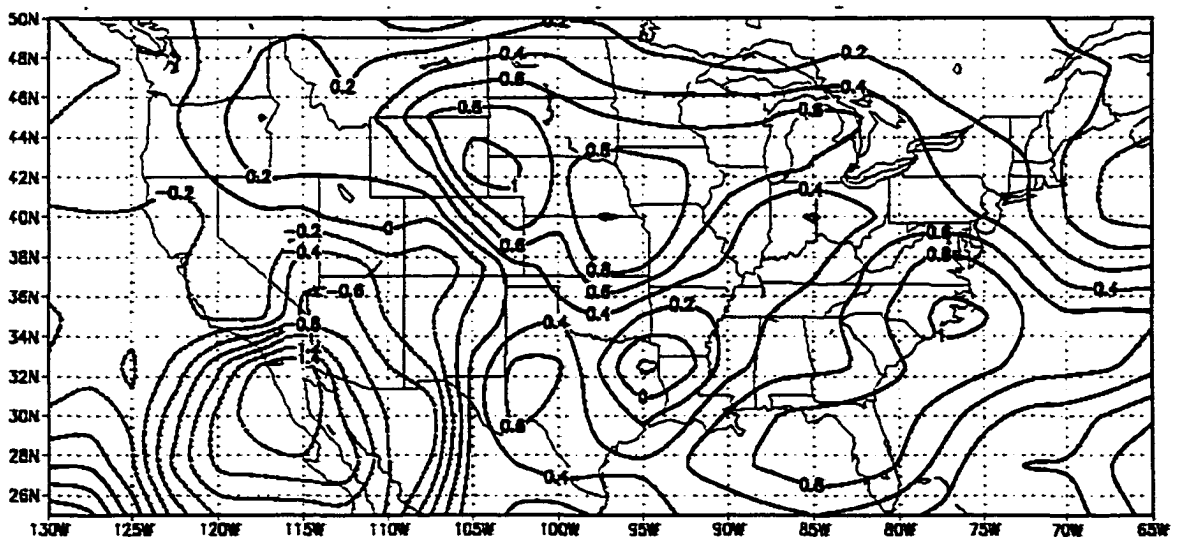

Figure 45. Event 1 - Event 4 July 850 mb Specific Humidity. Contours are 0.2 g kg^{-1}

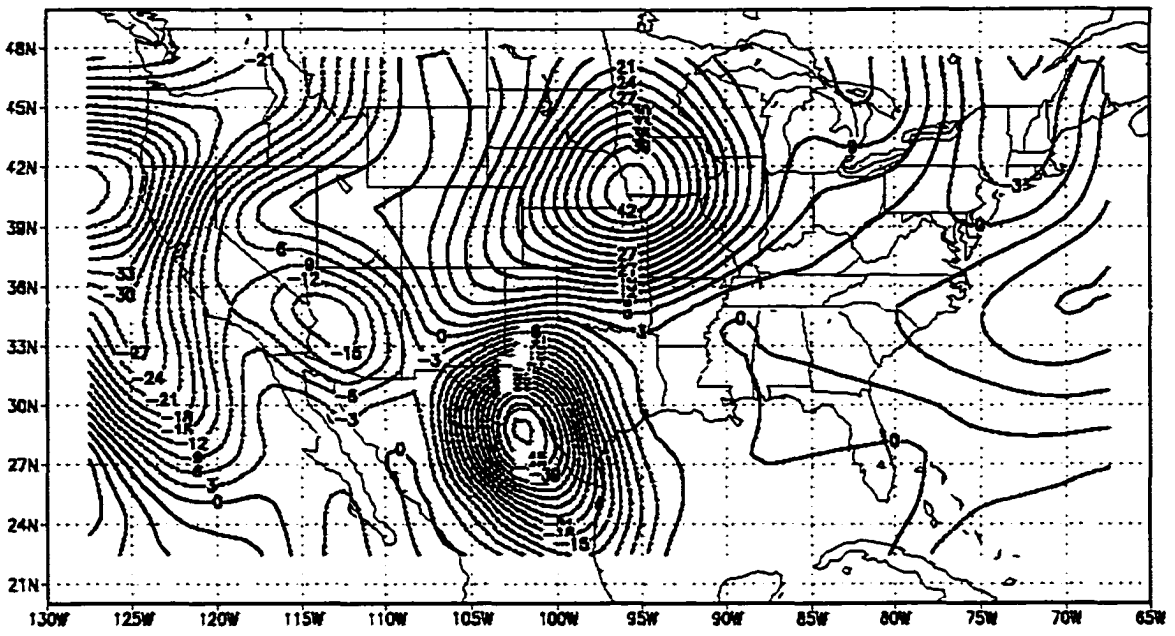

Figure 46. Event 1 July Temperature Advection. Contours are $3x10^{-6}$ K s^{-1}

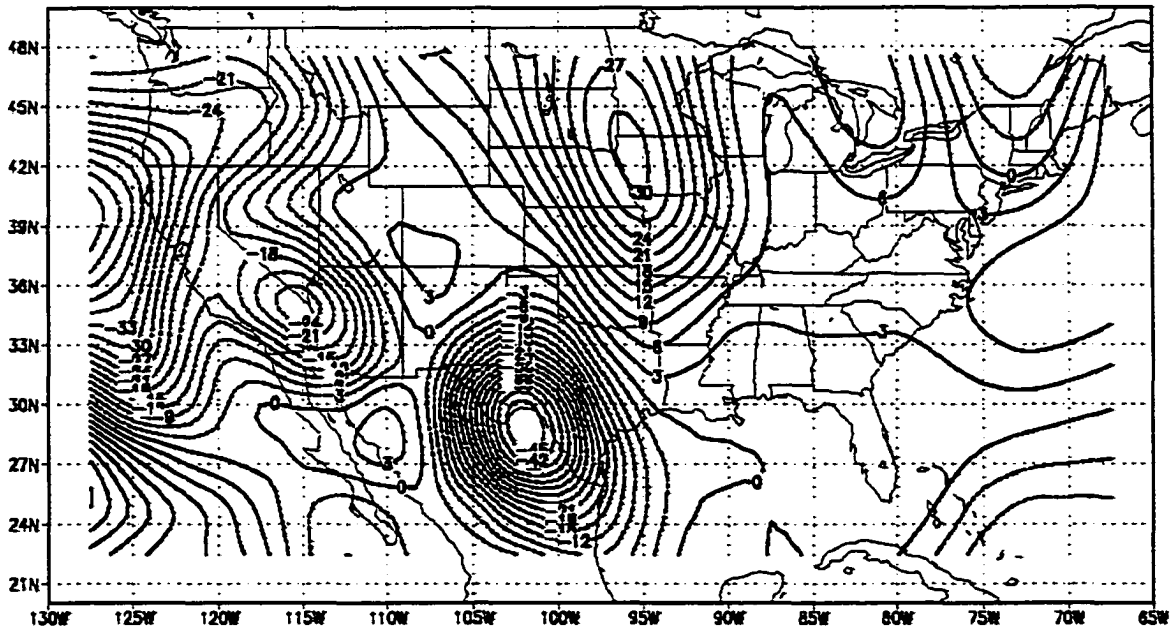

Figure 47. Event 4 July Temperature Advection. Contours are $3x10^{-6}$ K s^{-1}

The difference field (Figure 48) depicts a maximum of warm air advection in northwestern Kansas, a location near the initiation region of the mean MCC track (Cotton et al. 1989; Augustine and Howard 1991). It is interesting to note that the area of significant precipitation differences between Event 1 and 4 years (Figure 14) are located between a local maximum and minimum in the thermal advection difference field (Figure 48). A similar feature, the positioning of the significant precipitation differences between a thermal advection difference field couplet is also present in August.

The spatial location of statistically significant July precipitation (DWIM region) is addressed by analysis of the 500 mb geopotential height pattern. Recall that MCCs, once initiated and organized, begin to move along the periphery of a 500 mb ridge (Augustine and Howard (1991). Figure 49 shows the presence of lower 500 mb heights across the MCC initiation region.

One has to be careful with the interpretation of the difference field as a trough (ridge) configuration across the western (eastern) portion of the U.S., since a decrease (increase) in heights can occur in a ridge (trough). Geopotential heights during an Event 1 year (not shown) depict low amplitude (zonal) flow across the region as compared to Event 4 years with high amplitude flow (a ridge axis located along 107^0 W). The interpretation here is of lower (higher) heights over the western (eastern) region during an Event 1 year.

The ridge axis found during Event 4 years would tend to steer MCCs equatorward of the DWIM region; whereas, during an Event 1 year, MCCs would tend to move east-northeast of the initiation region, which is in the path of the DWIM region.

Summary of July Atmospheric Parameters

July precipitation displays the most coherent spatial signal across the DWIM region during the warm season. This is in agreement with previous studies, which show similar warm season spatial precipitation characteristics (Bunker et al. 1996, Ting and Wang 1997). It is interesting to note that July, being one of the most critical months for supplying, or maintaining subsoil moisture, also coincides with the largest precipitation

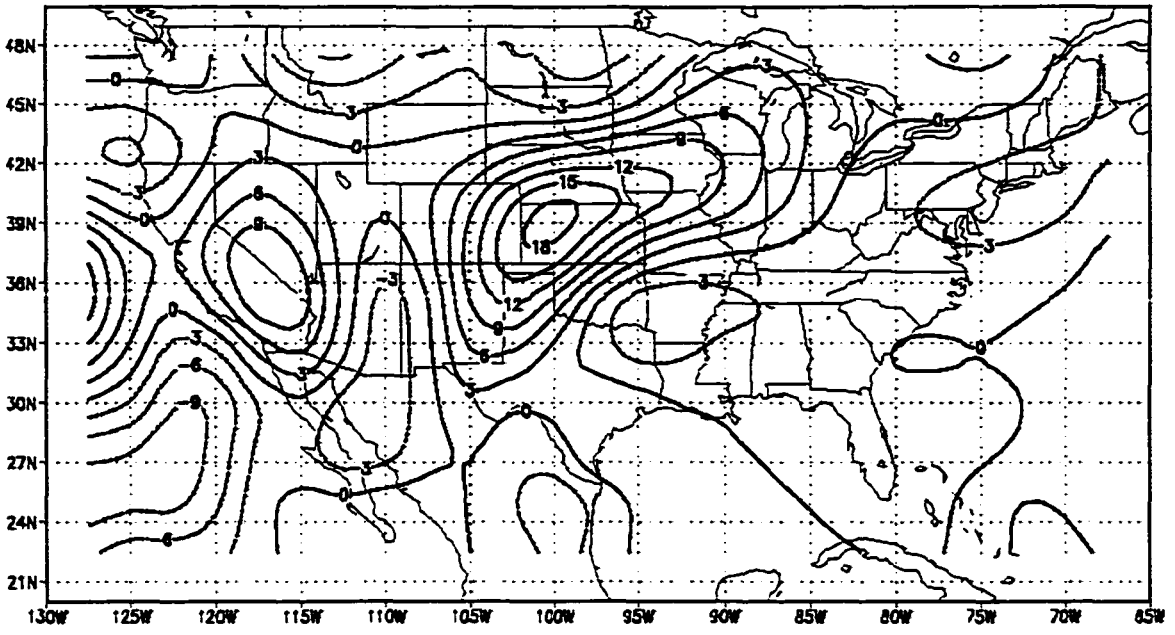

Figure 48. Event 1 - Event 4 July Temperature Advection. Contours are $3x10^{-6}$ K s^{-1}

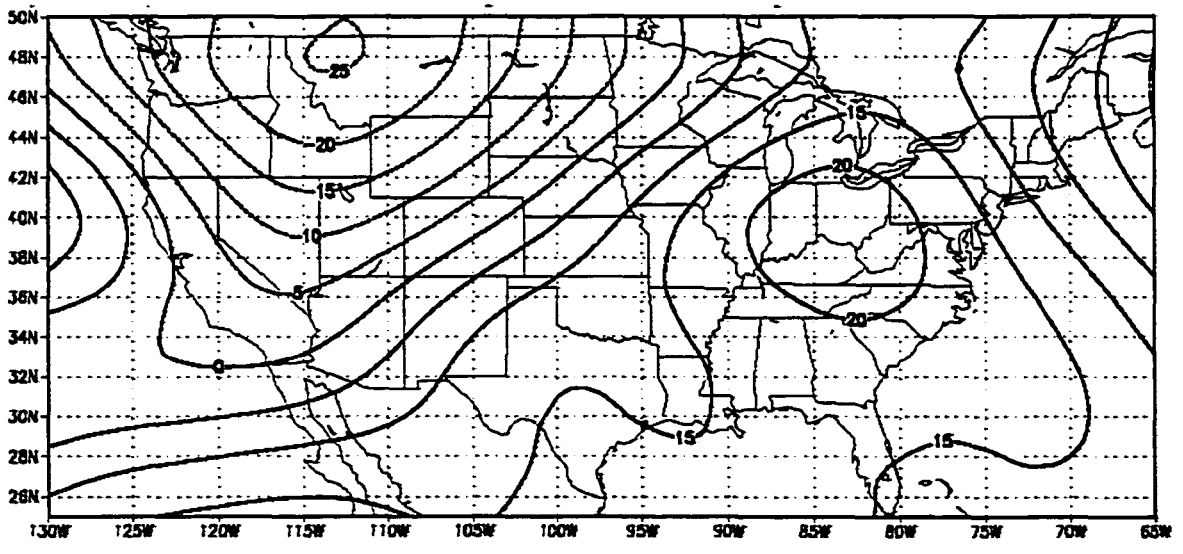

Figure 49. Event 1 - Event 4 July 500 mb Geopotential Heights. Contours are 5 m

differences between Event 1 and 4 years. This can be accounted for in part by July atmospheric parameters such as thermal advection fields, upper air divergence, and lower level convergence. Warm air advection is present in both Event 1 and 4 years, but magnitude differences are apparent, with Event 1 years exhibiting stronger values of warm air advection providing additional buoyant energy. Upper and lower-level fields of divergence and convergence, which are in phase over portions of the central Plains are due, in part, to the positioning of the upper and lower level jet streams. The difference field of 850 mb winds also suggests that the LLJ is the mechanism for movement of moisture into the area of MCC initiation. Once convective activity is initiated, it tracks to the east-northeast into the DWIM region following the periphery of enhanced 500 mb geopotential heights.

August Atmospheric Parameters

During August, statistically significant precipitation differences move equatorward into the central Plains region, with differences concentrated in portions of Nebraska, Iowa, Illinois, and Kansas (hereafter referred to as the NIIK region). During the previous months of April and July, the precipitation signal was enhanced in an Event 1 versus Event 4 year. This same trend continues in August. August precipitation remains important to continued crop development, but is not usually as crucial as July precipitation (Figure 50).

Nebraska experienced a median increase of 23.69 mm in an Event 1 versus Event 4 year, Iowa's median increase is 21.72 mm, Illinois' median increase is 38.10, and Kansas' median increase is 28.58 mm. August median precipitation differences are 26.14 mm across the NIIK region. This is near the April median precipitation difference of 27.30 mm across the KMI region, but less than the July median precipitation difference of 33.02 mm across the DWIM region.

August atmospheric parameters are favorably oriented to produce precipitation differences over the NIIK region in Event 1 and 4 years. The first parameter, the 200 mb jet stream, is stronger in Event 1 (Figure 51) as compared to Event 4 years (Figure 52).

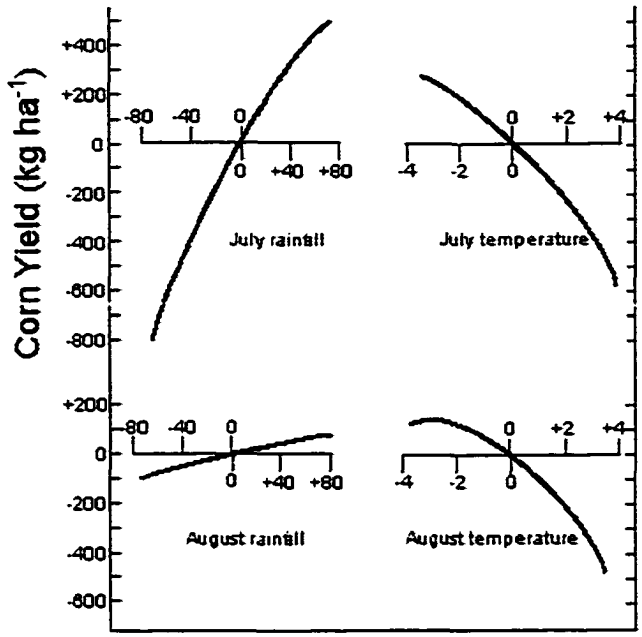

Figure 50. The response of corn yields to precipitation in mm. (Thompson 1986)

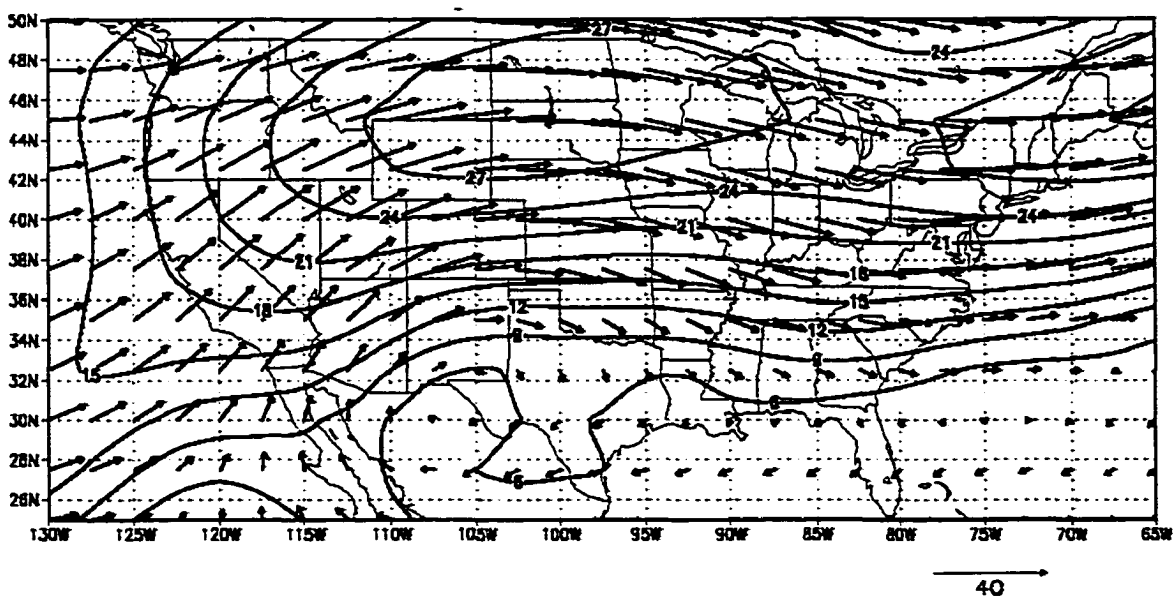

Figure 51. Event 1 August 200 mb Winds. Contours are 3 m s^{-1}

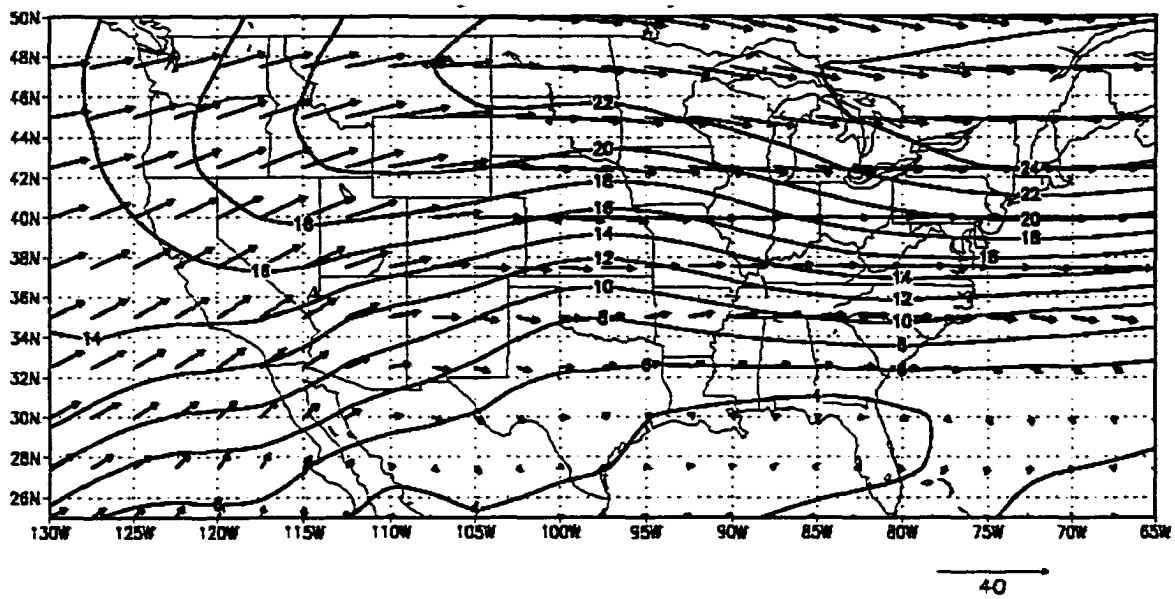

Figure 52. Event 4 August 200 mb Winds. Contours are 2 m s^{-1}

Also note the position of the jet streak in Event 1 as compared to Event 4 years. The jet streak is located over the NIIK region during Event 1 years (Figure 51). Event 4 years have the jet streak over the eastern portion of the U.S. (Figure 52). The difference field of the 200 mb jet stream also depicts an equatorward shift of the strongest winds to a position over western portions of the NIIK region (Figure 53).

The orientation of the 200 mb jet stream is also conducive to 200 mb divergence over portions of the NIIK region. Note that during an Event 1 year, Nebraska and Kansas are located near the right rear entrance of the jet streak (Figure 51), an area favorable for upper air divergence. Figure 54 shows that during an Event 1 year there is the presence of upper air divergence over Nebraska, Iowa, and portions of Kansas. While Illinois is in an area of upper air convergence during both Event 1 and 4 years (not shown), the convergence is weaker in an Event 1 year as shown by the 200 mb divergence difference field (Figure 55). It is interesting to note that during August, divergence (convergence) patterns at 200 mb are present in Event 1 (4) years. For instance, the months of April and July show large-scale convergence over their respective regions of precipitation differences (KMI and DWIM); in August, there is 200 mb divergence (convergence) present during

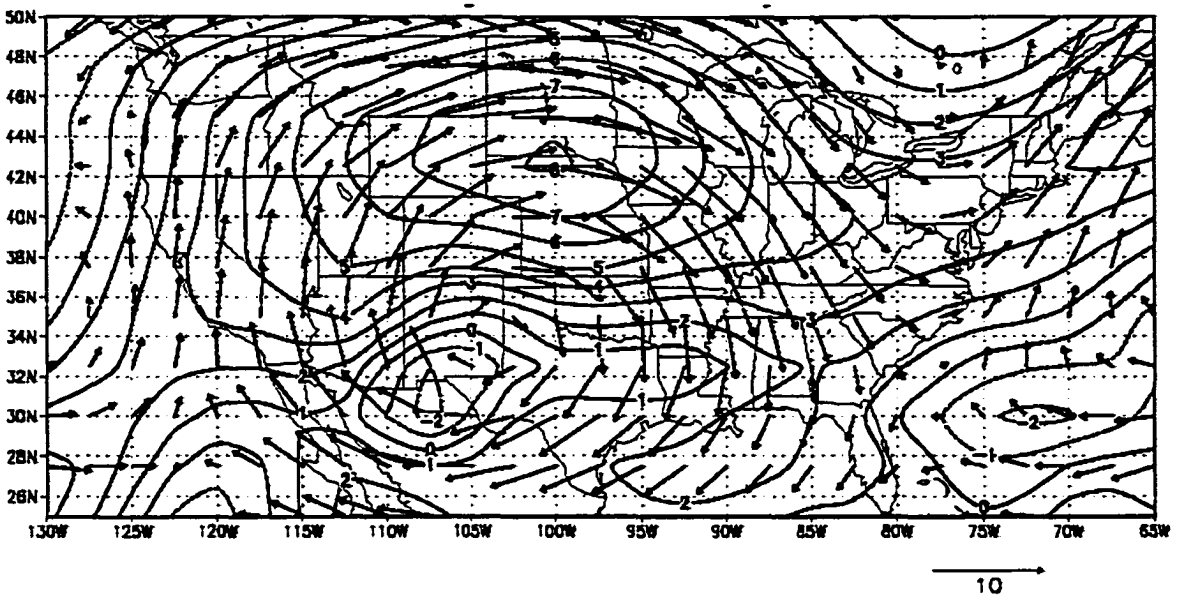

Figure 53. Event 1 - Event 4 August 200 mb Winds. Contours are 1 m s^{-1}

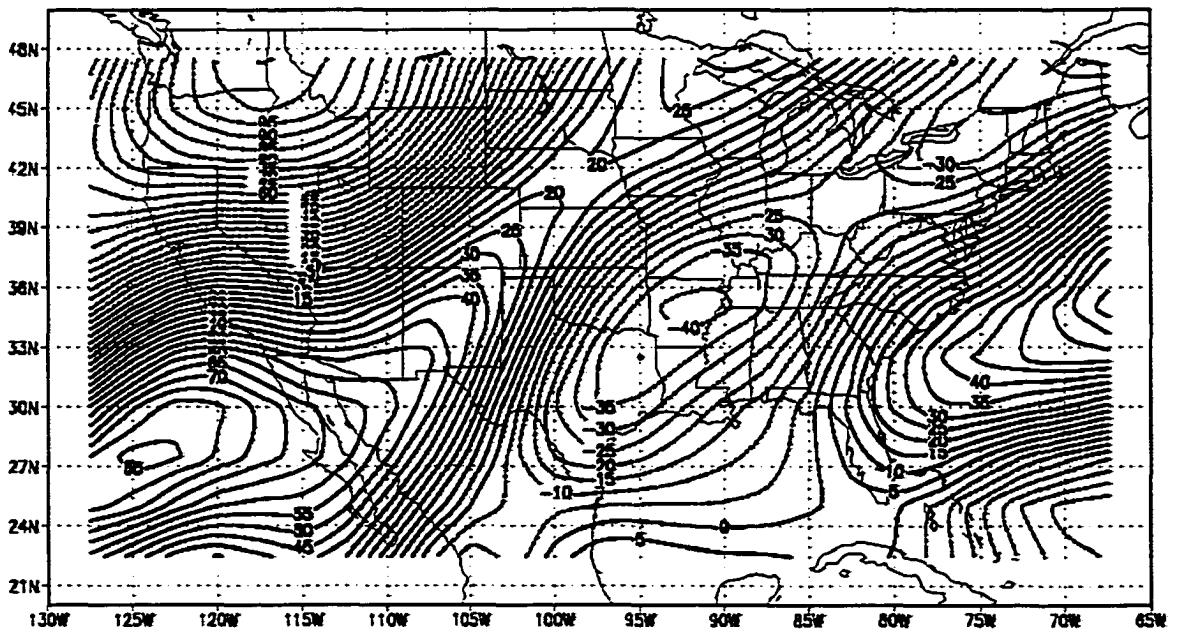

Figure 54. Event 1 August 200 mb Divergence. Contours are $5x10^{-7}$ s^{-1}

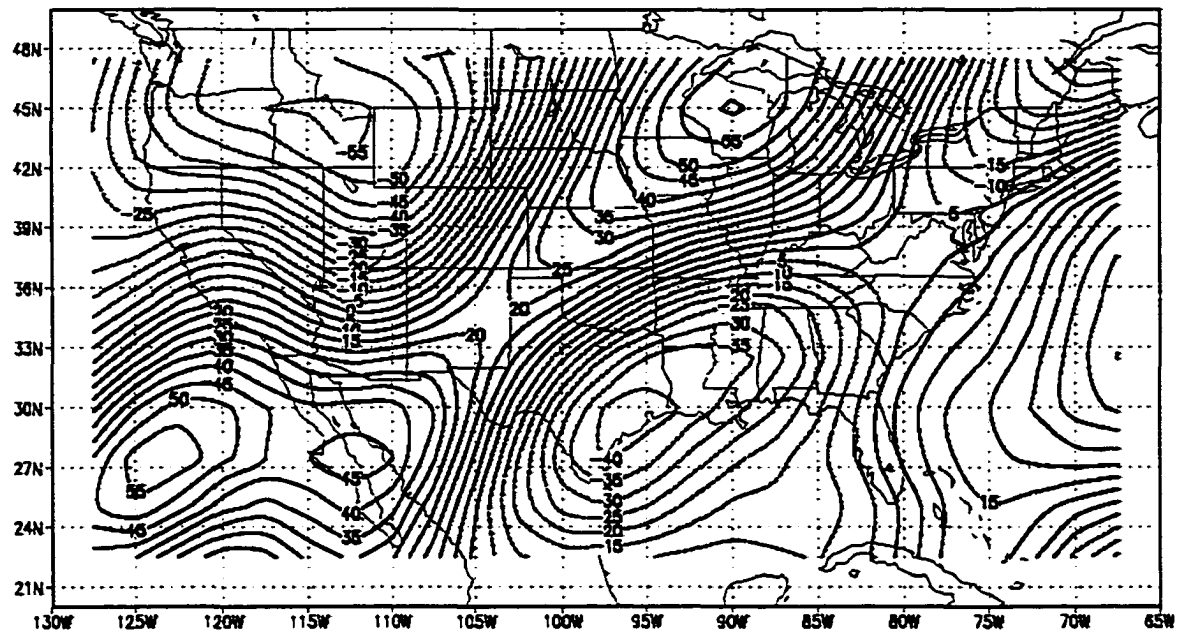

Figure 55. Event 1 - Event 4 August 200 mb Divergence. Contours are $5x10^{-7}$ s^{-1}

Event 1 (4) years. This well pronounced pattern may be related to the positioning and strength of the jet stream during August as compared to April and July. Pronounced 850 mb convergence appears over the NIIK region with a maximum over Nebraska and Kansas during Event 1 years (Figure 56).

Conversely, the NIIK region exhibits 850 mb divergence during Event 4 years (Figure 57). This is yet another atmospheric parameter that appears to exhibit opposite phases based upon the Event year that is in occurrence. The difference field of 850 mb convergence (Figure 58) shows that the maximum occurs over the Nebraska and Kansas border; again, an area that is typically recognized for initiation of convective activity such as the MCC.

Unlike July difference fields of 200 mb divergence and 850 mb convergence, there is an absence of vertical phasing present in August between the maximum of the two parameters. The 200 mb divergence maximum (Figure 55) is located northeast of the 850 mb convergence field maximum (Figure 57), although, the overall difference field in the

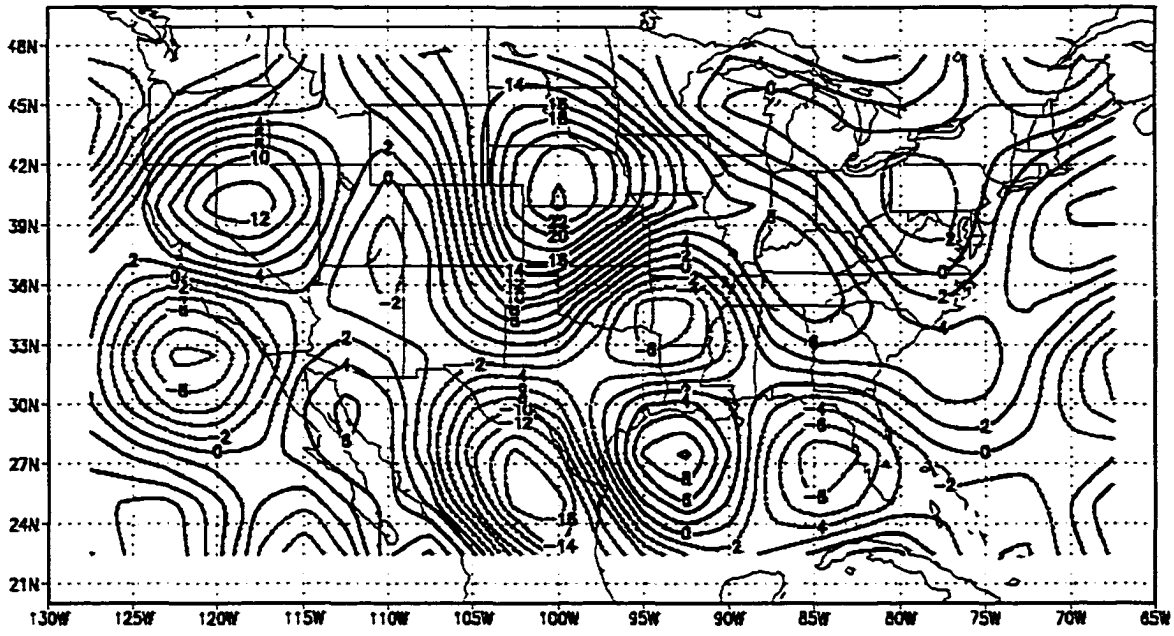

Figure 56. Event 1 August 850 mb Convergence. Contours are $2x10^{-7}$ s^{-1}

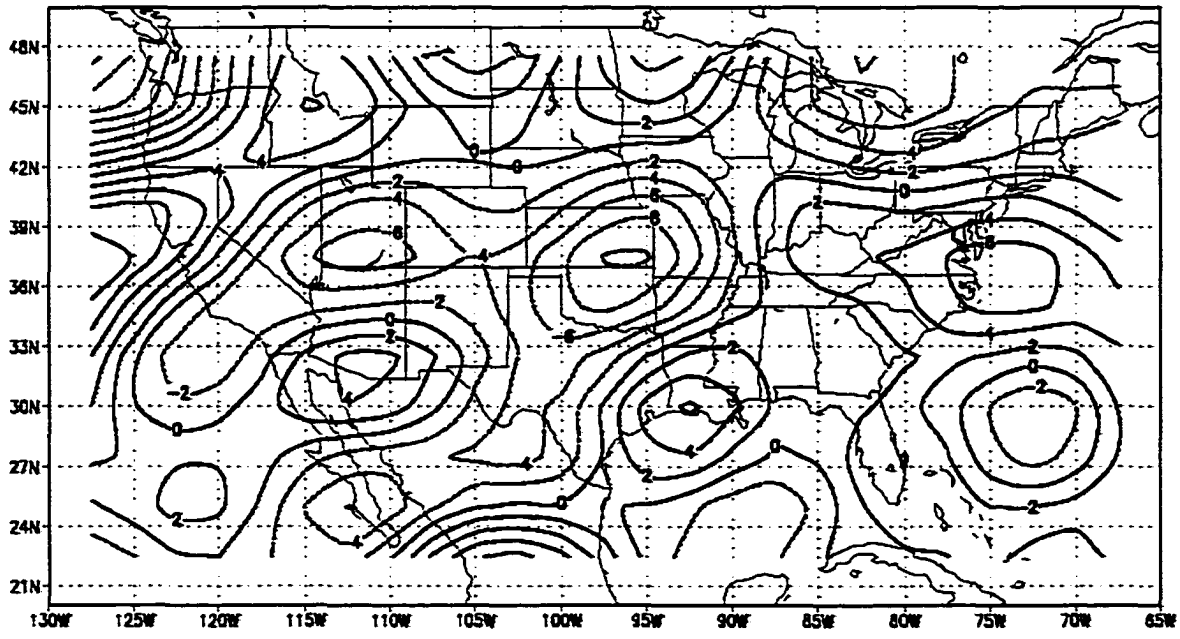

Figure 57. Event 4 August 850 mb Convergence. Contours are $2x10^{-7}$ s^{-1}

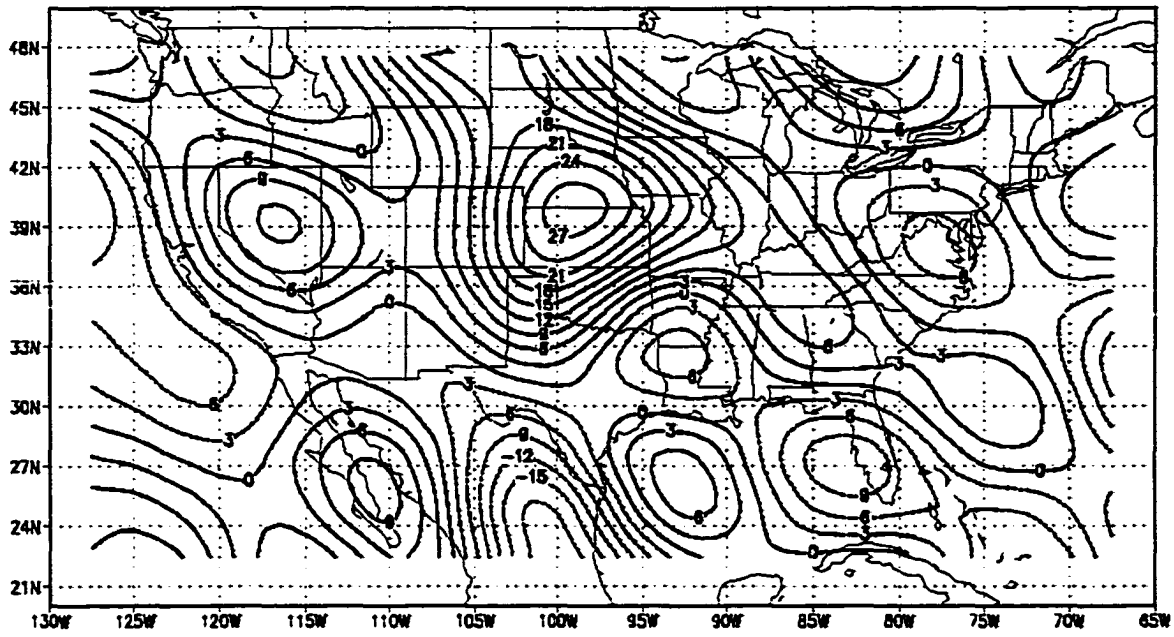

Figure 58. Event 1 - Event 4 August 850 mb Convergence. Contours are $3x10^{-7}$ s^{-1}

central and northern Plains shows general vertical phasing; this is notable evidence of Dines Compensation within the NIIK region.

The July difference fields of 850 mb winds and convergence were collocated with each other but such a pattern did not emerge between the two parameters in August. The August difference field of 850 mb winds shows weaker magnitudes over the NIIK region (Figure 59). This may be evidence for the weaker spatial pattern of August precipitation differences (Figure 15) as compared to July precipitation differences (Figure 14).

The weaker 850 mb wind field over this region, during an Event 1 year, may be a partial result of the pressure gradient pattern. Notice in the August difference field of 850 mb geopotential heights (Figure 60) that higher heights are present over the Rocky Mountain region, as contrasted to lower heights over the same region in July (Figure 44). The pressure gradient force is in the opposite direction from July, reducing the poleward extension of the maximum winds in the 850 mb wind field.

The difference field of low-level moisture shows the presence of additional moisture during an Event 1 year over the MCC initiation region (Figure 61). The low-

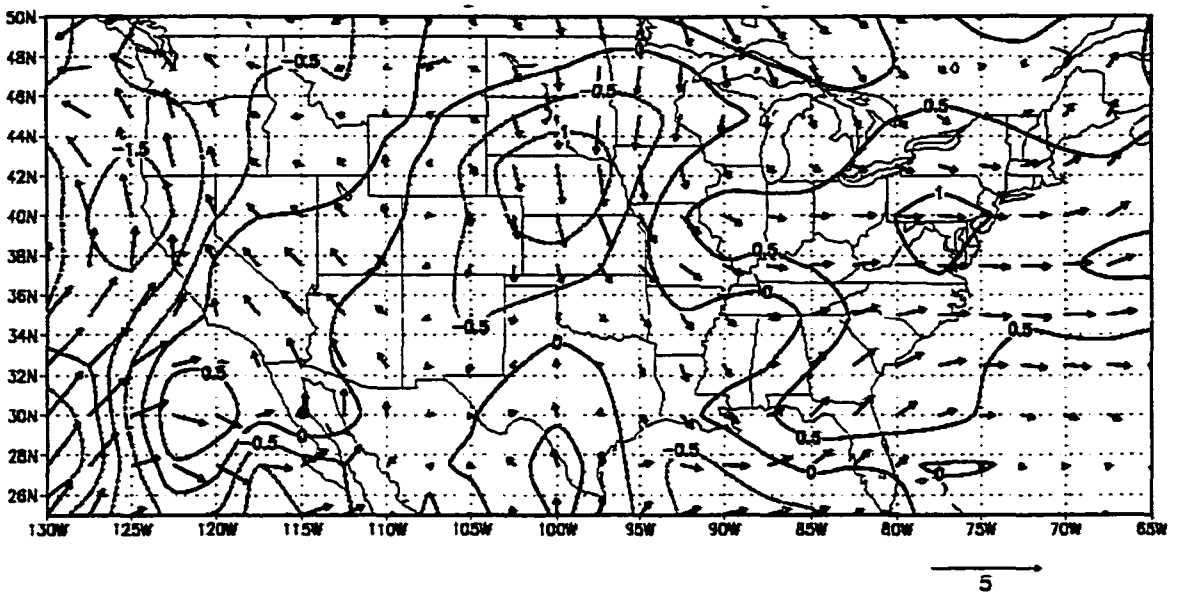

Figure 59. Event 1 - Event 4 August 850 mb Winds. Contours are 0.5 m s^{-1}

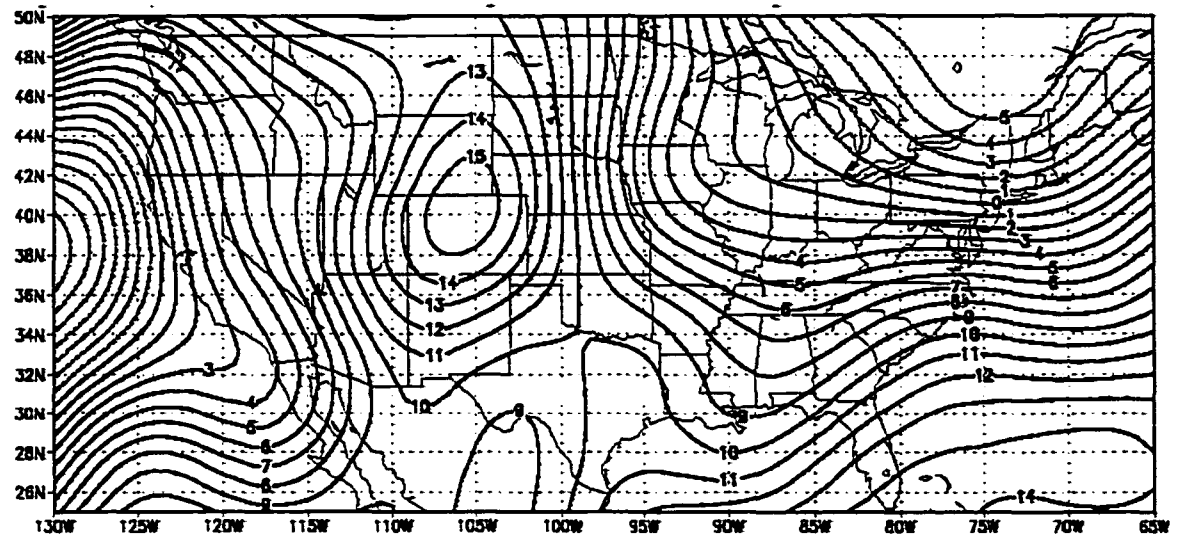

Figure 60. Event 1 - Event 4 August 850 mb Heights. Contours are 1 m

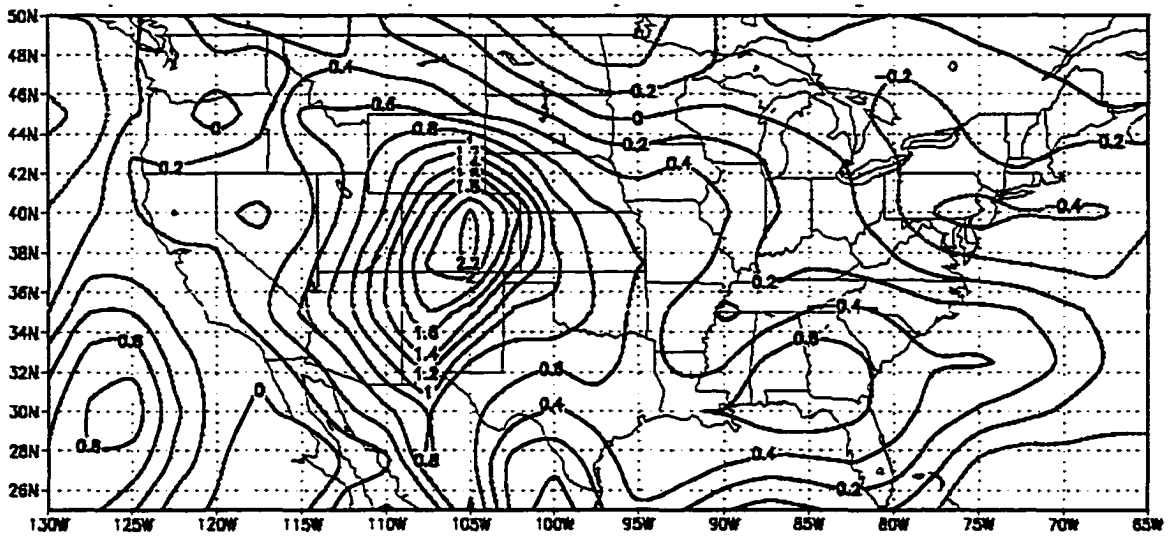

Figure 61. Event 1 - Event 4 August 850 mb Specific Humidity. Contours are 0.2 g kg^{-1}

level moisture ranges from 0.2 to 2.2 g kg^{-1} across the area, with the maximum occurring along the lee of the Rocky Mountains in eastern Colorado. The additional 2.2 g kg^{-1} in an Event 1 year is the largest magnitude increase of all warm season months. Again, putting the moisture content in terms of the dewpoint temperature, this is an additional increase of approximately 1.7^0 C at 850 mb. Additional moisture content in the lower level of the atmosphere plays a key role in precipitation differences upstream and across the NIIK region.

While the thermal advection patterns for Event 1 and 4 years are similar in magnitude, their spatial location exhibits a slight north-south difference. During Event 1 (4) years, the warm air advection maximum is located in southwest (northwest) Iowa. This slight spatial difference creates an interesting thermal advection pattern in the difference field. The difference field of thermal advection depicts a north-south couplet over the central and northern Plains region (Figure 62) (recall that the negative values of thermal advection correspond to smaller magnitudes of warm air advection). The west-east oriented axis of the couplet is located in the NIIK region, which is the location of the significant precipitation differences in August (Figure 15).

An additional explanation for the movement of convective systems along the NIIK region deals with the orientation of the 500 mb geopotential height pattern. The difference field of 500 mb geopotential heights depicts an amplified ridging (troughing) pattern in the western (eastern) portion of the NIIK region (Figure 63). Assuming as before, that convective systems move along the periphery of a 500 mb ridge, the NIIK region would be downstream from the initiation of convective systems, thus the movement and location of statistically significant precipitation differences can be explained.

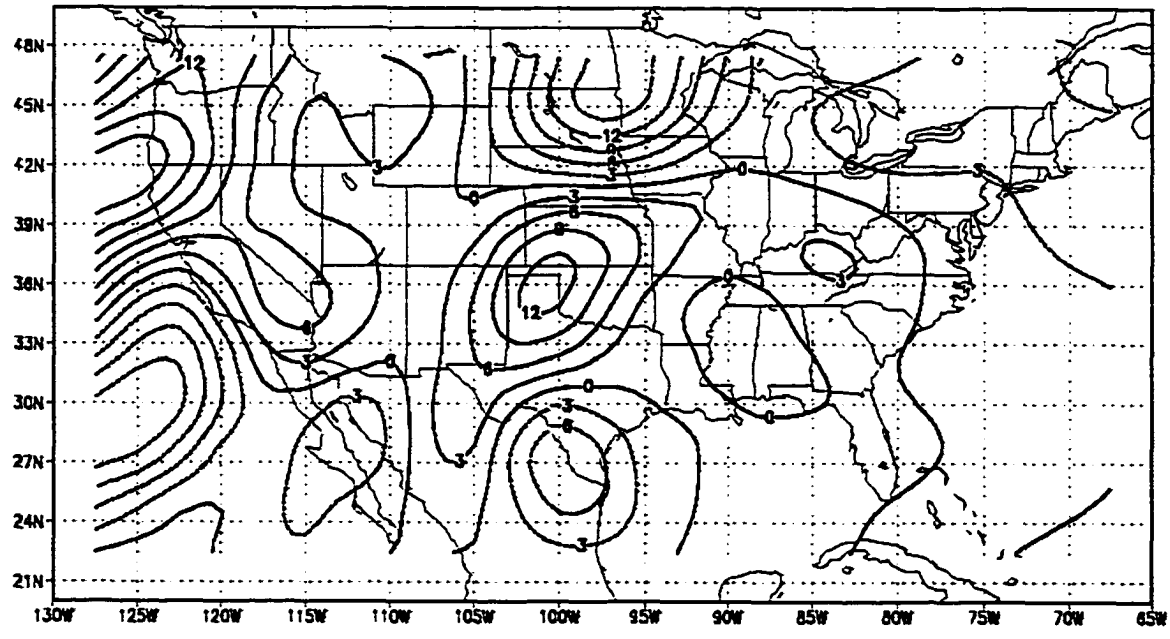

Figure 62. Event 1 - Event 4 August Temperature Advection. Contours are $3x10^{-6}$ K s^{-1}

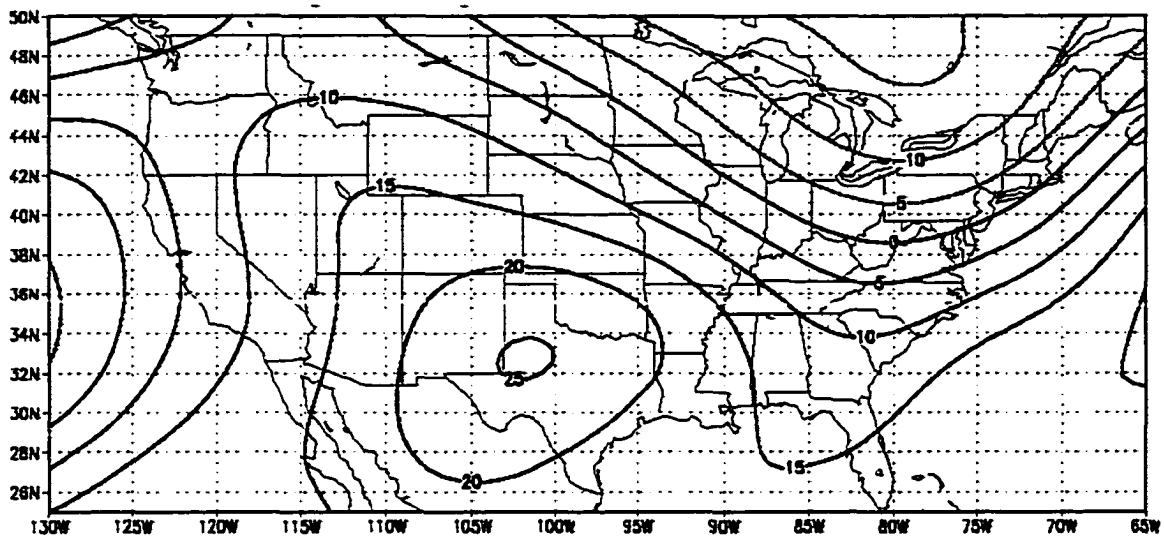

Figure 63. Event 1 - Event 4 August 500 mb Geopotential Heights. Contours are 1 m

Summary of August Atmospheric Parameters

August atmospheric parameters show differences in magnitude and spatial orientation between Event 1 and 4 years, which account for a portion of the differences in precipitation amounts across the NIIK region. There are several interesting contrasts with July's parameters, such as in the 850 mb thermal advection field (presence of a pronounced couplet in August versus a weak couplet in July), 850 mb specific humidity field (an additional 1 g kg^{-1} in August versus July), and the 500 mb geopotential height field (anomalous ridge out west in August which may have contributed to a diminished LLJ in an Event 1 year). It does appear that a favorable positioning of the upper air jet stream enhances divergence patterns in the upper atmosphere. Lower-level convergence is in phase with the above divergence patterns, promoting large scale lifting. Enhanced lower-level moisture along with a thermal advection couplet contributes positively to enhanced precipitation during Event 1 years.

September Atmospheric Parameters

Statistically significant precipitation differences in September move both poleward and eastward into the northern Plains and Ohio Valley, respectively (Figure 16). States that depict this precipitation difference are South Dakota, Minnesota, Wisconsin, Michigan, and Ohio (hereafter referred to as the SOWMM region). The number of state divisions that show statistically significant precipitation differences between Event 1 and 4 years is less than the July and August months, but similar to April (Appendix D). As in other months of the warm season, Event 1 years are wetter than their Event 4 counterparts, with the exception of Ohio, which shows enhanced precipitation during Event 4 years.

South Dakota experienced a median increase of 0.25 mm in an Event 1 versus Event 4 year; Ohio's median decrease is 12.51 mm; Wisconsin's median increase is 30.86 mm; Minnesota's median increase is 14.10 mm; and Michigan's median increase is 25.21 mm.

Note the lack of coherence within the SOWMM region. Wisconsin's median increase is 2.5 times the median increase in Minnesota, with South Dakota showing virtually no difference in precipitation based upon Event 1 versus Event 4 years. While Michigan and Ohio are spatially close, the precipitation differences are of opposite phase with Michigan (Ohio) receiving more (less) precipitation in Event 1 years. September, like April, is a month in which synoptic scale frontal systems are active across the grain-producing region of the U.S., therefore, as in April, atmospheric parameters that account for precipitation variability may not be as readily identifiable as in July and August.

The 200 mb difference field depicts an enhanced (reduced) jet stream over the southern (northern) portion of the U.S. during Event 1 years (Figure 64). The weaker winds at this level during Event 1 years will not contribute positively to large scale lifting over the SOWMM region.

Upper-level convergence is present during both Event 1 and 4 years over the SOWMM region. However, the difference field shows that convergence aloft is weaker during Event 1 years, allowing for a slightly less inhibiting environment for large scale lifting across the SOWMM region (Figure 65).

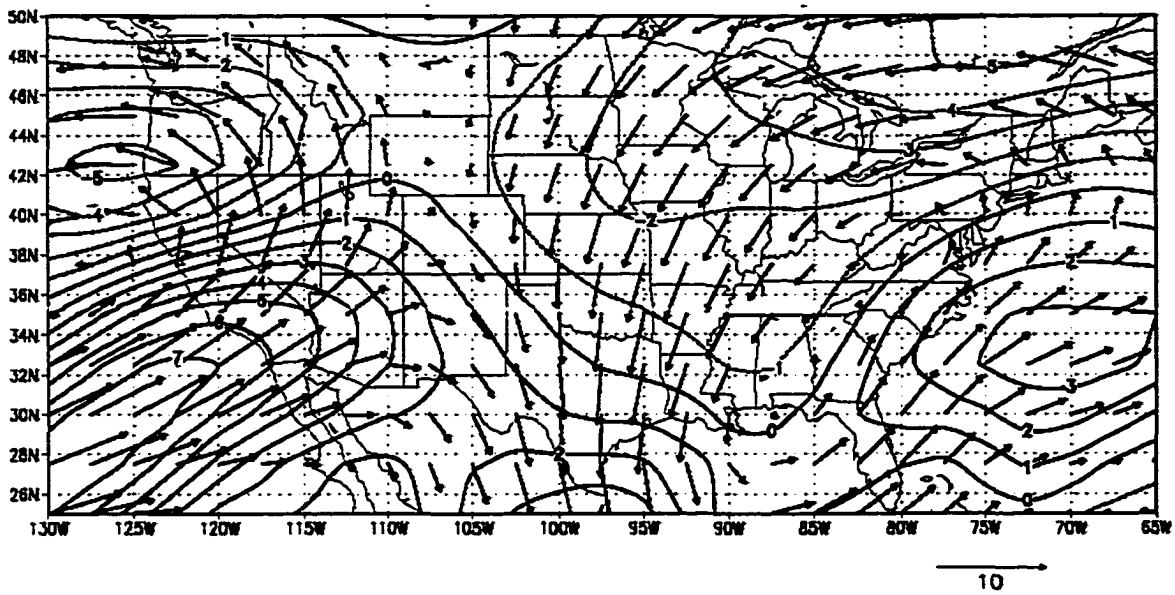

Figure 64. Event 1 - Event 4 September 200 mb Winds. Contours are 1 m s^{-1}

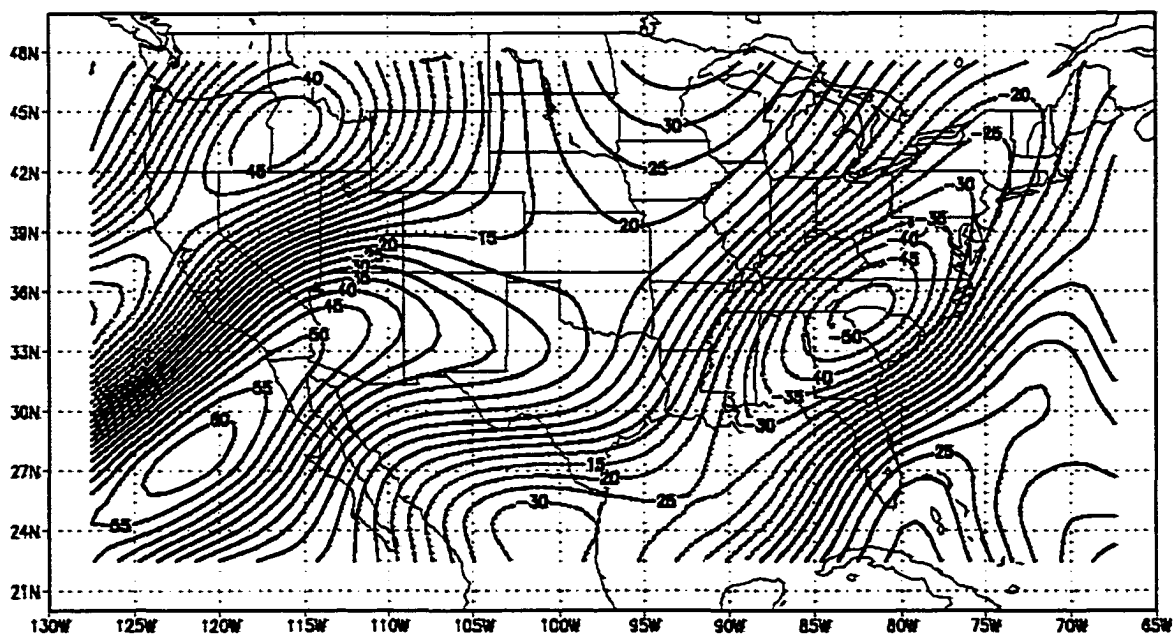

Figure 65. Event 1 - Event 4 September 200 mb Divergence. Contours are 5x10^{-7} s^{-1}

Earlier, it was shown that precipitation differences between Event 1 and 4 years in South Dakota were not very pronounced. In portions of South Dakota, Event 4 years show an increase in median precipitation amounts over Event 1 years. This may be due to the lower-level convergence field across the SOWMM region. In Event 1 years, the lower-level convergence field is weak (near 0-1x10^{-7} s^{-1}) across South Dakota but increases (2-4x10^{-7} s^{-1}) northeastward into the heart of the SOWMM region, where there are significant precipitation differences (Figure 66). The increased precipitation in an Event 1 year over northern Ohio is difficult to account for by the convergence field. There is an area of lower-level divergence over northern Ohio, which would be an environment not conducive to upward motion. During Event 4 years lower-level convergence is stronger and displaced poleward into Nebraska and South Dakota. Western portions of South Dakota show an increase in median precipitation during Event 4 years near the convergence area (Figure 67).

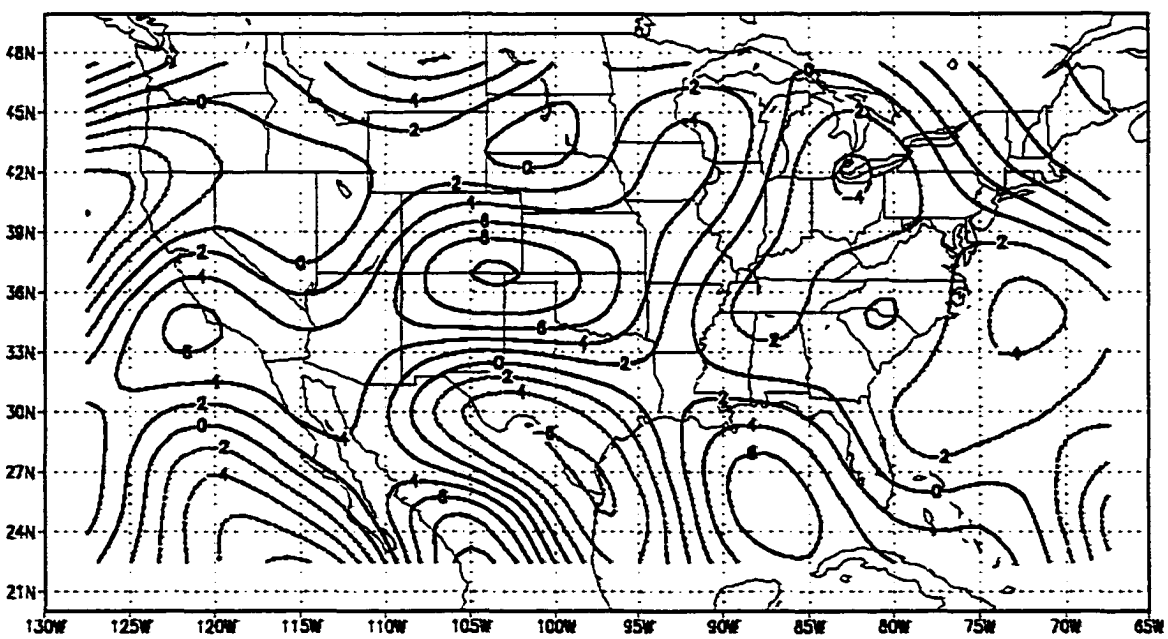

Figure 66. Event 1 September 850 mb Convergence. Contours are 2x10^{-7} s^{-1}

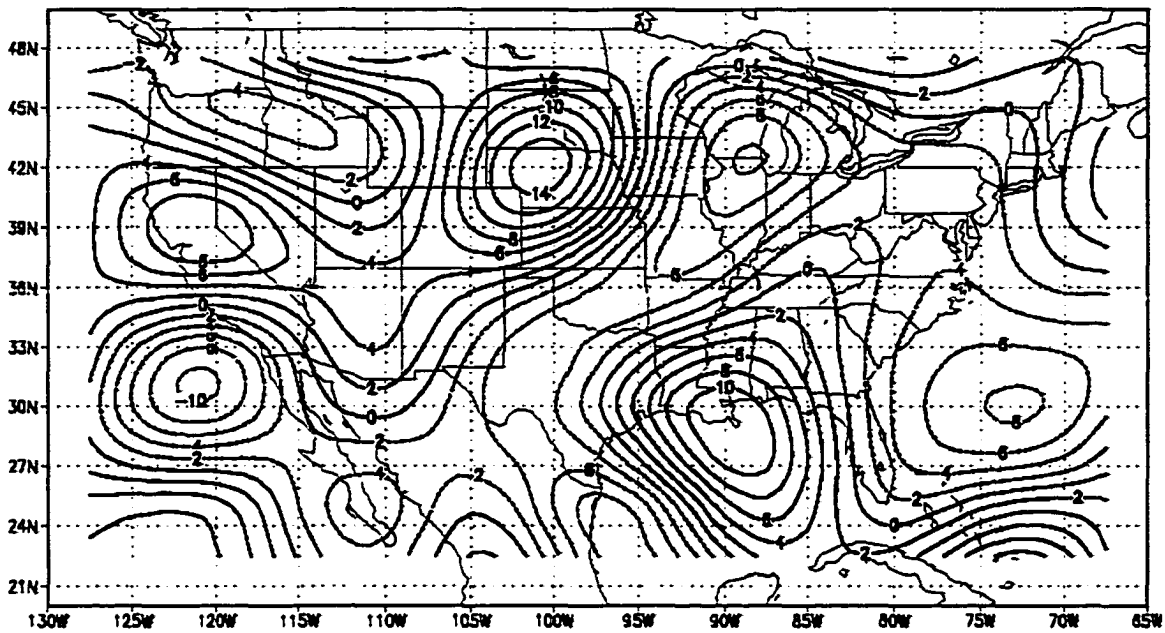

Figure 67. Event 4 September 850 mb Convergence. Contours are $2x10^{-7}$ s^{-1}

The difference field of lower-level convergence depicts an east-west couplet. The western portion of the couplet shows the predominance of convergence during Event 4 years and the lack of divergence over the eastern portion during Event 1 years (Figure 68).

The difference field of the 850 mb winds shows little difference (less than 0.5 m s^{-1}) between Event 1 and 4 years (Figure 69). The wind field was oriented southwest to northeast across the SOWMM region during both Event 1 and 4 years (not shown), which does imply some spatial phasing with the convergence difference field (Figure 68).

The small magnitude difference between the 850 mb wind speeds in Event 1 and 4 years can be attributed to a weak pressure gradient between the western Plains and the Bermuda High (Figure 70). The weak pressure gradient is attributed to an absence of a dipole between the Rockies and the Gulf coast in August (Figure 60) and September (Figure 70). During July, there was a pronounced pressure gradient between the two regions, which produced the differences in the low-level wind speeds (Figure 44).

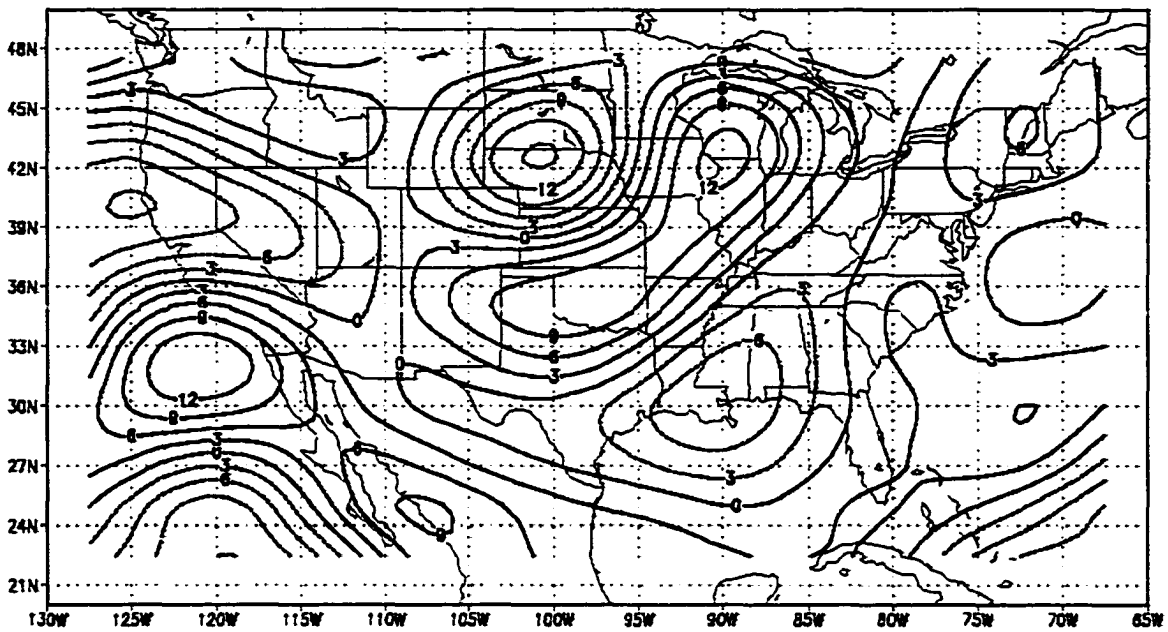

Figure 68. Event 1 - Event 4 September 850 mb Convergence. Contours are $3x10^{-7}$ s^{-1}

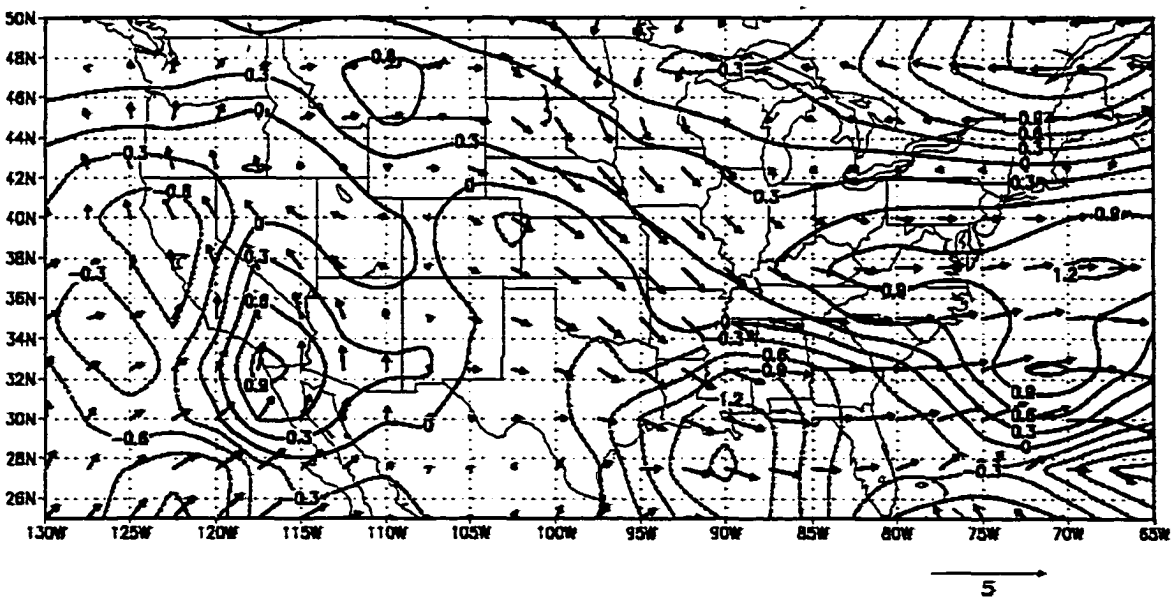

Figure 69. Event 1 - Event 4 September 850 mb Winds. Contours are 0.3 m s^{-1}

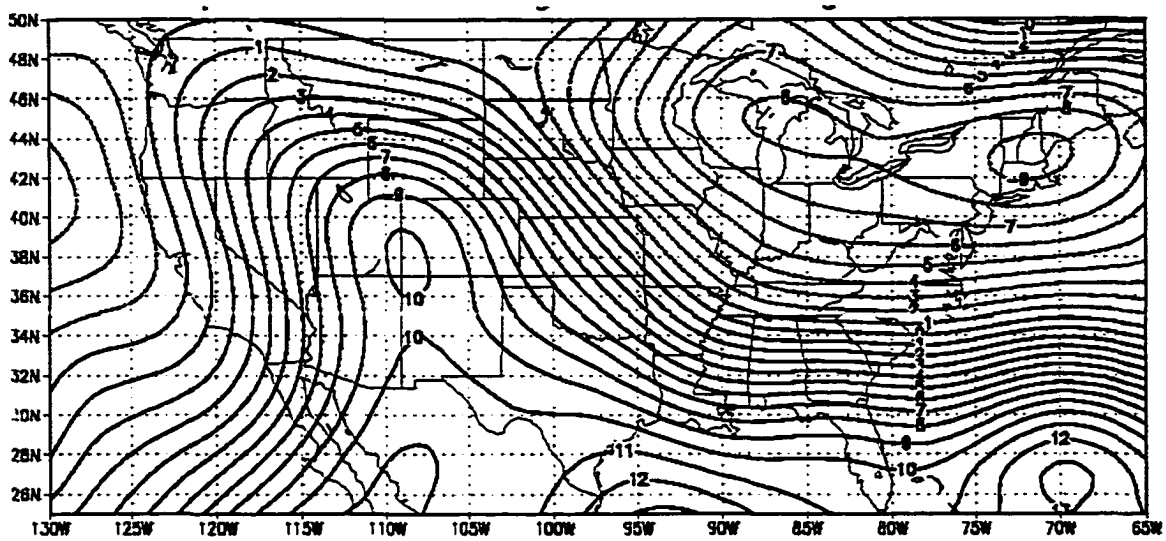

Figure 70. Event 1 - Event 4 September 850 mb Heights. Contours are 1 m

Lower-level moisture increases (0.2 -0.4 g kg^{-1}) across most of the SOWMM region during Event 1 years, with the exception of Ohio (Figure 71). Relating the values of specific humidity in terms of the dewpoint temperature, amounts to an increase of 1.3^0 C. There is also a maximum difference in the moisture field located at approximately 40^0 N and 110^0 W. This position is on the windward side of the Rocky Mountains, an area generally not associated with the initiation of MCC activity; most of the convective activity is concentrated along the leeward side.

Thermal advection patterns depict maximum warm air advection in the area south of the SOWMM region in both Event 1 and 4 years (not shown). Maximum differences in the thermal advection field are centered over Oklahoma, with stronger magnitude warm air advection during Event 1 years (Figure 72).

Mid-level geopotential height difference fields show the presence of a ridge axis over the western Plains during Event 1 years (Figure 73). Event 4 years depict a lower amplitude pattern that is zonal across the U.S. Convective activity along the periphery of the ridge axis would move downstream through the SOWMM region.

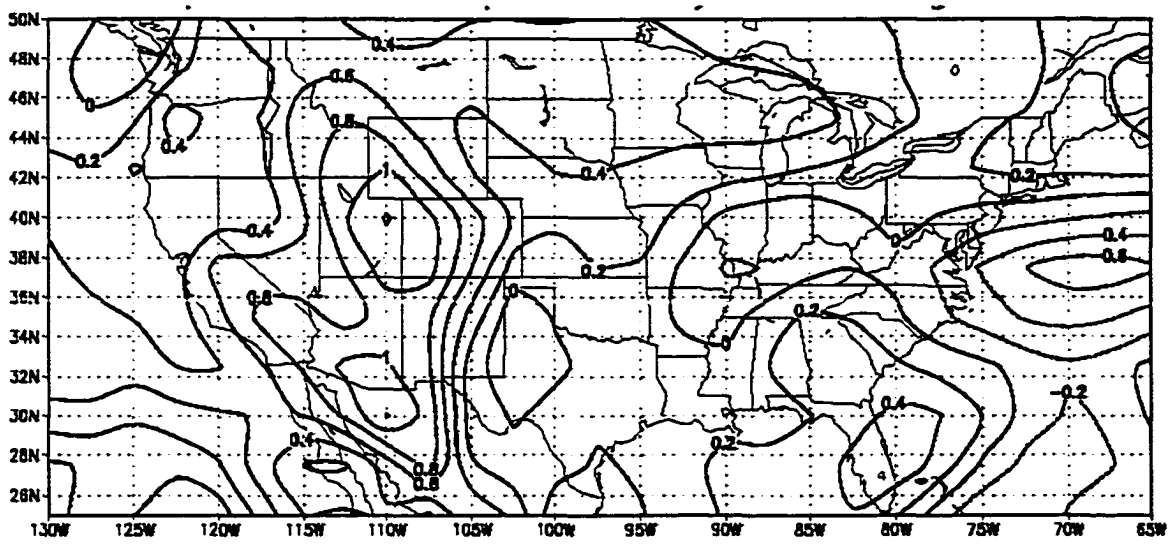

Figure 71. Event 1 - Event 4 September 850 mb Specific Humidity. Contours are 0.2 g kg^{-1}

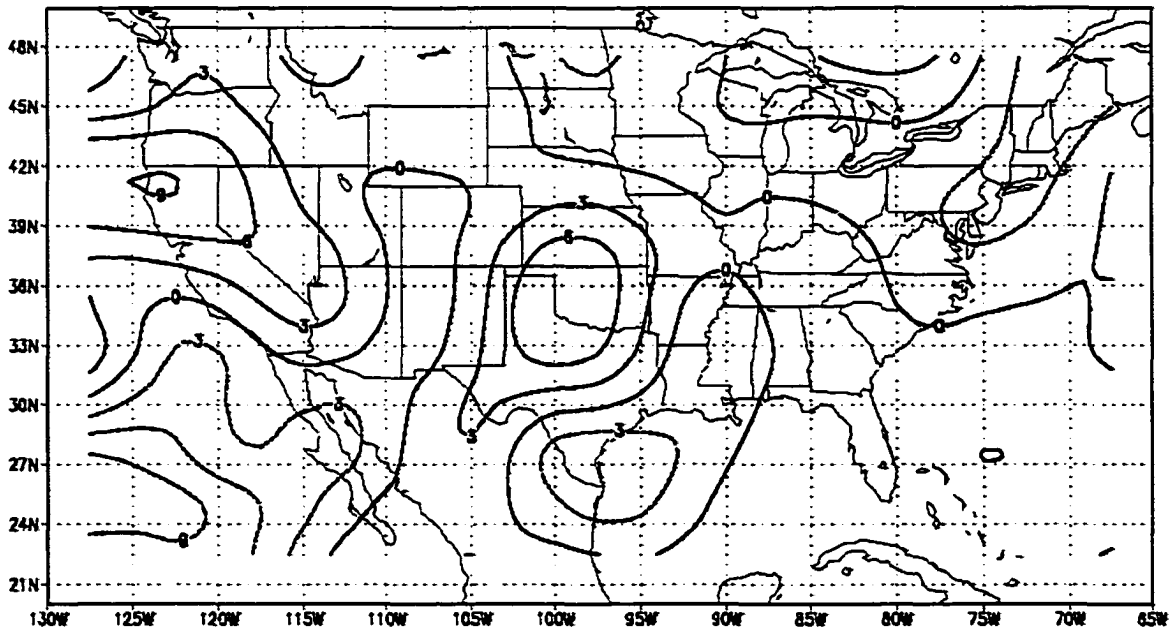

Figure 72. Event 1 - Event 4 September Temperature Advection. Contours are $3x10^{-6}$ K s^{-1}

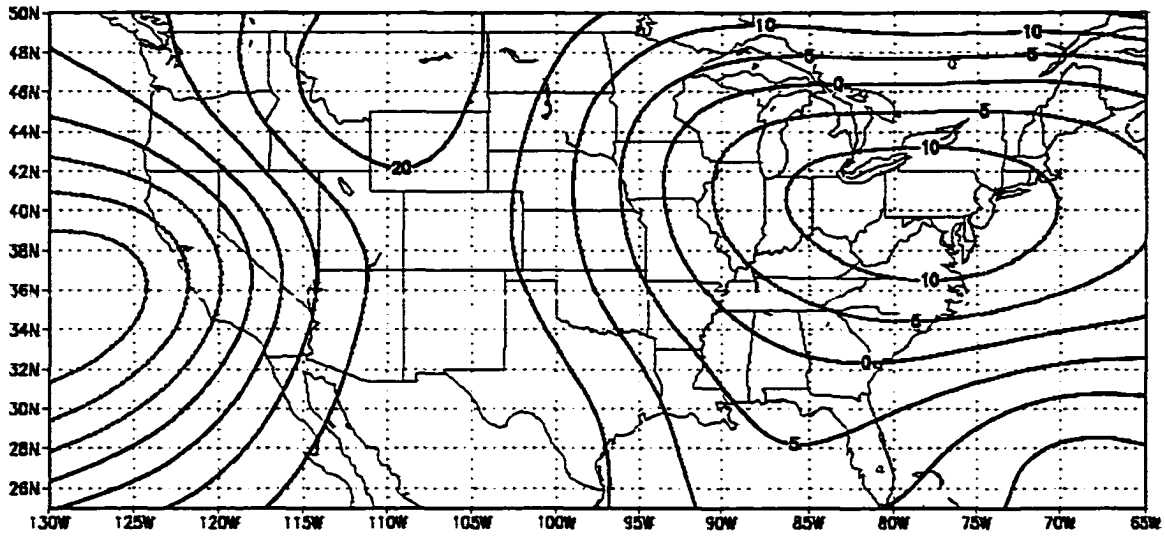

Figure 73. Event 1 - Event 4 September 500 mb Geopotential Heights. Contours are 5 m

Summary of September Atmospheric Parameters

Compared to July and August atmospheric parameters, September parameters are not as spatially coherent with the precipitation differences across their respective regions. Part of the reason for this spatial incoherency may be a result of September being a transition period from convective systems to a combination of both convective and stratiform systems.

There are some parameters that can be used to account for the precipitation differences across the SOWMM region. Parameters such as lower-level convergence and specific humidity appear to provide most of the physical basis behind the precipitation differences across the region.

During Event 1 years, lower-level convergence was a maximum over the southern Plains, but a lobe of convergence extended northward across portions of Minnesota and Wisconsin (Figure 66). In Event 4 years, lower-level convergence was stronger in magnitude and positioned poleward over South Dakota (Figure 67). The positioning and strength of this parameter corresponds with enhanced precipitation during Event 4 years over portions of South Dakota (Appendix C). The difference field of lower-level

convergence is a maximum over Wisconsin, which also corresponds to the largest median differences in precipitation across the SOWMM region (Figure 68). Specific humidity values depict the largest differences across the SOWMM region (Figure 71). Lifting and enhanced moisture are present and in phase over portions of the SOWMM region, with the exception of Ohio. Recall that portions of Ohio have enhanced precipitation during Event 4 years.

Marginal atmospheric parameters such as upper-level divergence, lower-level wind field and thermal advection may not enhance precipitation development in Event 1 years, but they do not suppress it. Upper-level convergence is present in both Event 1 and 4 years, but of weaker magnitude during Event 1 years (Figure 65). There is a weak maximum present in the lower-level wind field over the western portion of the SOWMM region (Figure 69). Thermal advection patterns are a maximum to the south of the SOWMM region, but exhibit little difference between Event 1 and 4 years (Figure 72).

Parameters such as the 200 mb wind field and the 850 mb geopotential height field do not contribute positively to the median precipitation difference across the SOWMM region. The 200 mb wind field indicates the location of the jet stream along the east coast of the U.S. during both Event 1 and 4 years, and a weaker magnitude over the SOWMM region during Event 1 years (Figure 64). The 850 mb geopotential height difference field shows the absence of a pronounced pressure gradient between the western Plains and the Gulf of Mexico, thus, little difference in the wind field between Event 1 and 4 years.

September atmospheric parameters are much like April in that it is difficult to identify more than a few parameters that are conducive to producing precipitation differences across a region. There is still an atmospheric parameter signal present, but not as strong as in July and August.

Global Significance in Geophysical Fields

Previous sections have discussed the physical relationship between atmospheric parameters (cause) and precipitation (effect). Both have exhibited differences based upon

the phase of the ENSO/LNSO and PDO, and this section presents a quantitative measure of the differences by using a field statistic method derived from Livezey and Chen (1983) and Madden et al. (1993).

Livezey and Chen (1983) pointed out that many studies do not take into account the problems introduced with multiplicity and spatial correlation in geophysical fields. The first-tier of testing for significance deals with the issue of multiplicity through application of a binomial experiment. The underlying assumption is of independence between grid points in a field; however, this is often an incorrect assumption, especially, with fields of atmospheric parameters. Atmospheric parameters often exhibit a high degree of spatial correlation between locations, one such example in the reanalysis grid being the two gridpoints across Iowa. Geopotential heights, wind fields, and other atmospheric parameters often have similar magnitudes because of the proximity to each other. This reduces the degrees of freedom in an atmospheric field, thus, providing the motivation for the second-tier of significance testing, accounting for spatial correlation. To estimate the RDOF in a geophysical field, a method developed by Madden et al. (1993) was used in this research project. An unanticipated result of using this method was the discovery of negative degrees of freedom in some of the atmospheric fields. Obviously, negative degrees of freedom are not possible, and an inspection of the correlation function and the full term in Equation 5 was performed to check for accuracy of the integral calculations. Summations over a finite width were performed on the correlation function and the entire term; results were found to be similar to the integral calculation. Inspection of the Bessel function reveals a negative contribution, but this would not be a source of the negative degrees of freedom since the Madden et al. (1993) domain was global. However, their model domain exhibited little negative correlation between gridpoints. In contrast to their study, the atmospheric fields here exhibit a pronounced negative correlation over a spatial distance approximately ranging from 600-2400 km. An examination of the integral in Equation 5 reveals that a significant portion of the weighting is on the negative correlation values, thus, producing negative values of RDOF in some of the atmospheric fields. These fields are not deemed as significant or insignificant but subject to future analysis with a

correlation function that is not as sensitive to negative correlations between gridpoints (Wikle personal communication 2000).

Results from the two-tiered testing of atmospheric fields are presented in the following section. If a field passes (fails) the two-tiered test, it is interpreted as statistically significant differences (no difference) between Event 1 and 4 years. Results of the two-tiered tests are discussed in detail for April in order to describe the method and interpretation of the analysis. Results for the months of April and July-September are presented in tabular form (Table 3), with corresponding figures appearing in Appendix A.

Two-Tiered Statistical Significance Results

During April, the 850 mb wind field shows differences between Event 1 and 4 years for the first-tier of significance testing. The darker shaded grid points make up approximately 32% (73/225 grid points) of the field (Figure 74). This is well above the minimum threshold of 12.9% (29/225 grid points) needed to pass the first-tier of significance testing (see Figure 9). Since the first-tier of testing (multiplicity) has passed, it is now possible to move to the second-tier of significance testing (spatial correlation).

Using an adapted version of the Madden et al. (1993) method to account for spatial correlation in a geophysical field, our results indicate that the DOF is reduced from 225 to approximately 35 RDOF. From Figure 9, it can be seen that the 850 mb field has passed the second-tier of testing, since the 35 RDOF fall within the region above the curve, thus, the field can be declared significantly different between Events 1 and 4.

One of the reasons that the April 850 mb wind field showed statistically significant differences between Event 1 and 4 years is the rapid decrease in spatial correlation. Note that a grid point spacing of approximately 1100 km is required to ensure independence (a spatial correlation of zero) between grid points (Figure 75), versus 1600 km in the April 500 mb geopotential height field (not shown). These results suggest more grid points being retained in the domain, which is reflective of the higher RDOF in the April 850 mb wind field. It is also possible to achieve statistical significance with a large percentage of

Table 3. Results of field significance test.[1]

Month	Parameter	%FS	DOF	RDOF	SC=0	GFS
April	200 mb Divergence Field	19 ¶	297	NDF	1200 km	N/A
April	200 mb Wind Field	3 #	225			
April	500 mb Geopotential	10 #	225			
April	850 mb Convergence	20 ¶	297	NDF	1400 km	N/A
April	850 mb Specific Humidity Field	18 ¶	225	NDF	800 km	N/A
April	850 mb Temperature	24 ¶	297	NDF	1600 km	N/A
April	850 mb Wind Field	32 ¶	225	35	1100 km	§
July	200 mb Divergence Field	18 ¶	297	NDF	1000 km	N/A
July	200 mb Wind Field	17 ¶	225	NDF	1000 km	N/A
July	500 mb Geopotential	39 ¶	225	8	2000 km	§
July	850 mb Convergence	14 ¶	297	31	800 km	NS
July	850 mb Specific Humidity Field	28 ¶	225	18	2000 km	§

[1] %FS = percent field significance (first-tier test). DOF = Degrees of freedom (number of grid points in field). RDOF = Reduced degrees of freedom calculated from equation 5. SC = Distance where correlation equals zero. GFS = Global field significance (second-tier test). #, ¶, and §, indicates failure to pass the first-tier test at 15% level, passed the first-tier test at 15% level, and passed the two-tiered test at 10% level, respectively. NDF, N/A, and NS indicate negative degrees of freedom, not available due to the negative degrees of freedom, and not significant (failure to pass the second-tier test).

Table 3 (continued)

July	850 mb Temperature	15 ¶	297	96	800 km	§
July	850 mb Wind Field	15 ¶	225	81	800 km	§
August	200 mb Divergence Field	34 ¶	297	NDF	1200 km	N/A
August	200 mb Wind Field	36 ¶	225	16	1400 km	§
August	500 mb Geopotential	42 ¶	225	12	1800 km	§
August	850 mb Convergence	21 ¶	297	21	1800 km	§
August	850 mb Specific Humidity Field	24 ¶	225	NDF	1400 km	N/A
August	850 mb Temperature	24 ¶	297	NDF	1200 km	N/A
August	850 mb Wind Field	22 ¶	225	8	2400 km	NS
September	200 mb Divergence Field	18 ¶	297	NDF	1000 km	N/A
September	200 mb Wind Field	14 ¶	225	9	1700 km	NS
September	500 mb Geopotential	23 ¶	225	NDF	1400 km	N/A
September	850 mb Convergence	7 #	297	NDF	600 km	N/A
September	850 mb Specific Humidity Field	18 ¶	225	14	2000 km	NS
September	850 mb Temperature	11 #	297			
September	850 mb Wind Field	10 #	225			

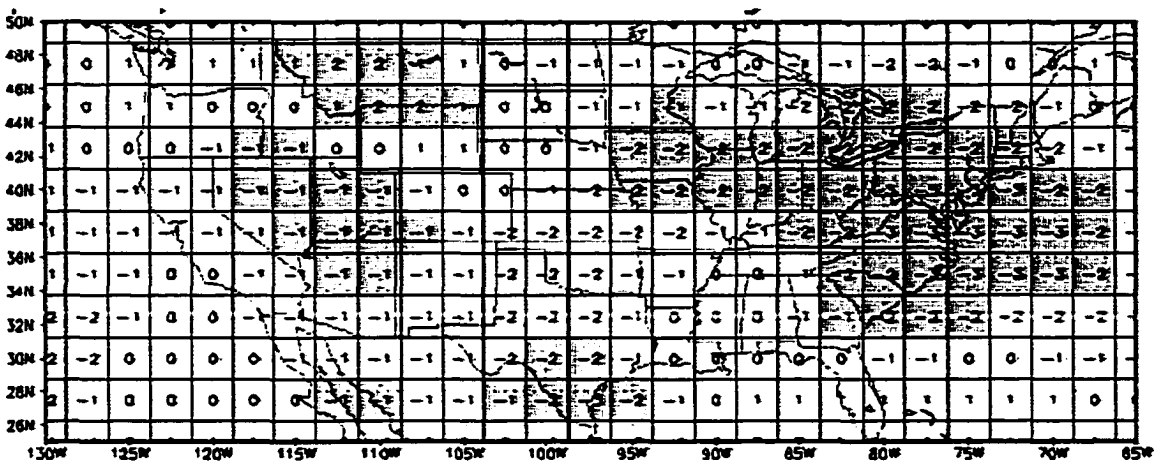

Figure 74. April difference field of 850 mb wind field in m s^{-1}. Darker shaded areas correspond to Student's t-test significance at the 10% level

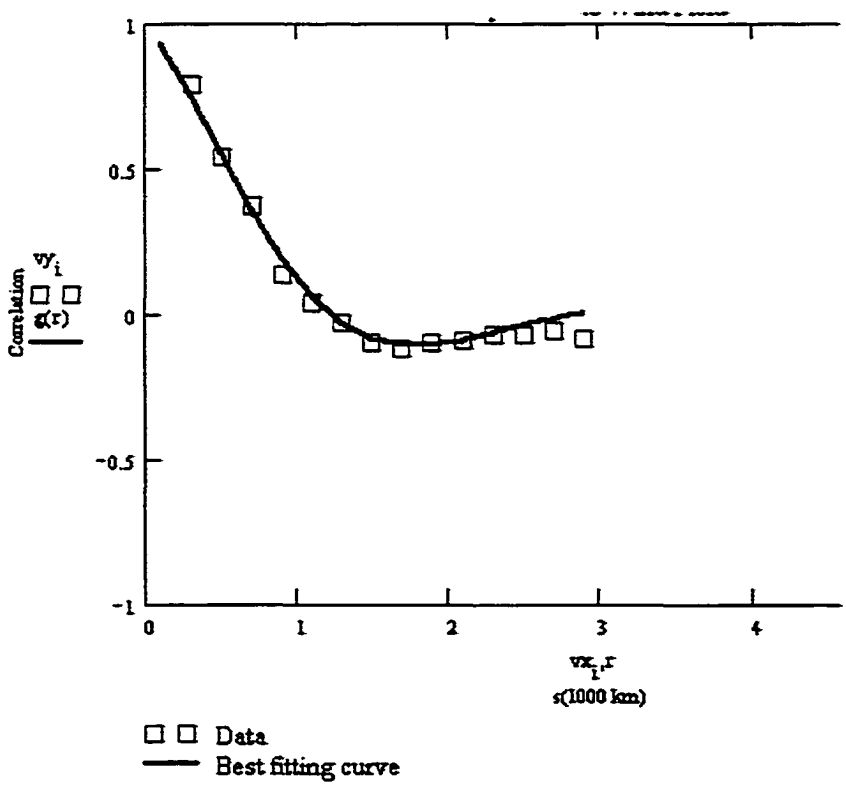

Figure 75. Spatial correlation between April 850 mb wind field grid points separated by an approximate distance of s

the field (greater than 30%) showing differences.

The RDOF for the April 850 mb wind field is larger than results from Livezey and Chen's (1983) RDOF of 30-60 over a global domain during the warm season; recall that this domain is limited to the continental U.S. An explanation for the larger RDOF in this study is due, in part, to the fields used. Their study was based on the 700 mb geopotential height field, which is typically more spatially correlated than the 850 mb wind field in the current study. Results with the April 500 mb geopotential height field (not shown) from this study compares favorably (RDOF=5) with the Livezey and Chen (1983) study.

Table 3 presents some interesting results in that most of the statistically significant fields are in July and August. It is difficult to glean much information from April and September atmospheric parameters since most fields exhibited negative DOF (with the exception of the April 850 mb wind field which shows global significance). However, July parameters exhibit global significance in four of the seven fields. This is an interesting result when you recall that during July the precipitation differences were the most spatially coherent of any warm season month (Figure 14). Global significance is concentrated in the middle and lower levels of the atmosphere. Three of the 850 mb fields, wind, specific humidity, and thermal advection all are globally significant. This is expected since all three are connected physically by the wind field. August parameters exhibited global significance at low (850 mb convergence field), middle (500 mb geopotential field), and upper (200 mb wind field) regions of the atmosphere.

From Table 3, it is apparent that most of the global field significance is concentrated in July and August. These two months exhibit the most spatially coherent precipitation signal (Figures 14 and 15) due to the favorable positioning of atmospheric parameters conducive to lifting and moisture presence, which is being reflected by the statistically significant fields.

CONCLUSIONS

This research project found its genesis in the previous work of Carlson et al. (1996). Their work identified a distinct warm season precipitation signal across portions of the grain belt. The precipitation signal was strongest when segregated by the phase of the SOI, with values less (greater) than 0.8 representative of wet (dry) and cool (warm) conditions across portions of the grain belt. The goal of this research is to extend their work into identifying physical mechanisms responsible for the precipitation variability across the grain producing regions of the U.S.

Physical mechanisms that account for warm season precipitation variability across the grain belt can be difficult to link directly from the tropics (teleconnections), due to the trapping of poleward propagating waves by the tropical easterlies (Lau and Peng 1992). Therefore, in addition to segregating the data by conditions in the tropics (ENSO/LNSO), it was decided to include the extratropics (PDO) since this region is in an environment that may be more conducive to downstream teleconnections during the warm season.

Corn yields, precipitation, and atmospheric parameters were segregated by Event 1 and 4 years (Table 1). Results of this segregation produced identifiable and spatially coherent precipitation signals across portions of the grain-producing region during the warm season. Most notable were the months of April and July-September. Precipitation amounts were elevated during Event 1 years over most of the grain-producing region of the U.S. (with a few exceptions during September. Precipitation fields also exhibited a high degree of spatial coherence (Figures 13-16). The most coherent of all months, July, featured a strong spatial signal over the northern Plains. The location of the statistically significant (at the 15% level) precipitation fields is in good agreement with other studies such as Bunkers et al. (1996) and Ting and Wang (1997); which discovered detectable precipitation signals over the Dakotas and Northern Plains, respectively.

While the results from the precipitation analysis in this study are also in good agreement with Carlson et al. (1996), analyses of atmospheric parameters were performed to elucidate the connection between cause (atmospheric parameters) and effect

(precipitation). Results are very encouraging, especially during July and August. During July, contributions came from all levels of the atmosphere and were located upstream of the DWIM region (Dakotas, Wisconsin, northeast Iowa, and Minnesota). The lower-levels provide lifting in the form of thermal advection and convergence (which is also in phase with upper-level divergence). The moisture field, represented by specific humidity, depicts excess moisture on the order of 1 g kg^{-1} over a large region during Event 1 years (Figure 45). The 500 mb geopotential height field depicts lower (higher) heights upstream (downstream) of the DWIM region. This configuration is similar to the 1993 flood year presented in Arritt et al. (1997) and Bell and Janowiak (1995). This configuration tends to act as a duct for convective systems into the DWIM region.

August atmospheric parameters were favorable for producing additional (less) precipitation in an Event 1 (4) year. As compared to July, the statistically significant precipitation differences between Event 1 and 4 years move southward into the NIIK region during August. The main atmospheric forcing during August tends to be in the form of Dines Compensation and thermal advection fields. The distinct thermal advection couplet appears to be the most interesting feature in August. The precipitation field tends to fall within the west-east axis of the thermal advection couplet. This is also seen with the weak southwest-northeast oriented couplet in July.

Carlson (personal communication 2000) has segregated 99 years of corn yields by all four combinations of ENSO/LNSO and PDO (Figure 5). The corn yield response that he has discovered is one of enhanced (diminished) yields during Event 1 (2) and 3 (4) years (Figure 5). Notice that the most consistent signal (yield reduction between 5 and 10% below trend) occurs in Event 4 years when yields are below trend over the entire grain-producing region. This is similar to the results in this study where the strongest (moderate) statistical signals in corn yield distributions occur in Event 4 (1) years (Table 2). From this information, it can be stated that a decrease of precipitation during portions of the warm season (especially during July and August) can negatively impact corn yields. The cause for the decrease in precipitation can be ascribed to unfavorable atmospheric parameters present over the grain-producing region. Some of the unfavorable parameters

consist of a decrease in the amount of low-level moisture present across the region during Event 4 years (the inverse of Figures 45 and 61). An absence of low-level forcing, as seen by the presence of divergence over a large region where MCC genesis typically occurs (Figure 57), and reduced 850 mb winds (inverse of Figure 41) play a role in diminished precipitation during Event 4 years.

The physical arguments presented above are further supported by the statistical results discovered by this research. Most notably the identification of global significance of atmospheric parameter fields during July and August. Results from the statistical analysis found fields such as the 500 mb geopotential heights, 850 mb specific humidity, 850 mb temperature advection, 850 mb winds, 200 mb winds, and 850 mb convergence that are globally significant.

The above results reflect a sense of cohesiveness, especially in July and August, between corn yields, precipitation, and the atmospheric parameters that account for a portion of the variability in precipitation, which in turn affects corn yield variability. Results from this research can be used to infer tendencies in crop yields and precipitation fields over portions of the grain-producing regions of the U.S. based upon the phase of the ENSO/LNSO and PDO. This gives forecasters a six to 12 month lead-time due to the predictability of ENSO/LNSO events and the stability of PDO. This work also provides a useful method to evaluate the overall significance of geophysical fields, an application useful to atmospheric modelers.

There are many opportunities to extend the work of this research. An obvious extension would be the determination of global significance in fields that exhibit pronounced negative correlations, which in turn leads to negative degrees of freedom with the use of the current correlation function. The most obvious choice for a solution would be the use of a correlation function that is not as sensitive to negative correlations in the field.

Recall that an assumption of this project was that MCWS account for a significant portion of the warm season precipitation variability across the grain-producing region of the U.S. Atmospheric parameters that are conducive to development (non-development) of

MCWS were identified in this research; therefore, another possible extension would be an analysis of MCWS variability based upon Event 1 and 4 years.

Finally, while the results presented here identify spatial patterns within atmospheric fields that account for a portion of the precipitation variability, and by extension corn yield variability, it masks the magnitude of the quantitative results due to averaging monthly fields. It is suggested that future work decrease the time scale from monthly to daily averaging of events, which in turn will further elucidate the magnitudes of atmospheric parameters that account for a portion of precipitation and corn yield variability.

APPENDIX A. FIRST-TIER TEST AND CORRELATION VERSUS DISTANCE.[1]

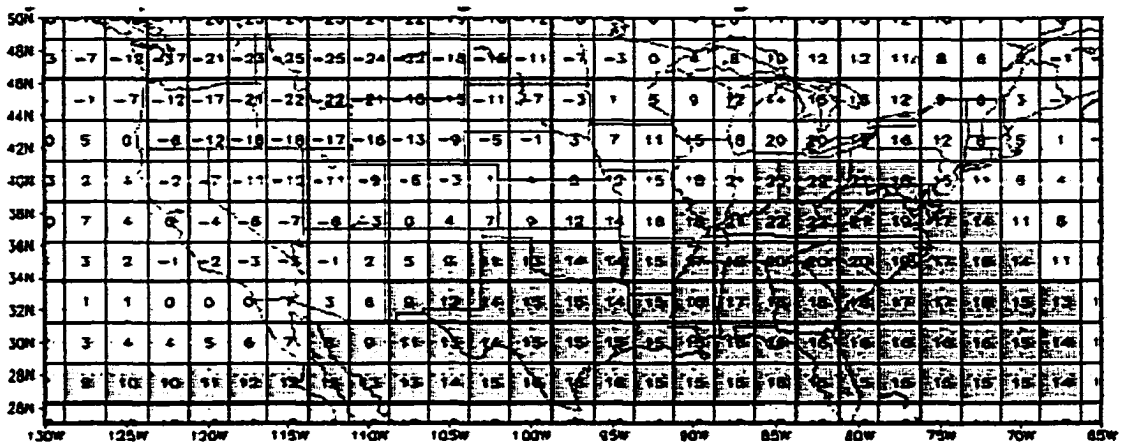

July difference field of 500 mb Geopotential heights in m. Darker shaded areas correspond to Student's t-test significance at the 10% level

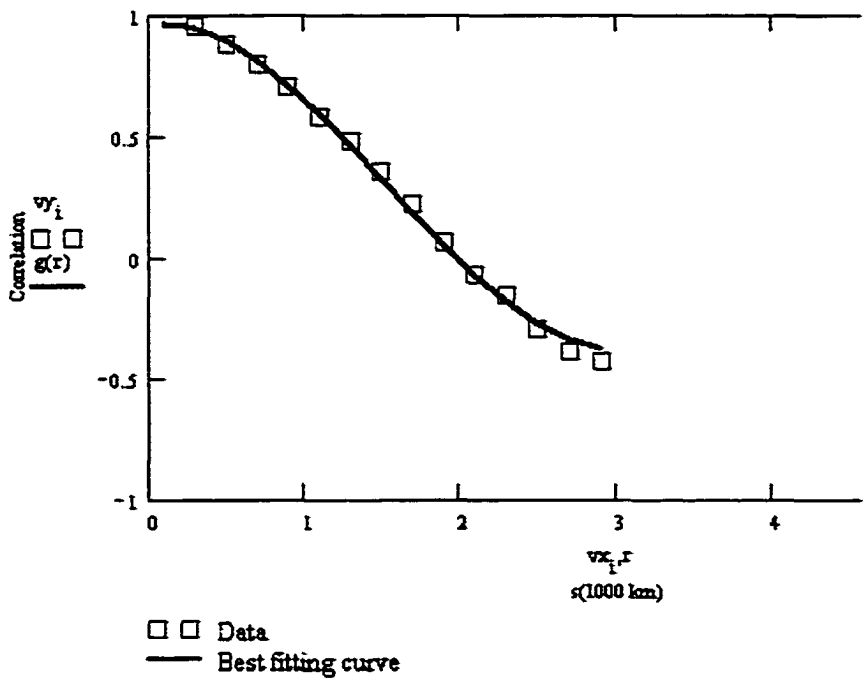

Spatial correlation between July 500 mb geopotential height field grid points separated by an approximate distance of s.

[1]**Shaded grid points indicate significance at the 10% level.**

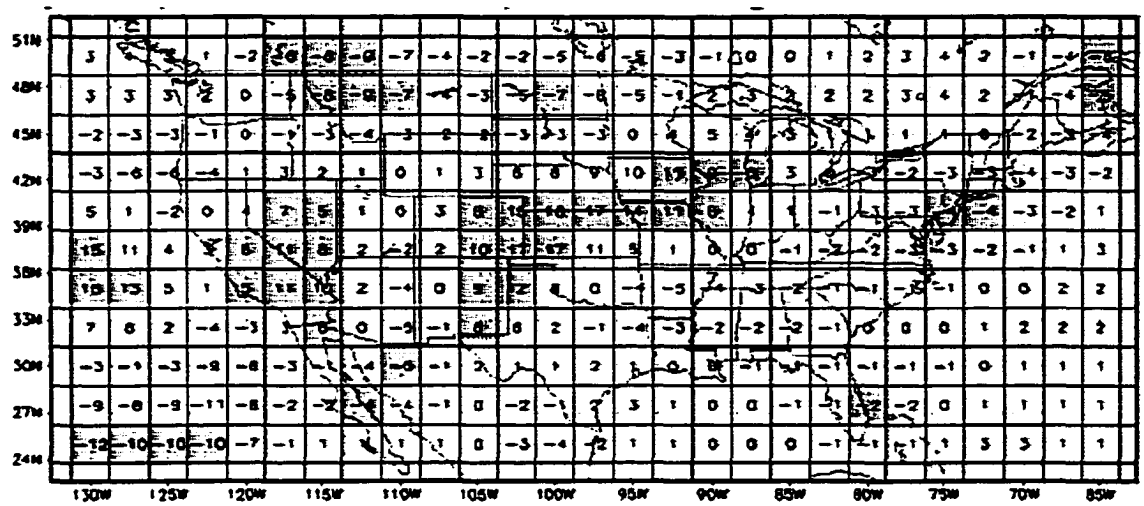

July difference field of 850 mb temperature advection in K s^{-1}. Darker shaded areas correspond to Student's t-test significance at the 10% level

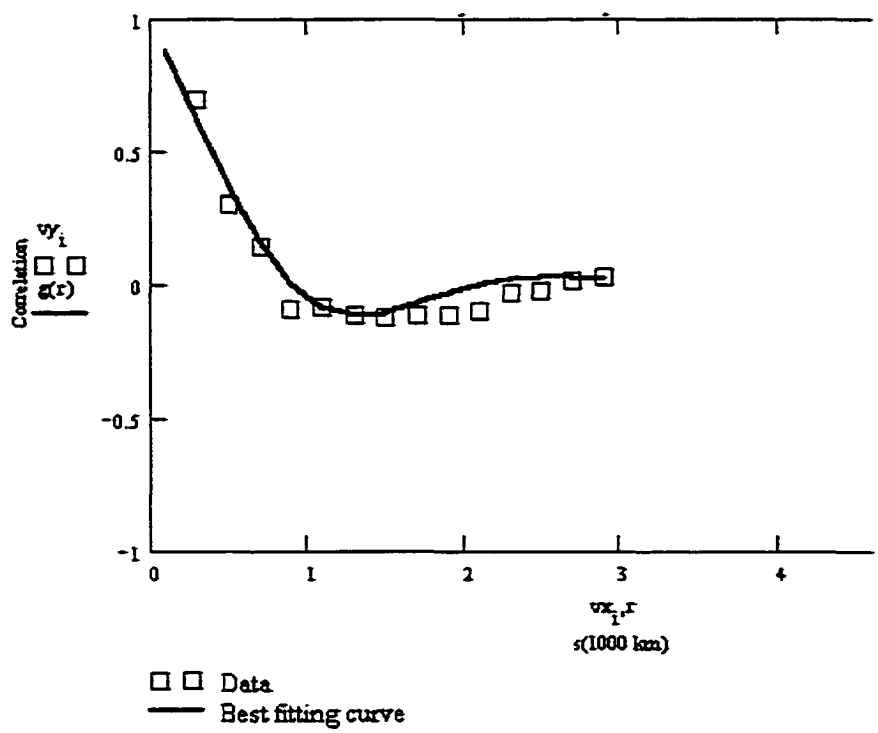

Spatial correlation between July 850 mb temperature advection field grid points separated by an approximate distance of s.

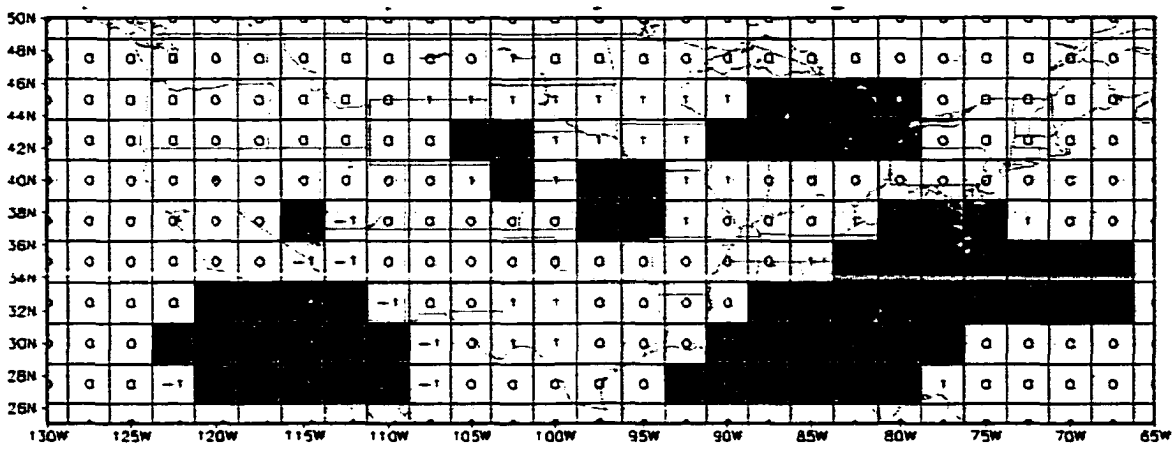

July difference field of 850 mb Specific Humidity in g kg^{-1}. Darker shaded areas correspond to Student's t-test significance at the 10% level

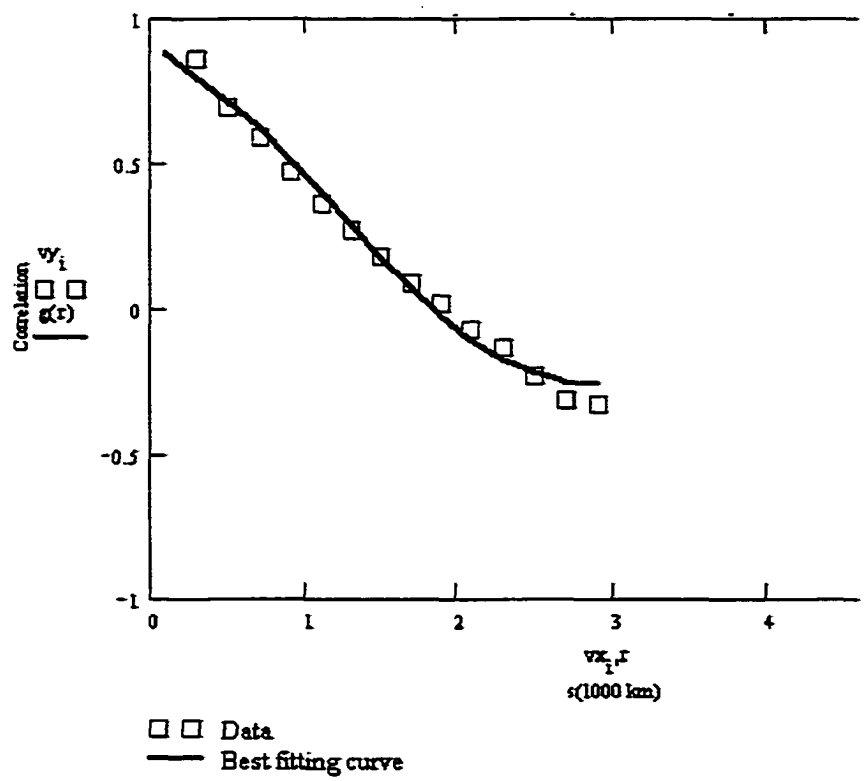

Spatial correlation between July 850 mb Specific Humidity field grid points separated by an approximate distance of s.

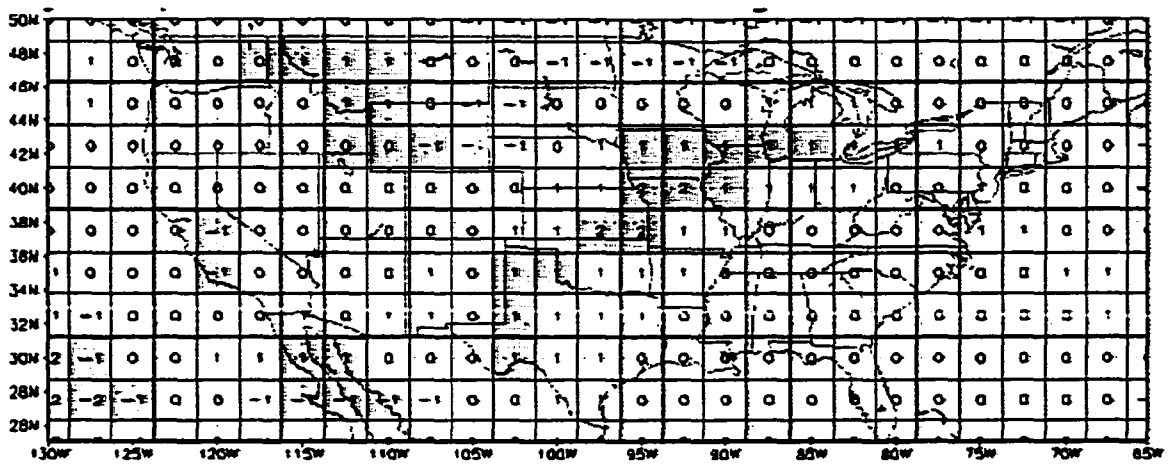

July difference field of 850 mb winds in m s^{-1}. Darker shaded areas correspond to Student's t-test significance at the 10% level

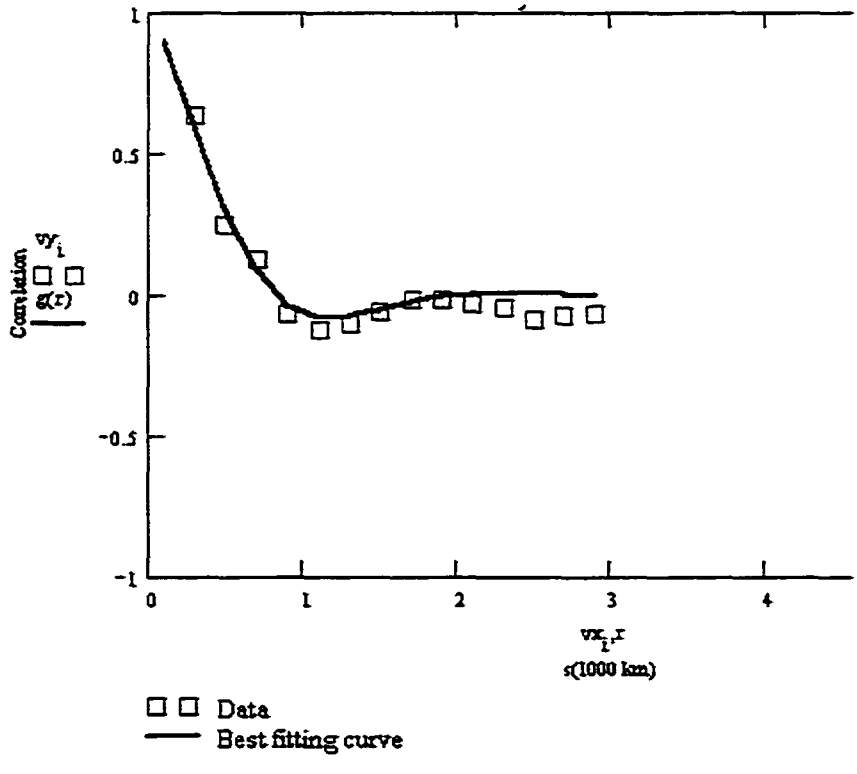

Spatial correlation between July 850 mb wind field grid points separated by an approximate distance of s.

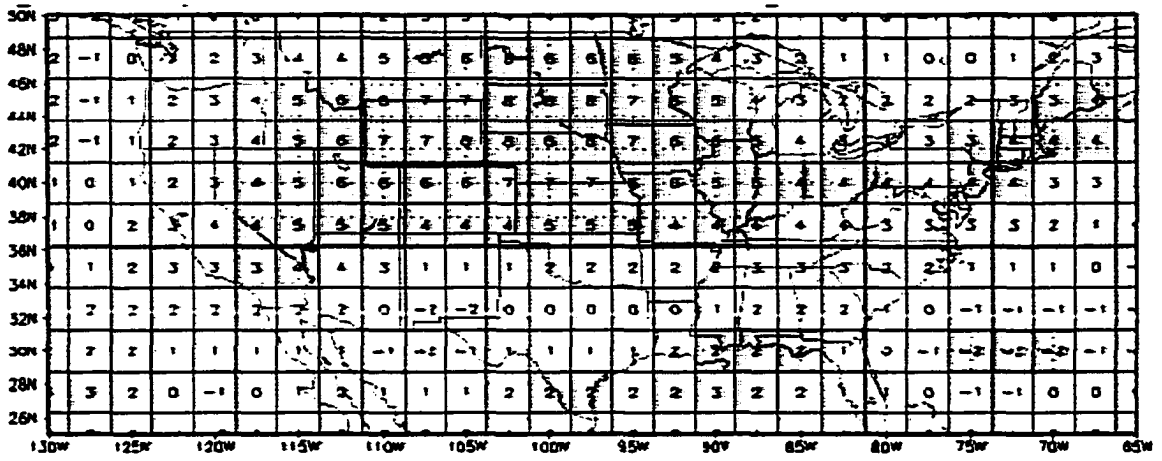

August difference field of 200 mb winds in m s^{-1}. Darker shaded areas correspond to Student's t-test significance at the 10% level

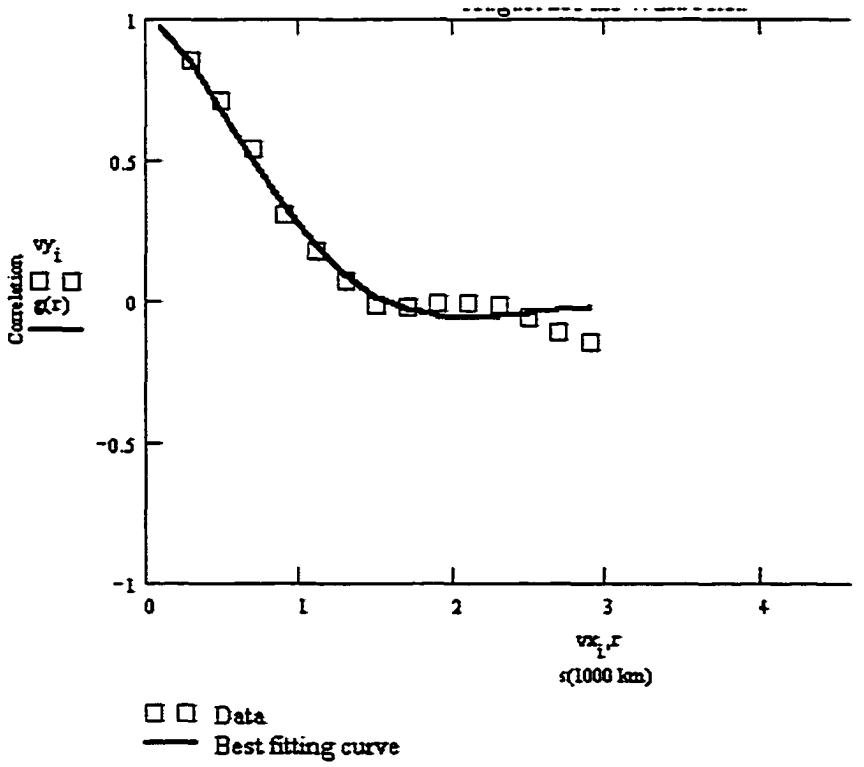

Spatial correlation between August 200 mb wind field grid points separated by an approximate distance of s.

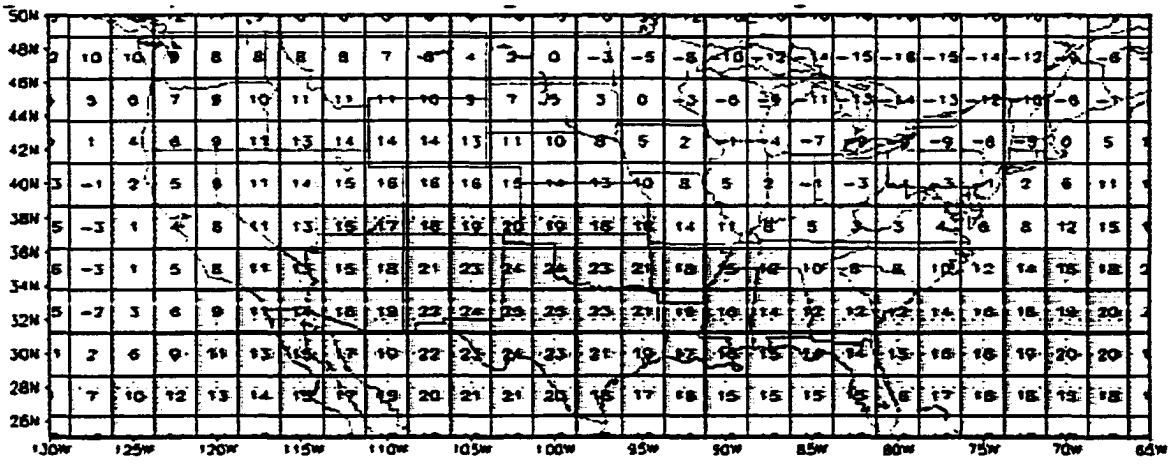

August difference field of 500 mb Geopotential heights in m. Darker shaded areas correspond to Student's t-test significance at the 10% level

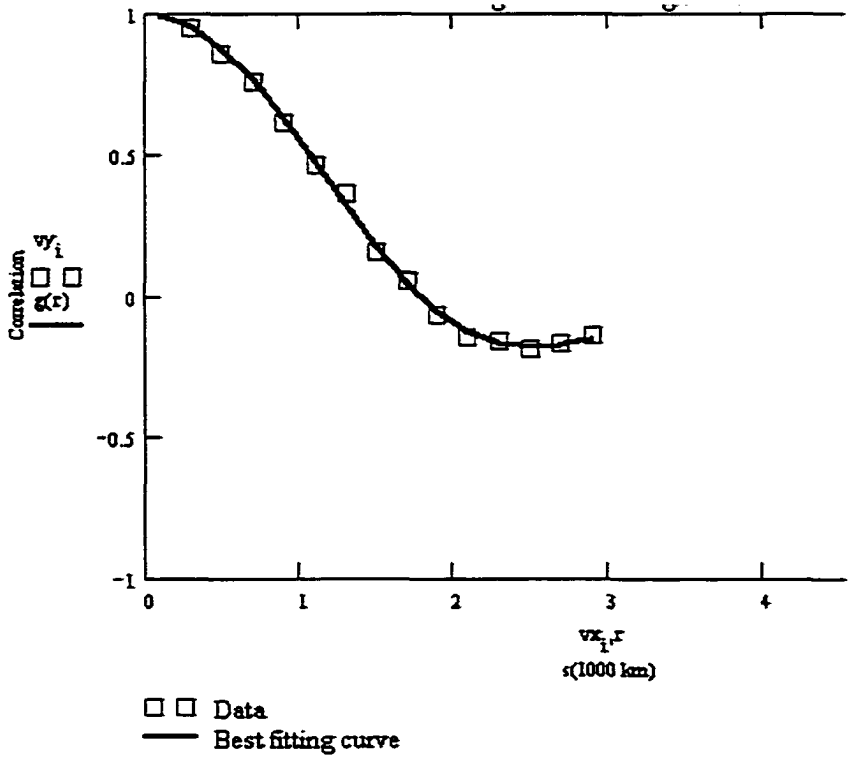

Spatial correlation between August 500 mb height field grid points separated by an approximate distance of s.

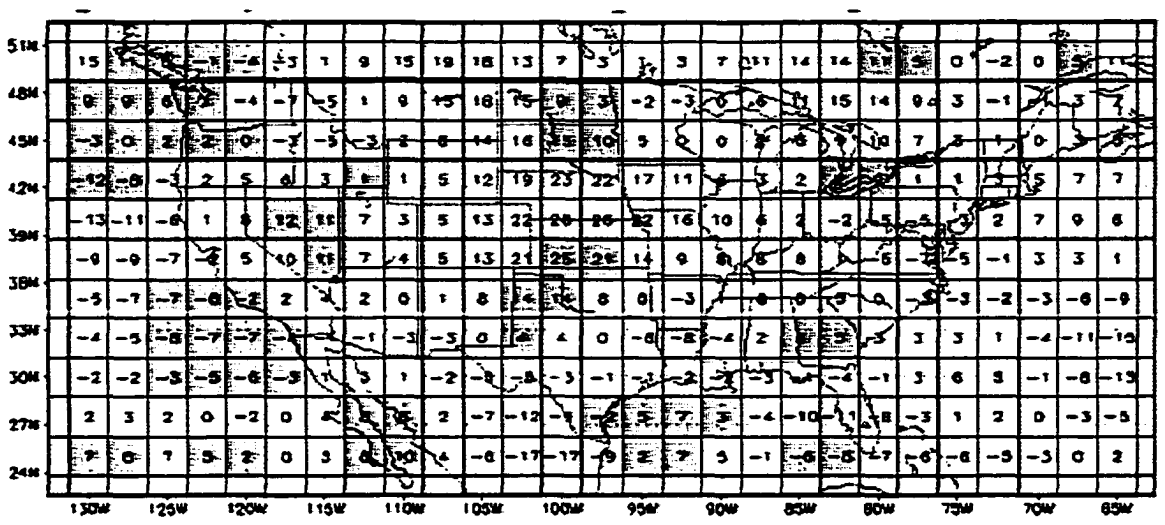

August difference field of 850 mb convergence in s^{-1}. Darker shaded areas correspond to Student's t-test significance at the 10% level

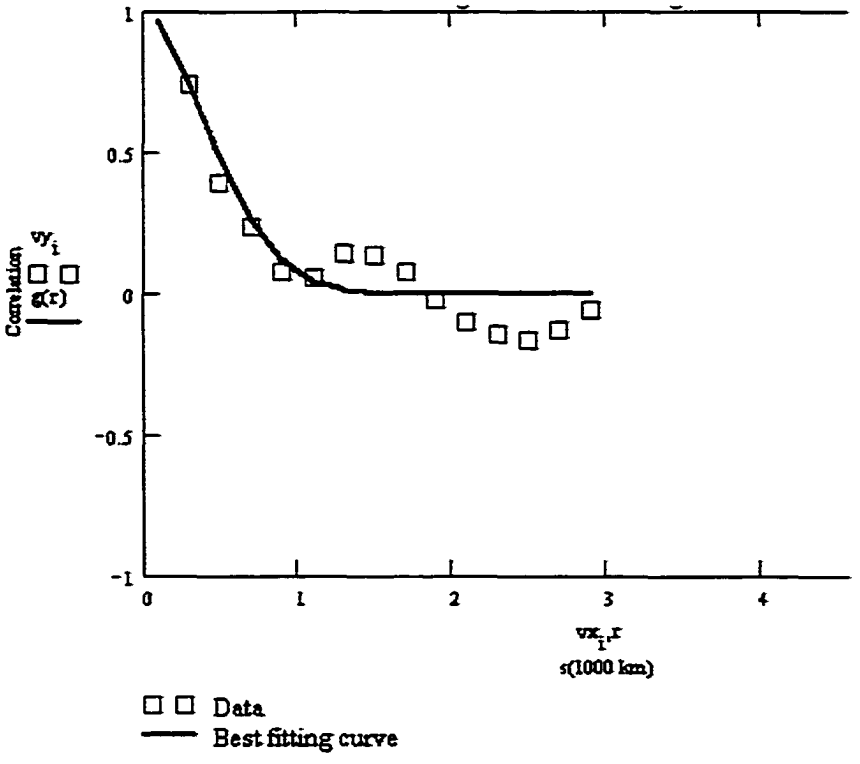

Spatial correlation between August 850 mb convergence field grid points separated by an approximate distance of s.

APPENDIX B. A RECONSTRUCTED VERSION OF THE GRAPH IN FIGURE 9.[2]

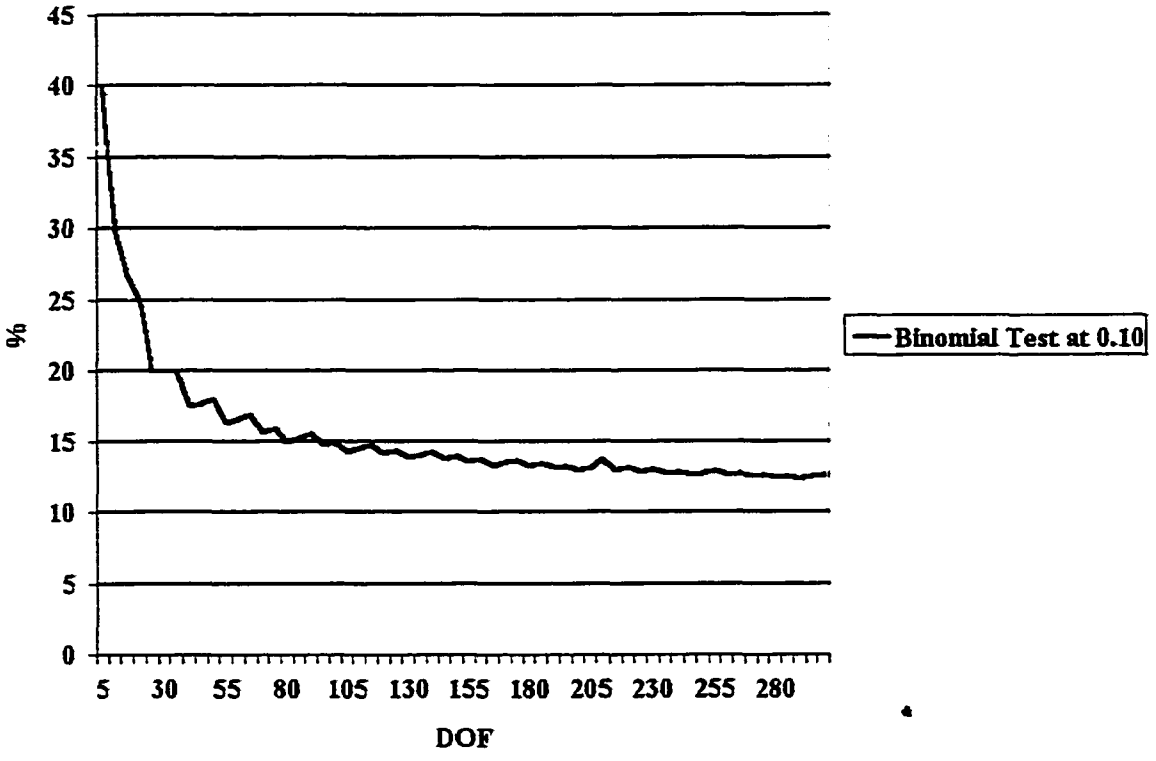

[2] This graph extends the % field of significance to 45%.

APPENDIX C. DESCRIPTION OF MONTHLY PRECIPITATION BY STATE AND DIVISION.[3]

July Precipitation

North Dakota- Seven of the nine state divisions show significant median precipitation differences between Events 1 and 4 at the 15% level. Event 1 median precipitation values are larger in magnitude than Event 4 for all nine divisions. Differences range from 10 mm to 54 mm, with the largest differences (> 30 mm) located in state divisions 3, 4, 5, 6, and 9.

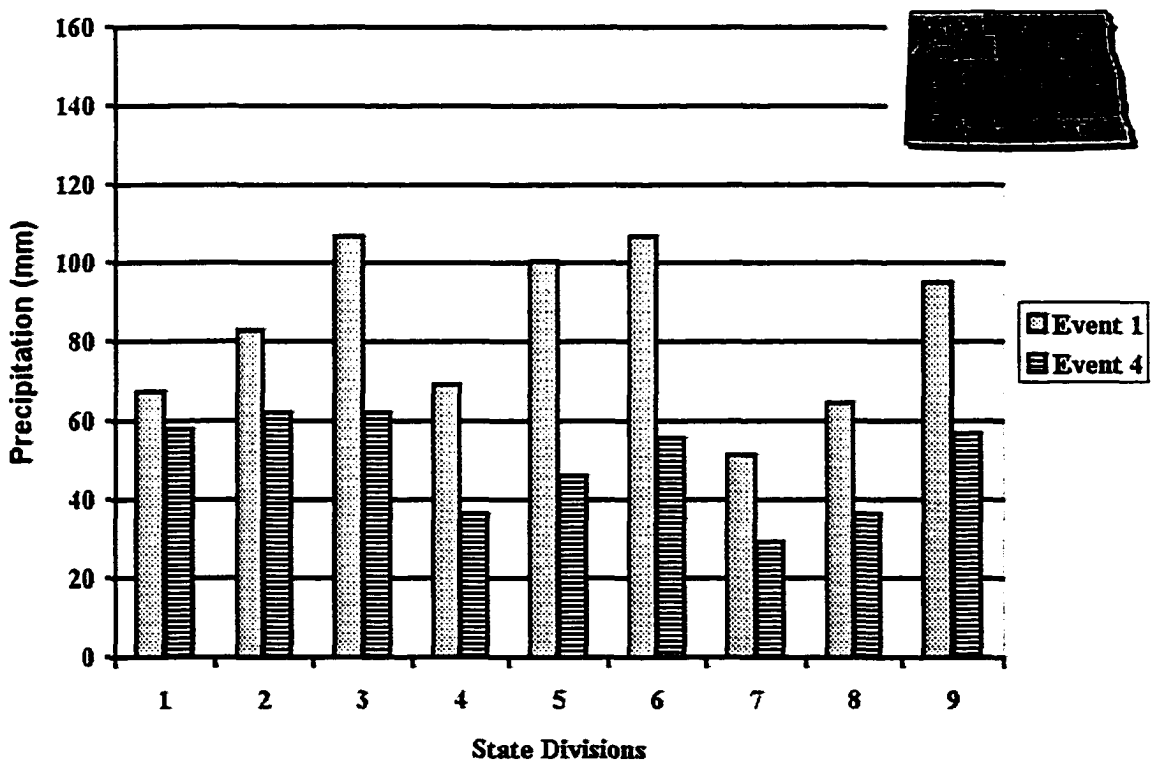

July North Dakota median precipitation by Events 1 and 4. Significance at the 15% level (p-value at 0.15) is denoted by shaded state divisions in upper right portion of graph.

[3]Shaded divisions in each state map indicate significant differences between Events 1 and 4 at the 10% level.

South Dakota- Five of the nine state divisions show significant median precipitation differences between Events 1 and 4 at the 15% level (Figure 21). Event 1 median precipitation values are larger in magnitude than Event 4 in all nine divisions. Differences range from 13 mm to 58 mm, with the largest differences (> 30 mm) located in state divisions 1, 3, 6, 7, and 8.

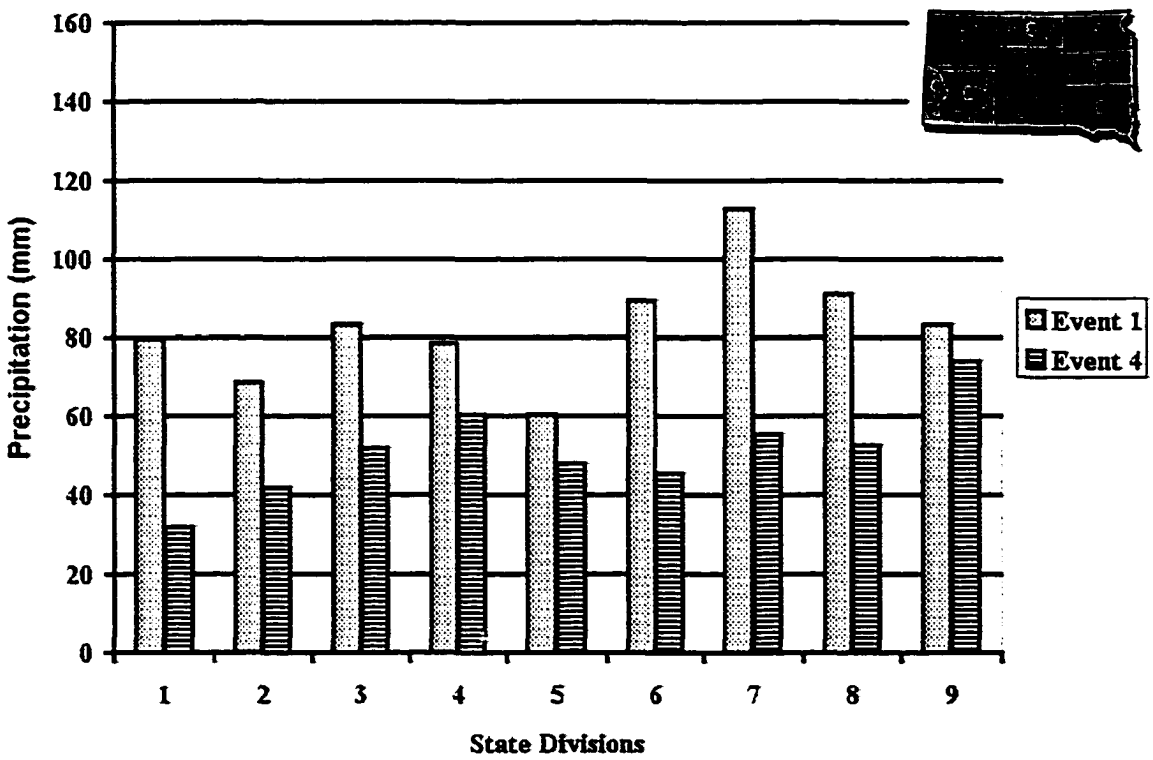

July South Dakota median precipitation by Events 1 and 4. Significance at the 15% level (p-value at 0.15) is denoted by shaded state divisions in upper right portion of graph.

Minnesota- Six of the nine state divisions show significant median precipitation differences between Events 1 and 4 at the 15% level (Figure 22). Event 1 median precipitation values are larger in magnitude than Event 4 in all nine divisions. Differences range from 21 mm to 55 mm, with the largest differences (> 30 mm) located in all state divisions except 4.

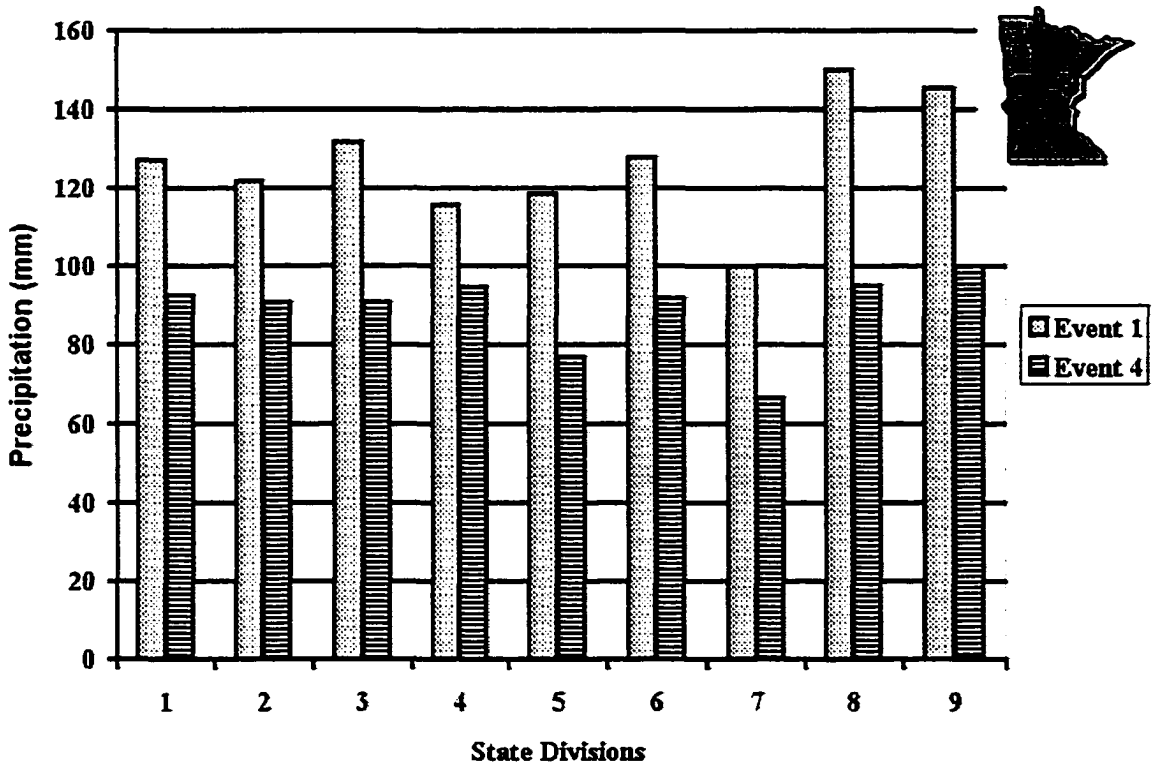

July Minnesota median precipitation by Events 1 and 4. Significance at the 15% level (p-value at 0.15) is denoted by shaded state divisions in upper right portion of graph.

Wisconsin- Seven of the nine state divisions show significant median precipitation differences between Events 1 and 4 at the 15% level (Figure 23). Event 1 median precipitation values are larger in magnitude than Event 4 in all nine divisions. Differences range from 14 mm to 80 mm, with the largest differences (> 30 mm) located in state divisions 1, 4, 7, 8, and 9.

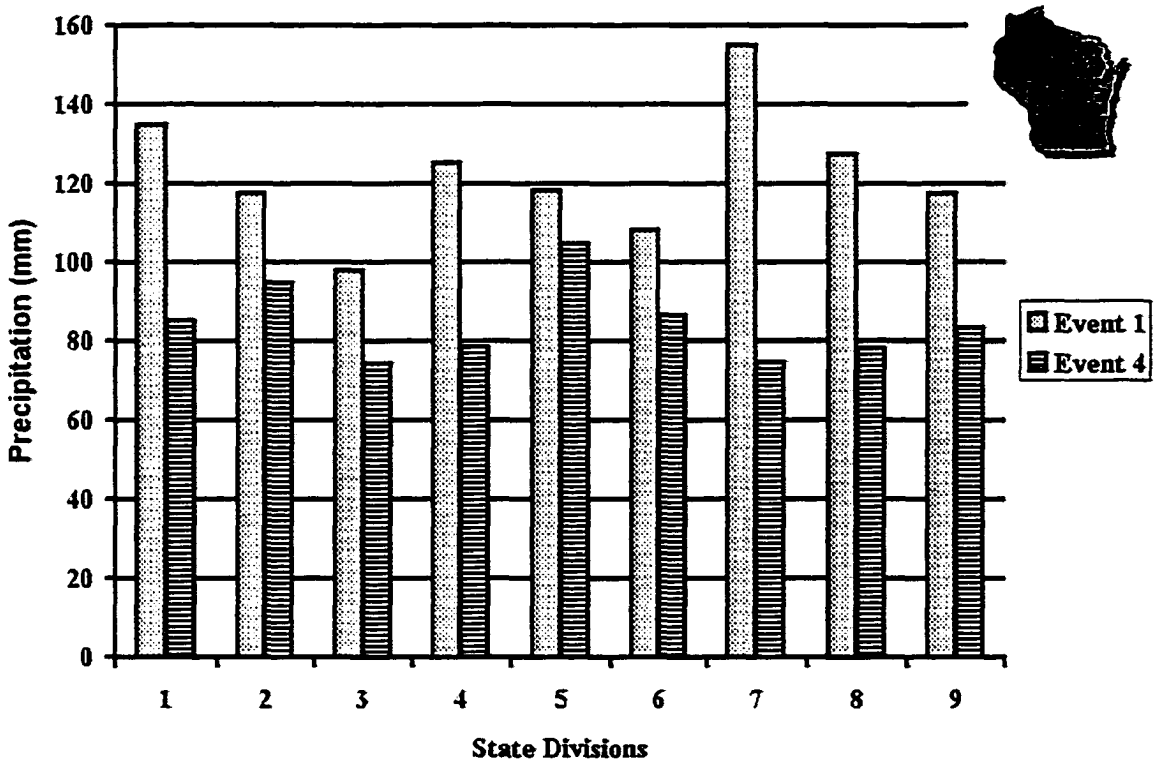

July Wisconsin median precipitation by Events 1 and 4. Significance at the 15% level (p-value at 0.15) is denoted by shaded state divisions in upper right portion of graph.

Iowa- Two of the nine divisions show significant median precipitation differences between Events 1 and 4 at the 15% level (Figure 24). Event 1 median precipitation values are larger in magnitude than Event 4, with the exception of state divisions 8 and 9. Differences range from 4 mm to 39 mm, with the largest differences (> 30 mm) located in state divisions 2, 3, and 7.

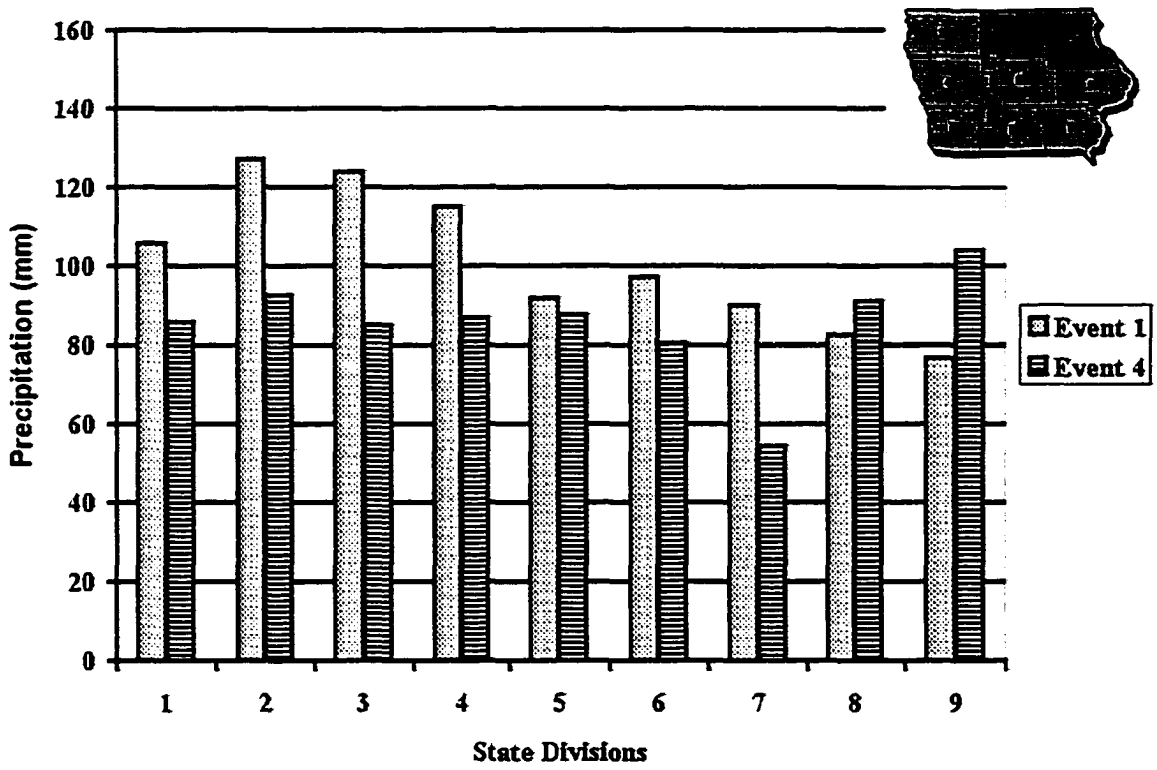

July Iowa median precipitation by Events 1 and 4. Significance at the 15% level (p-value at 0.15) is denoted by shaded state divisions in upper right portion of graph.

August Precipitation

Illinois- Four of the nine state divisions show significant median precipitation differences between Events 1 and 4 at the 15% level (Figure 25). Event 1 median precipitation values are larger in magnitude than Event 4 in all nine divisions. Differences range from 3 mm to 60 mm, with the largest differences (> 30 mm) located in state divisions 1-5.

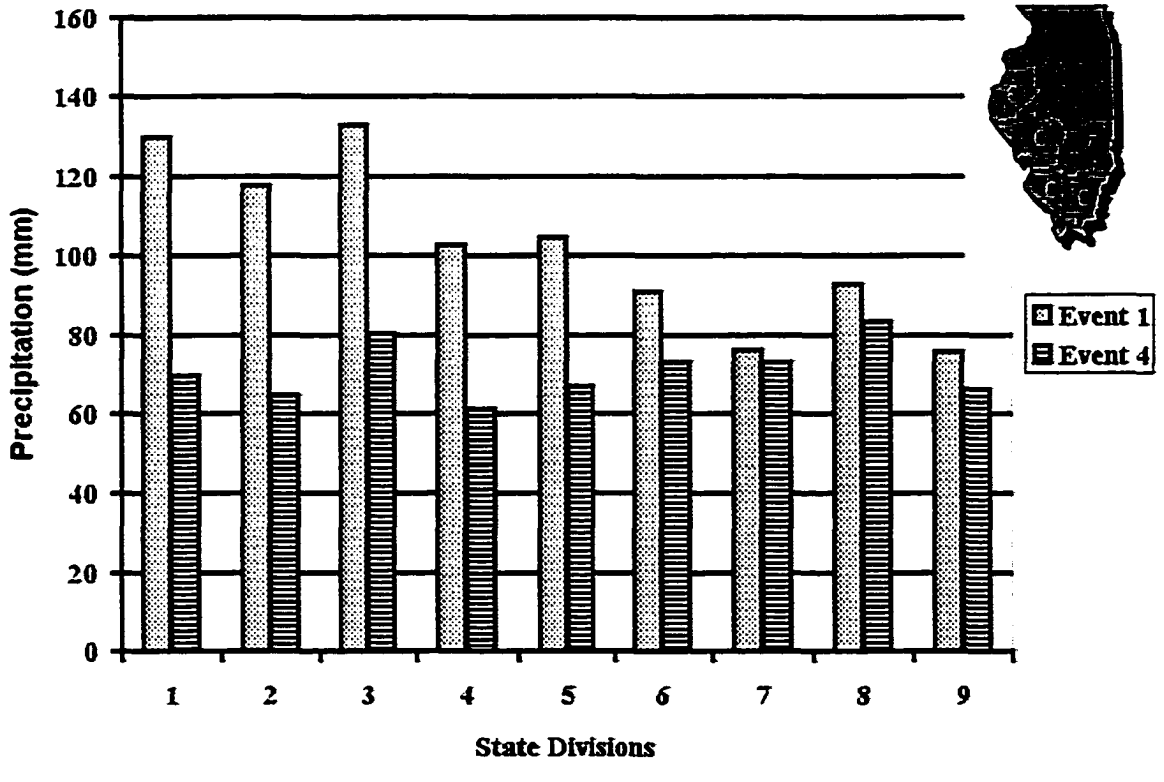

August Illinois median precipitation by Events 1 and 4. Significance at the 15% level (p-value at 0.15) is denoted by shaded state divisions in upper right portion of graph.

Iowa- Four of the nine state divisions show significant median precipitation differences between Events 1 and 4 at the 15% level (Figure 26). Event 1 median precipitation values are larger in magnitude than Event 4 in all nine divisions. Differences range from 10 mm to 50 mm, with the largest differences (> 30 mm) located in state divisions 2, 6, and 9.

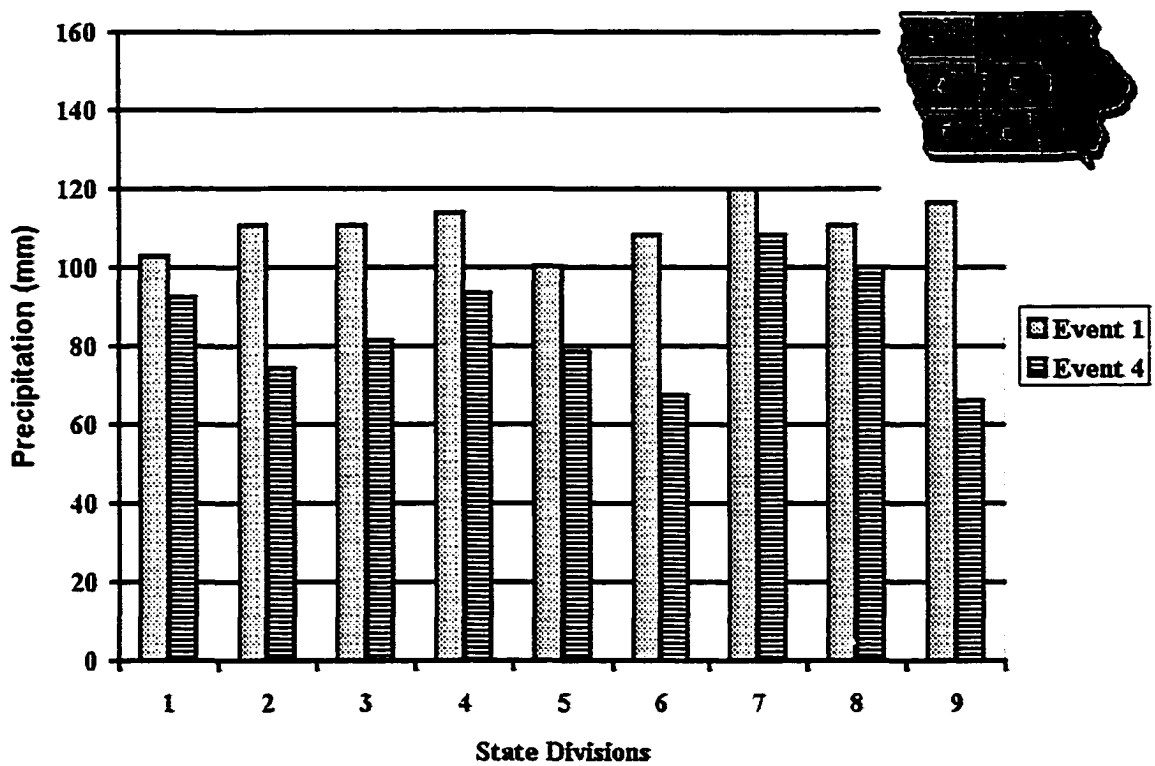

August Iowa median precipitation by Events 1 and 4. Significance at the 15% level (p-value at 0.15) is denoted by shaded state divisions in upper right portion of graph.

Kansas- Two of the nine state divisions show significant median precipitation differences between Events 1 and 4 at the 15% level (Figure 27). Event 1 median precipitation values are larger in magnitude than Event 4 in all nine divisions. Differences range from 3 mm to 52 mm, with the largest differences (> 30 mm) located in state divisions 1 and 2.

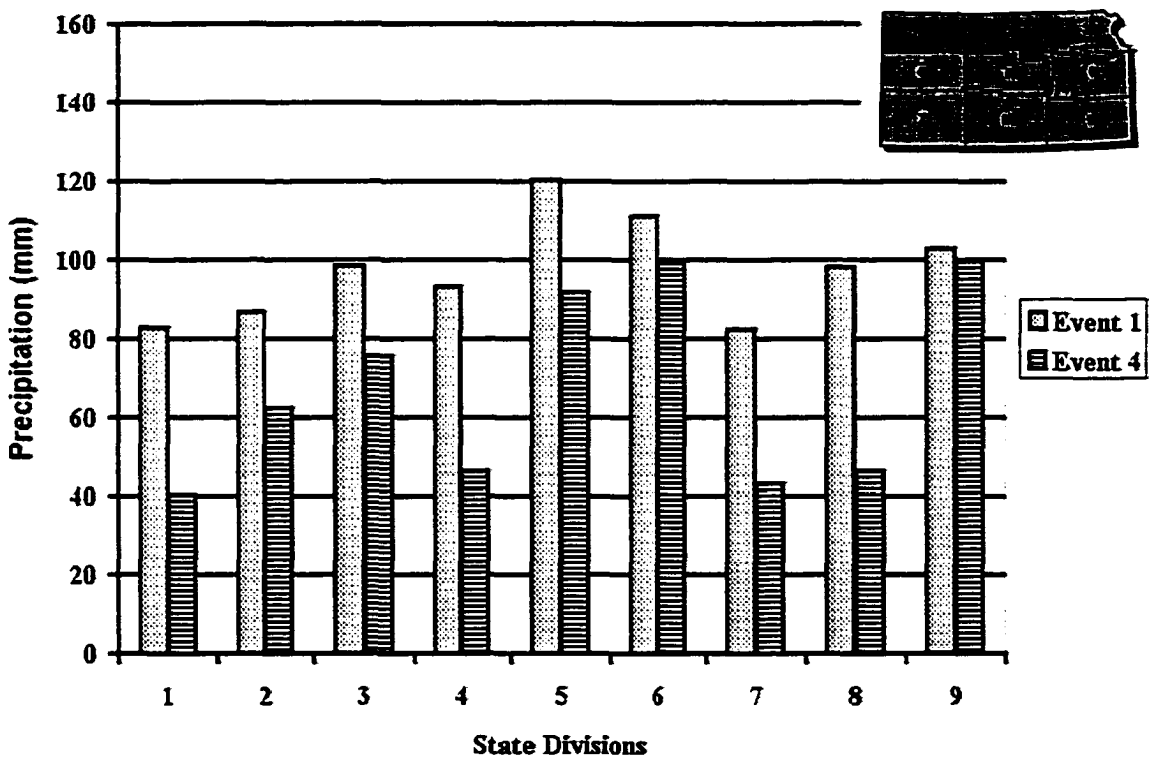

August Kansas median precipitation by Events 1 and 4. Significance at the 15% level (p-value at 0.15) is denoted by shaded state divisions in upper right portion of graph.

Nebraska- Five of the eight state divisions show significant median precipitation differences between Events 1 and 4 at the 15% level (Figure 28). Event 1 median precipitation values are larger in magnitude than Event 4 in all nine divisions. Differences range from 16 mm to 48 mm, with the largest differences (> 30 mm) located in state divisions 5 and 7.

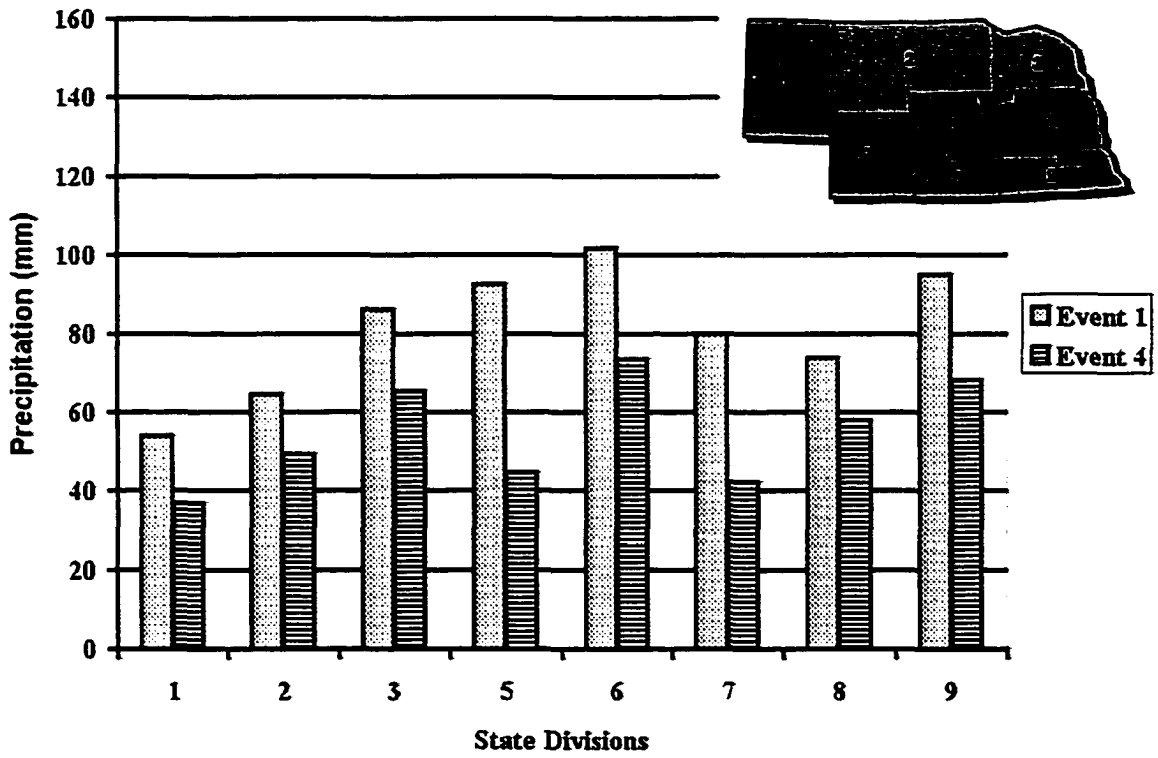

August Nebraska median precipitation by Events 1 and 4. Significance at the 15% level (p-value at 0.15) is denoted by shaded state divisions in upper right portion of graph.

September Precipitation

Michigan- Three of the ten state divisions show significant median precipitation differences between Events 1 and 4 at the 15% level (Figure 29). Event 1 median precipitation values are larger in magnitude than Event 4, with the exception of state division 6. Differences range from 14 mm to 49 mm, with the largest differences (> 30 mm) located in state divisions 5, 7, 9, and 10.

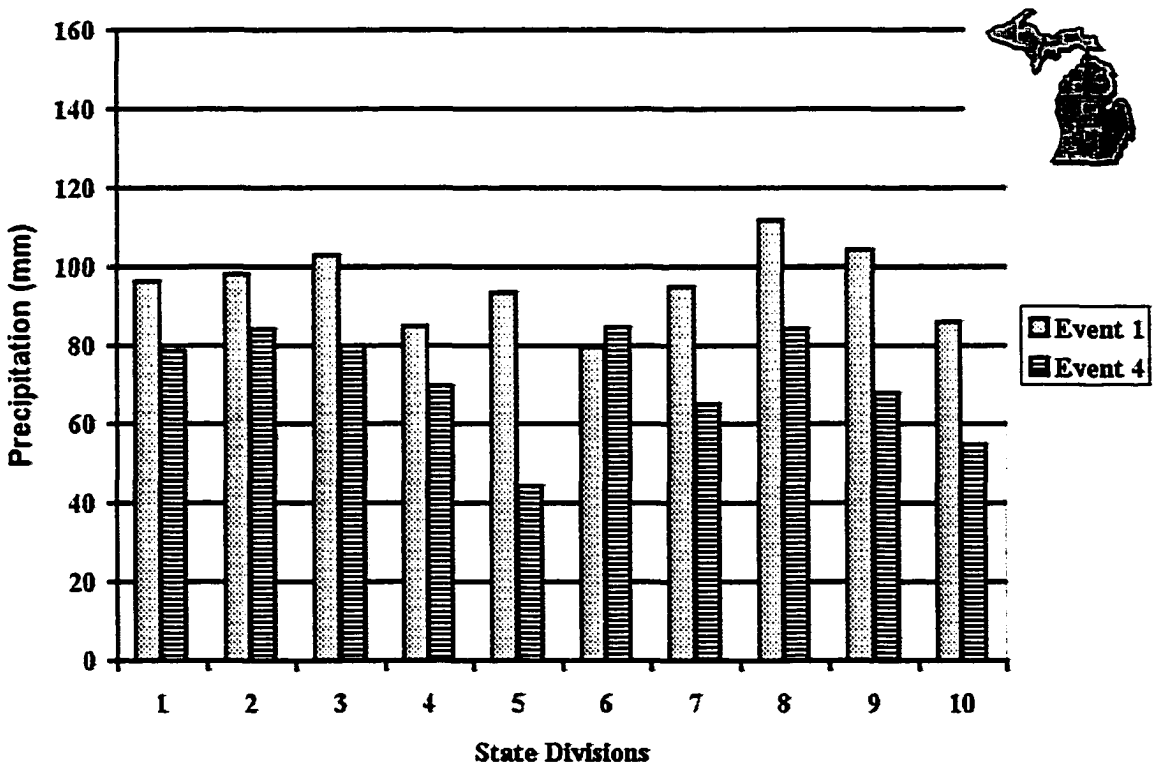

September Michigan median precipitation by Events 1 and 4. Significance at the 15% level (p-value at 0.15) is denoted by shaded state divisions in upper right portion of graph.

Minnesota- Three of the nine state divisions show significant median precipitation differences between Events 1 and 4 at the 15% level (Figure 30). Event 1 median precipitation values are larger in magnitude than Event 4, with the exception of state division 2. Differences range from 4 mm to 62 mm, with the largest differences (> 30 mm) located in state divisions 8 and 9.

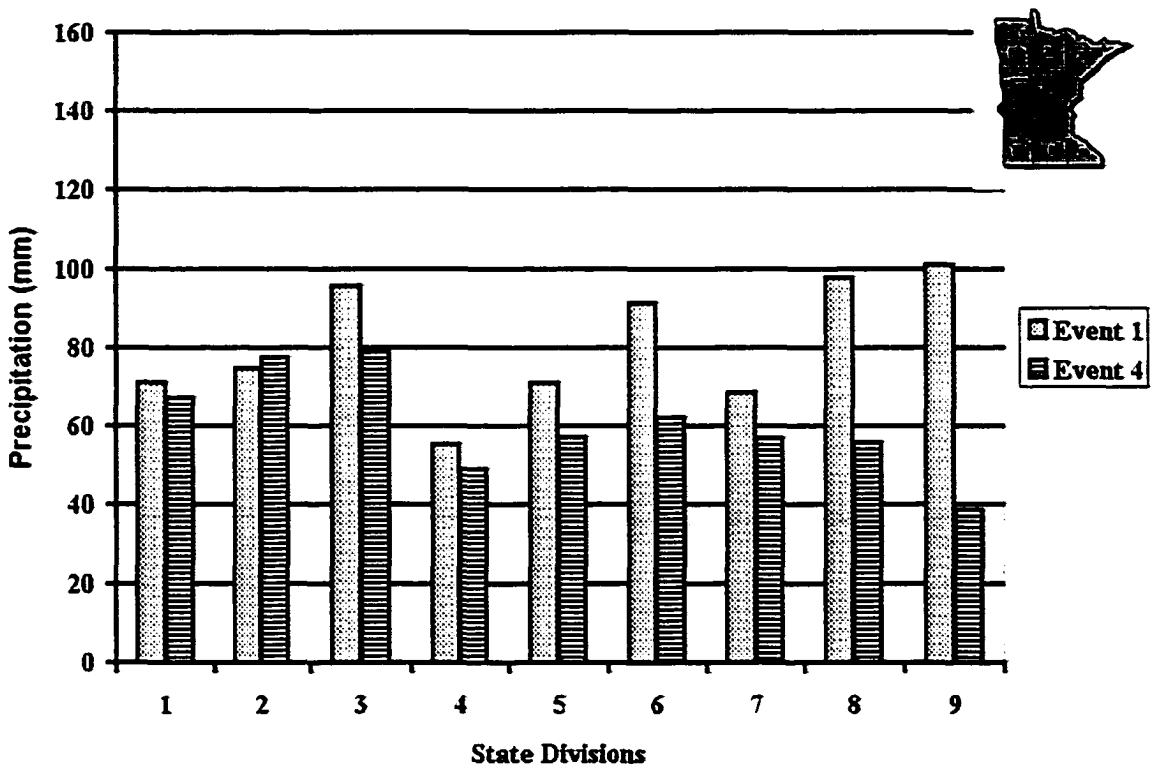

September Minnesota median precipitation by Events 1 and 4. Significance at the 15% level (p-value at 0.15) is denoted by shaded state divisions in upper right portion of graph.

Ohio- Three of the ten state divisions show significant median precipitation differences between Events 1 and 4 at the 15% level (Figure 31). Event 4 median precipitation values are larger in magnitude than Event 1, with the exception of state divisions 1-3. Differences range from 8 mm to 64 mm, with the largest differences (> 30 mm) located in state divisions 4, 8, and 9. Note that central and southern Ohio shows a positive response to Event 4 precipitation events.

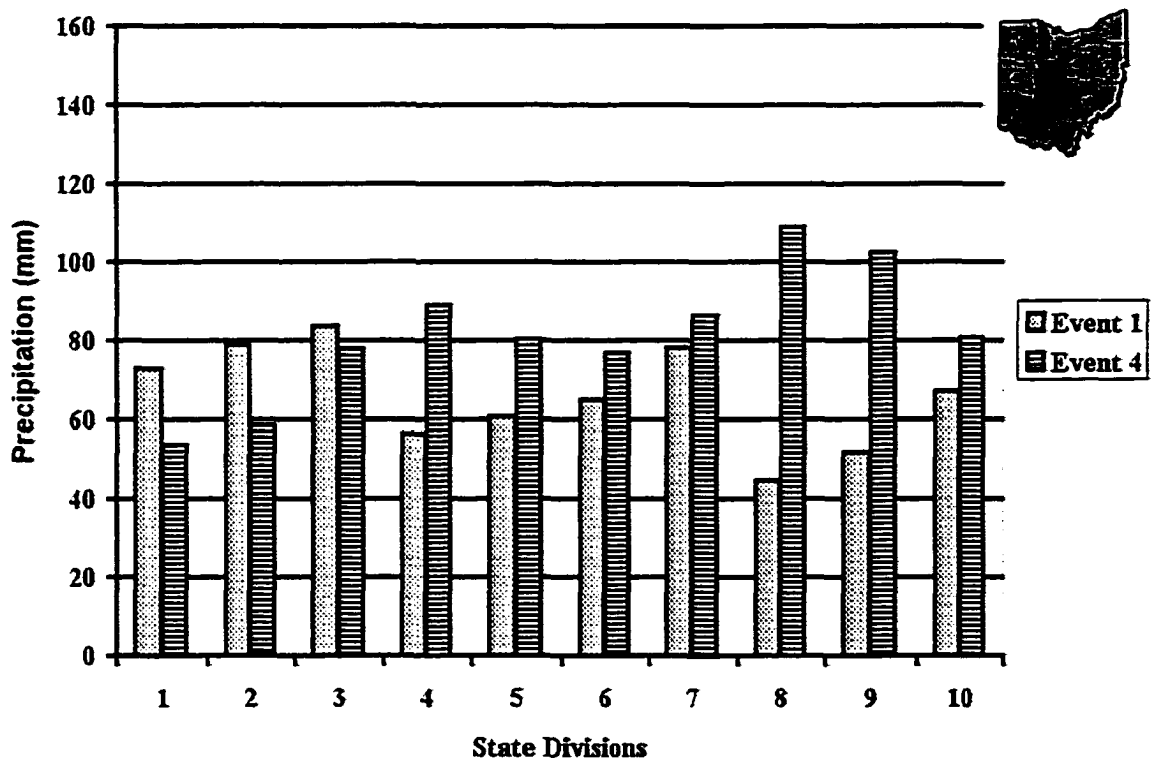

September Ohio median precipitation by Events 1 and 4. Significance at the 15% level (p-value at 0.15) is denoted by shaded state divisions in upper right portion of graph.

South Dakota- Two of the nine state divisions show significant median precipitation differences between Events 1 and 4 at the 15% level (Figure 32). Event 1 median precipitation values are larger in magnitude than Event 4 in five of the nine divisions. Differences range from 0 mm to 25 mm, with smaller differences (< 30 mm) compared to other states.

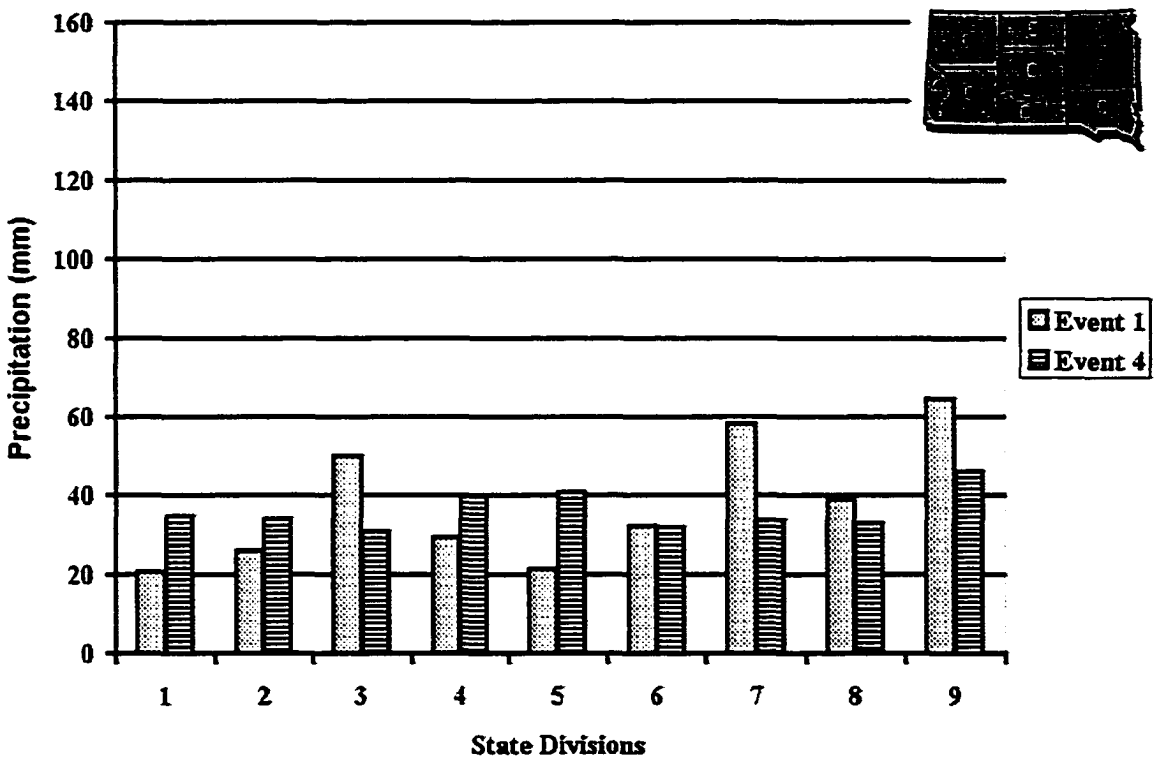

September South Dakota median precipitation by Events 1 and 4. Significance at the 15% level (p-value at 0.15) is denoted by shaded state divisions in upper right portion of graph.

Wisconsin- Three of the nine state divisions show significant median precipitation differences between Events 1 and 4 at the 15% level (Figure 33). Event 1 median precipitation values are larger in magnitude than Event 4 in all nine divisions. Differences range from 6 mm to 46 mm, with the largest differences (> 30 mm) located in state divisions 2, 4, 5, 8, and 9.

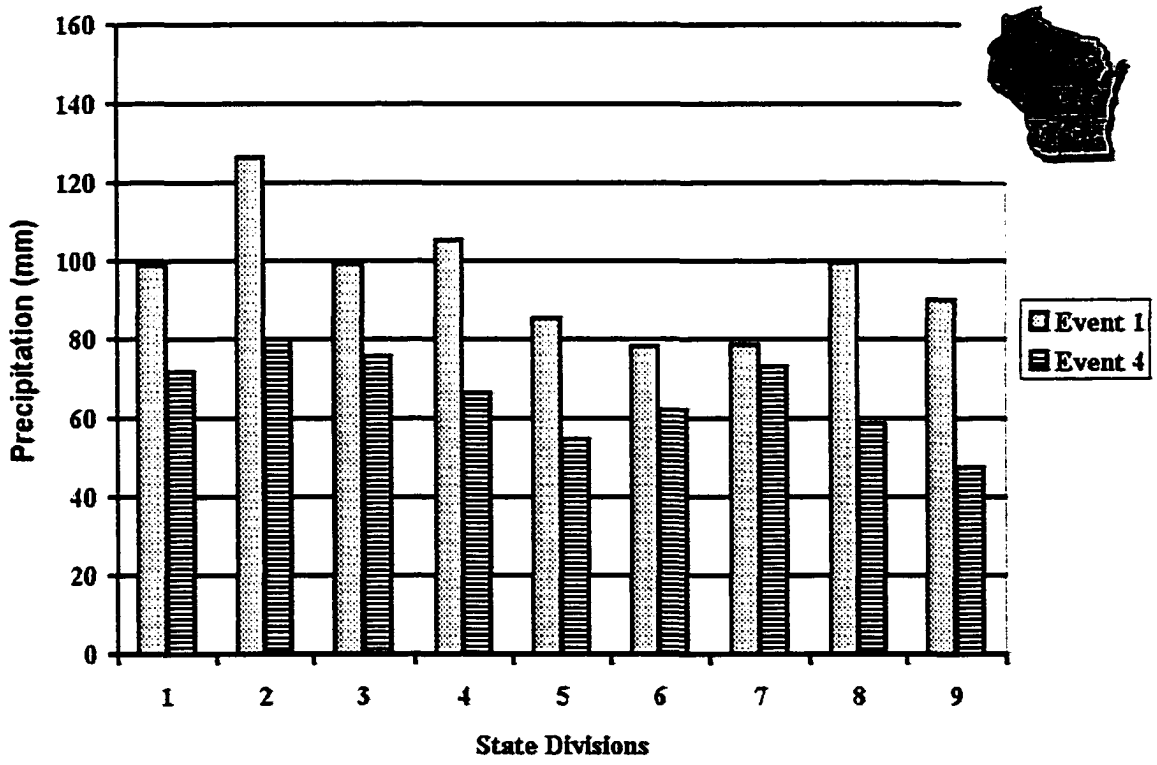

September Wisconsin median precipitation by Events 1 and 4. Significance at the 15% level (p-value at 0.15) is denoted by shaded state divisions in upper right portion of graph.

APPENDIX D. PRECIPITATION DIFFERENCES (EVENT 1 - EVENT 4) BY STATE DIVISIONS AND MONTHS (APRIL, JULY-SEPTEMBER).[4]

Month	State	1	2	3	4	5	6	7	8	9	10
April	IL	-19.9	-18.9	10.2	4.1	4.7	6.1	8.4	-2.0	-5.2	N/A
April	IN	-21.6	11.6	12.1	25.4	21.5	4.3	11.7	-0.5	-3.8	N/A
April	IA	30.6	0.1	-5.0		16.6	0.6	27.3			N/A
April	KS	4.4			-7.4	14.7			33.1		N/A
April	MI	-9.1	0.0	-10.4	-1.7	-21.1	11.3	26.2	-29.3	-21.6	5.2
April	MN	-12.4		-7.1	-6.7	-0.4	-11.0	5.1	21.2	20.2	N/A
April	MO		19.2		6.3	1.7		N/A	N/A	N/A	N/A
April	NE	-14.4	12.1	28.8	N/A	3.6	25.3	-1.1	-3.6	27.4	N/A
April	ND	-19.1	-14.1	-20.1	-14.9	-1.9		-12.2	-38.1	9.3	N/A
April	OH	30.1	23.7	-5.1	20.6	17		7.2	10.7	39.8	14.4
April	SD	-27.7	-39.2	14.1	-11.4	-22.2	-9.0	19.3	10.2	8.1	N/A
April	WN	-5.0	-15.5	-11.4	8.9	0.6	12.3	-5.6	-2.9	-10.2	N/A
July	IL	-14.5	1.5	-24.4	-37.8	3.3	-32.3	-48.3	-13.5	-9.4	N/A
July	IN	3.8	-27.4	-13.7	5.1	-9.1	-6.6	-15.2	7.4	-0.5	N/A
July	IA	20.1			28.4	4.3	16.8	35.8	-8.6	-26.9	N/A
July	KS		-4.3	-13.0	14.7	36.3	-24.1	-1.3	-10.9	15.2	N/A
July	MI	14.2	19.3	-12.7	-15.0	13.5	7.9	-0.8	1.8	-11	19.6
July	MN		31.0	41.1							N/A
July	MO	-17.8	46.5	-23.9	-16.3	-15.0	-38.1	N/A	N/A	N/A	N/A
July	NE	21.8	19.1	7.1	N/A	13.5	9.4	-4.3	-6.9	-2.3	N/A
July	ND	10.0								38.4	N/A
July	OH	-19.6	-21.3	-12.0	-36.1	4.6	-6.4	10.2	-25.7		10.2
July	SD		26.9		18.5	12.7		57.7			N/A
July	WN			23.4			21.8				N/A
August	IL			52.5			18.2	3.2	9.4	9.4	N/A

[4] Shaded regions indicate significant differences at the 10% level.

Appendix D (continued)

August	IN	36.4	[redacted]	3.8	[redacted]	13.7	5.5	16.9	33.5	[redacted]	N/A
August	IA	10.3	[redacted]	[redacted]	20.3	21.7	[redacted]	11.9	10.9	[redacted]	N/A
August	KS	[redacted]	[redacted]	22.9	46.7	28.6	11.7	39.1	51.8	3.2	N/A
August	MI	-12.8	0.8	12.1	28.7	41.3	6.5	19.4	[redacted]	12.2	15
August	MN	3.8	-2.2	-13.1	[redacted]	-2.7	-26	4.2	[redacted]	27.3	N/A
August	MO	-4.8	32.4	0.1	28.2	5.7	-39.8	N/A	N/A	N/A	N/A
August	NE	[redacted]	15.6	20.6	N/A	[redacted]	[redacted]	[redacted]	[redacted]	26.8	N/A
August	ND	-5	1.7	-3.3	4.2	1.8	2.9	10.4	3.4	-9.4	N/A
August	OH	7.5	23.5	24.5	-7.6	11	9.3	-1.4	12.3	1.5	8.6
August	SD	2.2	11.3	9.7	-0.1	9.1	9.1	-0.9	12.4	6.7	N/A
August	WN	[redacted]	[redacted]	-9.7	12.4	5.5	18.3	21.3	14	[redacted]	N/A
September	IL	15.7	5.7	-11.6	-0.4	-3.2	-5.7	-14	22.7	42.2	N/A
September	IN	-25.3	-2.2	26.8	-34.2	-24.1	-3.6	9.4	-8.1	[redacted]	N/A
September	IA	44.1	17.5	14.4	[redacted]	30.4	12.7	15.2	-14	-6.2	N/A
September	KS	-11.2	4.4	20.3	-11.9	-19.4	-1.5	-7	-8.9	-34.5	N/A
September	MI	17.5	13.8	22.9	15.4	[redacted]	-5.1	[redacted]	27.6	36.6	[redacted]
September	MN	3.8	-2.7	16.6	[redacted]	[redacted]	[redacted]	11.8	42.2	62.4	N/A
September	MO	4.7	12.7	-20.2	-4.6	5	-8.5	N/A	N/A	N/A	N/A
September	NE	6.1	4.2	35.7	N/A	-0.9	33.7	-5.6	-9.8	-2	N/A
September	ND	-26.7	-18.8	-18.9	-25	12.4	-3.2	-7.7	-12.4	4.8	N/A
September	OH	19.3	20.4	5.8	-32.5	[redacted]	-11.6	-8.1	[redacted]	[redacted]	-13.5
September	SD	-14.2	-7.9	[redacted]	-10.2	-19.1	0.3	[redacted]	6.1	18.8	N/A
September	WN	[redacted]	[redacted]	23.6	[redacted]	30.9	16.4	5.6	41.1	42.4	N/A

REFERENCES

Anderson, C. J., and R. W. Arritt, 1998: Mesoscale convective complexes and persistent elongated convective systems over the United States during 1992 and 1993. *Mon. Wea. Rev.*, **126**, 578-599.

Arritt, R. W., T. D. Rink, M. Segal, D. P. Todey, C. A. Clark, M. J. Mitchell, and K. M. Labas, 1997: The Great Plains low-level jet during the warm season of 1993. *Mon. Wea. Rev.*, **125**, 2176-2192.

Augustine, J. A., and K. W. Howard, 1991: Mesoscale convective complexes over the United States during 1986 and 1987. *Mon. Wea. Rev.*, **119**, 1575-1589.

Bell, G. D., and J. E. Janowiak, 1995: Atmospheric circulation associated with the Midwest floods of 1993. *Bull. Amer. Meteor. Soc.*, **76**, 681-695.

Bonner, W. D., 1968: Climatology of the low-level jet. *Mon. Wea. Rev.*, **96**, 833-850.

Bunkers, M. J., J. R. Miller Jr., and A. T. DeGaetano, 1996: An examination of El Nino-La Nina-related precipitation and temperature anomalies across the northern Plains. *J. Climate*, **9**, 147-160.

Carlson, R. E., D. P. Todey, and S. E. Taylor, 1996: Midwestern corn yield and weather in relation to extremes of the southern oscillation. *J. Prod. Agric.*, **9**, 347-352.

Carlson, R. E., Personal Communication 2000.

Cotton, W.R., M.S. Lin, R.L. McAnelly, C.J. Tremback, 1989: A composite model of mesoscale convective complexes. *Mon. Wea. Rev.*, **117**, 765-783

Fleagle R. G. and J. A. Businger, 1980: An introduction to atmospheric physics. 2nd ed. Academic Press, Inc. Orlando, FL 432 pp.

Fraedrich, K. C. Ziehmann, and F. Sielmann, 1995: Estimates of spatial degrees of freedom. *J. Climate*, **8**, 361-369.

Fritsch, J. M., R. J. Kane, and C. R. Chelius, 1986: The contribution of mesoscale convective weather systems to the warm-season precipitation in the United States. *J. Climate Appl. Meteor.*, **25**, 1333-1345.

Garnett, E. R., M. L. Khandekar, and J. C. Babb, 1998: On the utility of ENSO and PNA indices for long-lead forecasting of summer weather over the crop-growing region of the Canadian prairies. *Theor. Appl. Climatol.*, **60**, 37-45.

Gershunov, A., and T. P. Barnett, 1998: Interdecadal modulation of ENSO teleconnections. *Bull. Amer. Meteor. Soc.*, **79**, 2715-2725.

Holton, J. R., 1979: An introduction to dynamic meteorology . 2nd ed. Academic Press Inc. San Diego, CA 511 pp.

Horel, J. D., and J. M. Wallace, 1981: Planetary-scale atmospheric phenomena associated with the Southern Oscillation. *Mon. Wea. Rev.*, **107**, 813-829.

Hoskins, B. J., I. Draghici, and H. C. Davies, 1978: A new look at the omega-equation. *Quart. J. Roy. Met. Soc.* **104**, 31-38.

Hoskins, B. J., and D. J. Karoly, 1981: The steady linear response of a spherical atmosphere to thermal and orographic forcing. *J. Atmos. Sci.*, **38**, 1179-1196.

Iowa Department of Agriculture. 1998. Agricultural Statisitics. Iowa Dep. Of Agric., Des Moines.

Kaiser, H.M., Drennen, T.E. eds, 1993: Agricultural Dimensions of Global Climate Change, St. Lucie Press, 311 pp.

Kalbfleisch, J. G., 1985: Probability and statistical inference. 2nd ed. Springer-Verlag New York, Inc. 343 pp.

Kalnay, E., and Co-authors, 1996: The NCEP/NCAR 40-year reanalysis project. *Bull. Amer. Meteor. Soc.*, **77**, 437-471.

Karl, T. R., C. N. Williams Jr., and P. J. Young, 1986: A model to estimate the time of observation bias associated with monthly mean maximum, minimum, and mean temperatures for the United States. *J. Climate Appl. Meteor.*, **25**, 145-160.

Lau, K. M., and L. Peng, 1992: Dynamics of atmospheric teleconnections during the northern summer. *J. Climate*, **5**, 140-158.

Leathers, D. J., B. Yarnal, and M. A. Palecki, 1991: The Pacific/North American teleconnection pattern and United States climate. Part I: Regional temperature and precipitation associations. *J. Climate*, **4**, 517-528.

List, R. J., 1966: Smithsonian meteorological tables. 6th ed. Smithsonian Institution Washington D. C. 527 pp.

Livezey, R. E., and W. Y. Chen, 1983: Statistical field significance and its determination by Monte Carlo techniques. *Mon. Wea. Rev.*, **111**, 46-59.

Livezey, R. E., and K. C. Mo, 1987: Tropical-extratropical teleconnections during the Northern Hemisphere winter. Part II: Relationships between monthly mean Northern Hemisphere circulation patterns and proxies for tropical convection. *Mon. Wea. Rev.*, **115**, 3115-3123.

Madden, R. A., D. J. Shea, G. W. Branstator, J. J. Tribbia, and R. O. Weber, 1993: The effects of imperfect spatial and temporal sampling on estimates of the Global mean temperature: experiments with model data. *J. Climate*, **6**, 1057-1066.

Maddox, R. A., 1980: Mesoscale convective complexes. *Bull. Amer. Meteor. Soc.*, **61**, 1374-1387.

Maddox, R. A., 1983: Large-scale meteorological conditions associated with midlatitude, Mesoscale convective complexes. *Mon. Wea. Rev.*, **111**, 1475-1493.

Mantua, N. J., 1999: The Pacific decadal oscillation and climate forecasting for North America. Available at: http://www.atmos.washington.edu/~mantua/REPORTS/PDO/PDO_cs.htm

Mantua, N. J., 2000: The Pacific Decadal Oscillation (PDO). Available at: http://tao.atmos.washington.edu/pdo/

Mauget, S. A. and D. R. Upchurch, 1998: El Nino and La Nina related climate and agricultural impacts over the continental United States. Technical Report #2. *U.S. Department of Agriculture-Agricultural Research Service Wind Erosion and Water Conservation Research Unit Cropping Systems Research Laboratory, Lubbock, Texas.*

McAnelly, R. L., and W. R. Cotton, 1989: The precipitation life cycle of mesoscale convective complexes over the central United States. *Mon. Wea. Rev.*, **114,** 784-808.

Mo, K. C., J. N. Paegle, and R. W. Higgins, 1997: Atmospheric processes associated with summer floods and droughts in the central United States. *J. Climate,* **10,** 3028-3046.

Phillips J., B. Rajagopalan, M. Cane, and C. Rosenzweig, 1999: The role of ENSO in determining climate and maize yield variability in the U.S. cornbelt. *Int. J. Climatol.*, **19,** 877-888.

Rasmusson, E. M., and J. M. Wallace, 1983: Meteorological aspects of the El Nino/Southern Oscillation. *Science,* **222,** 1195-1202.

Shibles, R., 1998: Agronomy 501: Crop growth and development. *Master of Science in Agronomy.* Iowa State Univ. Press, Ames, IA.

Thompson, L., 1986: Climate change, weather variability, and corn production *Agronomy Journal.*, **78,** 649-653.

Ting, M., and H. Wang, 1997: Summertime U.S. precipitation variability and its relation to Pacific sea surface temperatures. *J. Climate,* **10,** 1853-1873.

Todey, D. P., 1995: Extended range forecasting and ENSO effects in the corn belt. Ph.D. diss. Iowa State University, Ames, Iowa.

Tollerud E. I., and R. S. Collander, 1993: Mesoscale convective systems and extreme rainfall in the central United States. Preprints, *Symposium on Extreme Hydrological Events: Precipitation, Floods, and Droughts, Fourth Scientific Assembly of the International Association of Hydrological Sciences (IAHS)*, Yokohama, Japan, July 11-23.

Trenberth, K. E., and T. J. Hoar, 1996: *Geophysical Research Letters*, **23**, 57-60.

Stull, R. B., 1995: Meteorology today for scientists and engineers. *West Publishing Company*., Minneapolis/St. Paul 385 pp.

USDA. 1949-1998. Agricultural statistics. U.S. Gov. Print. Office, Washington, DC.

Wallace, J. M., and P. V. Hobbs, 1977: Atmospheric Science An Introductory Survey. Academic Press Inc., Orlando, FL 467 pp.

Wallace, J. M., and D. S. Gutzler, 1981: Teleconnections in the geopotential height field during the Northern Hemisphere winter. *Mon. Wea. Rev.*, **109**, 784-812.

Walpole R. E., and R. H. Myers: Probability and Statistics for Engineers and Scientists. Macmillan Publishing Company, New York, NY 765 pp.

Wikle, C. K., Personal Communication 1998-2000.

Wilks, D. S., 1995: Statistical methods in the atmospheric sciences. Academic Press Inc., San Diego, CA 467 pp.

Zhang, Y., J. M. Wallace, and D. S. Battisti 1997: ENSO-like interdecadal variability: 1900-93. *Journal of Climate,* **10,** 1004-1020.

ACKNOWLEDGMENTS

I am grateful to the guidance and patience provided by my major professor, Dr. Richard E. Carlson. You have been supportive with the genesis, development, and closing stages of the dissertation. Without your help, especially with the statistics and FORTRAN programming this project would have not been possible. I would also like to extend my gratitude to the members of my graduate committee, Dr. Raymond W. Arritt, Dr. Tsing-Chang Chen, Dr. William A. Gallus, and Dr. S. Elwynn Taylor. I also want to extend a special debt of gratitude to the three people that I have worked with in the introductory Agronomy/Meteorology class; Dr. Richard E. Carlson, Dr. S. Elwynn Taylor, and Dr. Douglas N. Yarger. I have seen three very distinct methods in the classroom and have components of all three within me. I am grateful to all three for providing a template for successful teaching.

Drs. Roland A. Madden and Christopher K. Wikle were important components with the spatial statistics. Dr. Madden graciously took the time to discuss the ideas behind using spatial statistics with geophysical fields and Dr. Wikle was very instrumental in the application of the spatial statistics on the geophysical fields. Dr. Wikle often took time out of a very busy schedule to answer questions and discuss problems along the way, a special thanks goes to him.

Many other people have made an impact on my graduate career here at Iowa State, I would like to recognize and thank them for their support. Charles and Verna Brown for their generous financial contribution to my graduate education. Dr. Dennis P. Todey has provided guidance and support throughout my tenure here. Christopher Anderson has provided a setting conducive to some interesting conversations regarding meteorology. Conversations with Seth Loyd have always provided support for the soul, and I will always be grateful to him.

My love goes out to my family. My wife, mother and sisters have always provided a strong support system for me and I will be eternally grateful to all of them. Last but certainly not least, Christ, who makes all things possible.